MODEL PARAMETER ESTIMATION

3.1: Teardown versus nonteardown approaches

- So far, we have eliminated redundant model parameters and have derived cell impedance models.

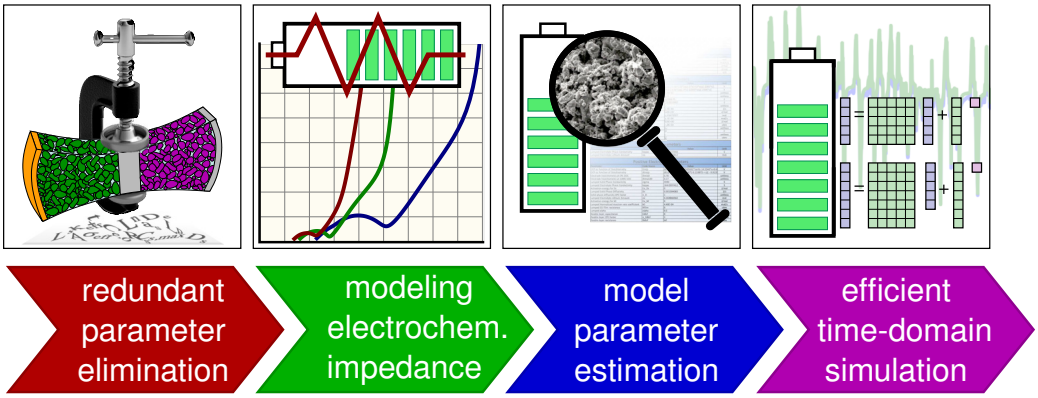

- It is now time to find accurate estimates of model parameter values.

Parameter estimation via cell teardown

- Two different approaches are reported in the literature: teardown and nonteardown.
- The teardown approach begins by disassembling the cell in a glovebox in an inert (e.g., argon gas) environment.

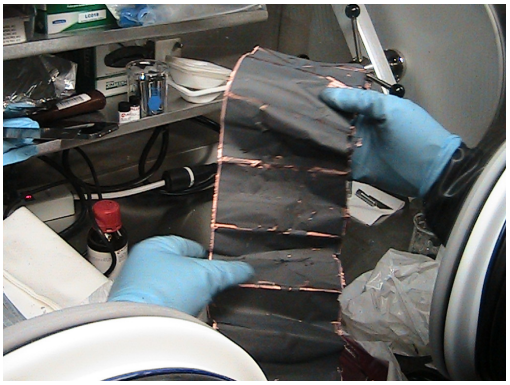

- Some measurements can be made directly.
- The current-collector's area A can be found by measuring its length and width using a ruler and then computing their product.
- A micrometer can measure electrode and separator thicknesses L^{r}.

- Can estimate particle sizes $R_{\mathrm{s}}^{\mathrm{r}}$ via SEM images of electrode samples.
- Can estimate porosity from FIB cross-sectional electrode slices.
- Electrode porosity can also be estimated using mercury porosimetry.
- Interfacial surface area of assumed spherical particles is $a_{\mathrm{s}}^{\mathrm{r}} = 3\varepsilon_{\mathrm{s}}^{\mathrm{r}}/R_{\mathrm{s}}^{\mathrm{r}}$.
- Other parameters require much more elaborate procedures.
- Electrode diffusivity $D_{\mathrm{s}}^{\mathrm{r}}$ can be estimated via galvanostatic intermittent titration technique (GITT) experiments performed on half cells.
- Inductively coupled plasma-optical emission spectrometry (ICP-OES) can determine the relative fractions of different atomic elements in a sample (e.g., is this electrode NCA, or NMC, or something else?).
- Values of $c_{\mathrm{s,max}}^{\mathrm{r}}$ can be found experimentally but are usually adopted from the literature for the electrode composition that is detected.
- Active-material volume fraction $\varepsilon_{\mathrm{s}}^{\mathrm{r}}$ can be found by comparing measured cell capacity to the maximum capacity of the materials.
- Electrode OCP vs. stoichiometry can be estimated as described later.
- Exchange-current density, double-layer capacitance hard to measure directly; instead, EIS data are regressed to a simplified model.
- Making half cells degrades $\sigma_{\mathrm{eff}}^{\mathrm{r}}$ measurements via modified contact resistance. $\sigma_{\mathrm{eff}}^{\mathrm{r}}$ doesn't dominate dynamics, so use literature values.
- Commercial cells contain very little electrolyte, so it is extremely difficult to identify electrolyte properties accurately.
  - Extract a sample via centrifuge; analyze via gas chromatography to determine its composition; reconstitute additional electrolyte having the same composition for more detailed analysis.

- A summary observation is that specialized (often very expensive) equipment and highly trained scientists are needed.
  - Experiments used to parameterize a PBM via direct measurement include FTIR, GC–MS, NMR, XRD, ICP–OES, TGA, DLS, PEIS, SSPP, PITT, SEM–EDS, pycnometry, and Hg-porosimetry.
- Experimental errors on the individual parameter values tend to add together when the entire PBM is evaluated. So, the final model still requires tuning of the parameter values to fit observed behaviors.
- Also, in many cases cell-supplier legal agreements prohibit cell teardown, and so alternate means to determine the PBM parameter values have appeal. Nonteardown methods provide such means.

Parameter estimation without cell teardown

- The nonteardown approach stimulates an intact physical cell electrically and/or thermally and measures its response.
- The same stimulus is applied to the cell model to compute its predicted response.
- Model parameter values are adjusted to make model predictions match physical measurements as closely as possible.

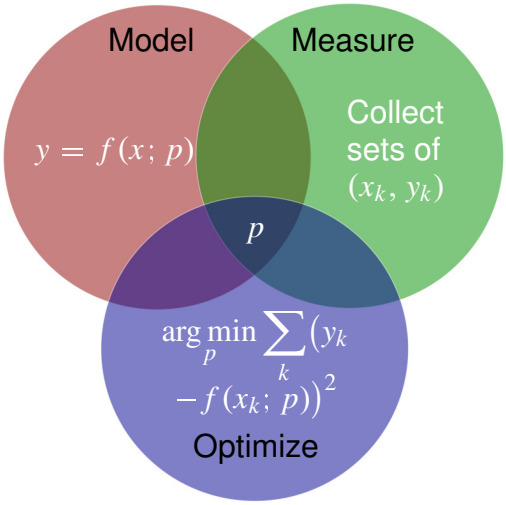

- Nonteardown parameter estimation is merely an application of nonlinear optimization methods and theory.
- Concept is fundamentally simple but hazardous to apply if insufficient consideration is given to known nonlinear-optimization risk factors.

Example of parameter-estimation ("system-ID") data processing

- An example will illustrate some of the common pitfalls.
- "Measured" data are first generated synthetically, then a model equation is fit to the data; summary results are plotted.

```
% First, generate some data to use in the identification
m = 0.1; b = 0.2; % true slope and y-intercept
x = rand(100,1);  % 100 random x locations
y = m*x + b + 0.01*randn(size(x)); % noisy "measured" data
figure(1); plot([0 1],[b m+b],x,y,'.','markersize',15); hold on

% Now, regress the data to a line "the hard way" (instead of using known
% optimal ways for fitting a line, assume we need to do nonlinear
% optimization)
cost = @(xx) rms(xx(1)*x+xx(2) - y); % "cost" to minimize
theta = fminsearch(cost,[0 0]); % init mhat=bhat=0; then seek best fit

plot([0 1],[theta(2),theta(1)+theta(2)]); grid on
xlabel('x coordinate); ylabel('y coordinate);
title('Parameter-estimation example');
legend('True line','"Meas" data','Estimated line','location','northwest')
text(0.61,0.192,{'Estimates of line','parameters:'},...
  'verticalalign','bottom');
text(0.61,0.187,sprintf('$$\\hat{m} = %4.4f$$, $$\\hat{b} = %4.4f$$',...
  theta(1),theta(2)),'interpreter','latex');
```

- Some sample results from this process are shown to the right.
- Line fit is good, but noise on the data in this example makes it impossible for perfect fit.
- We also will get imperfect cell-model system-ID results due to measurement noise.

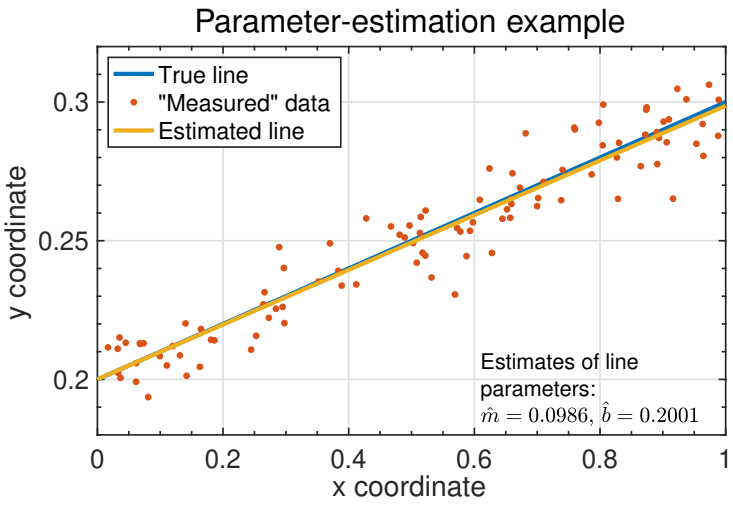

- In this example, the cost is "convex," having a single minima corresponding to the globally optimal solution.
- Generally, this won't be true, and we need to overcome challenges of cost functions having many "local minima".
- No known optimizing method guarantees the globally optimal solution; instead, we will find only locally optimal solutions.

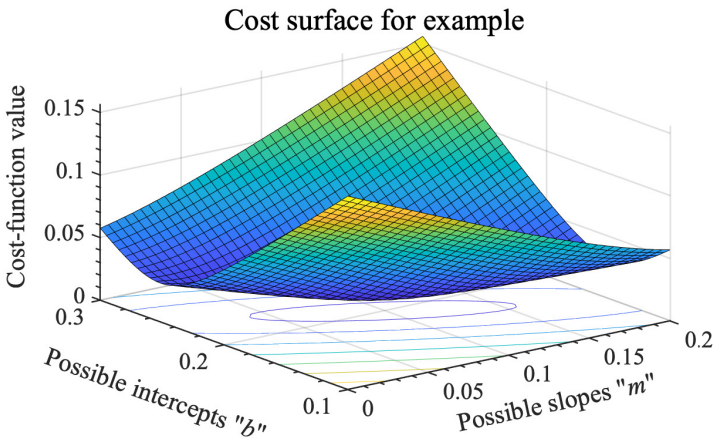

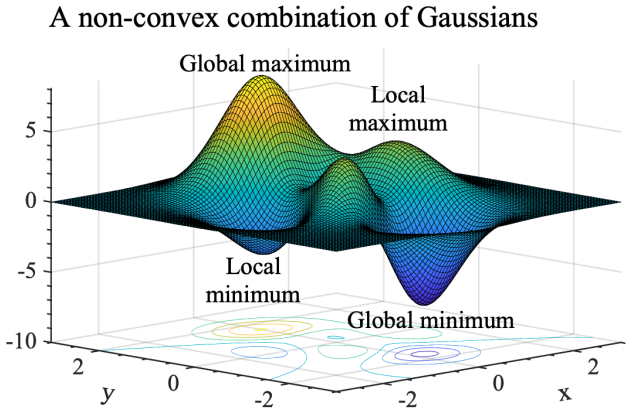

- So, solutions will be somewhat wrong; however, they may be close enough to predict cell electrochemical variables and voltage well.
- Also need to consider that models describe reality imperfectly.
- For example, we might fit a quadratic to the same data.
- The cost is lower but the physical meaning is lost.
- 1D DFN assumes spherical particles, and uniform properties and variables across 3D regions (none are true).

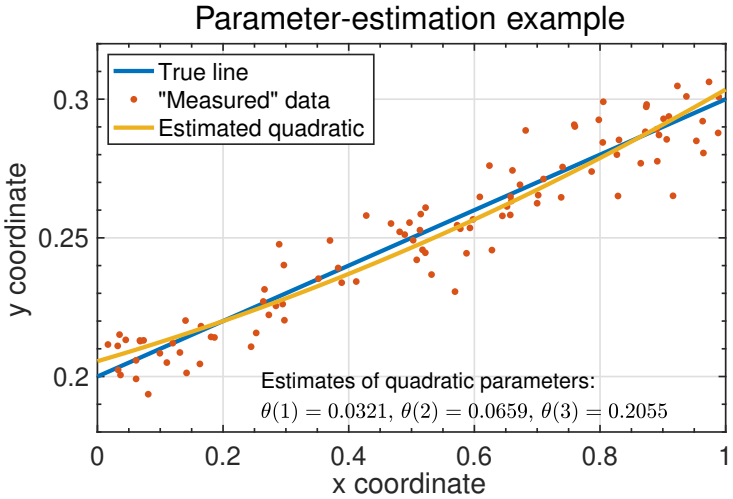

- Since the DFN/LMP model is "wrong," "true" parameters do not exist.

- Practical wisdom from the field of optimization suggests that in order to find a good solution to the optimization, it is helpful:
  - For initial parameter guesses to be close to their true values;
  - To have tight bounds on the range of possible parameter values;
  - To use a good global-optimization algo. to escape poor minima;
  - To weight data samples according to their quality and importance.
- Finally, we must recognize that our measured data will include biases, nonlinear errors, random noises, and even errors that are correlated.
- Parameter-estimation method must carefully calibrate raw test results to clean up measured data as much as possible before optimizations.

A balanced approach

- We now recognize that there are advantages and disadvantages to teardown and nonteardown approaches to estimate parameters.
- Teardown methods excel at measuring dimensions; nonteardown methods are better for estimating effective transport parameters.
- However, notice that the LPM formed from the DFN has eliminated all dimensional values. Maybe cell teardown can be avoided entirely?
- But we will later encounter fundamental obstacles to finding unique OCP functions without performing at least a minimal cell teardown.
- This is a rapidly-developing research topic: for now, I recommend performing teardown to find OCP functions and dimensions.
- I recommend nonteardown methods to estimate all other values: the figure illustrates the nonteardown strategy that I will present.

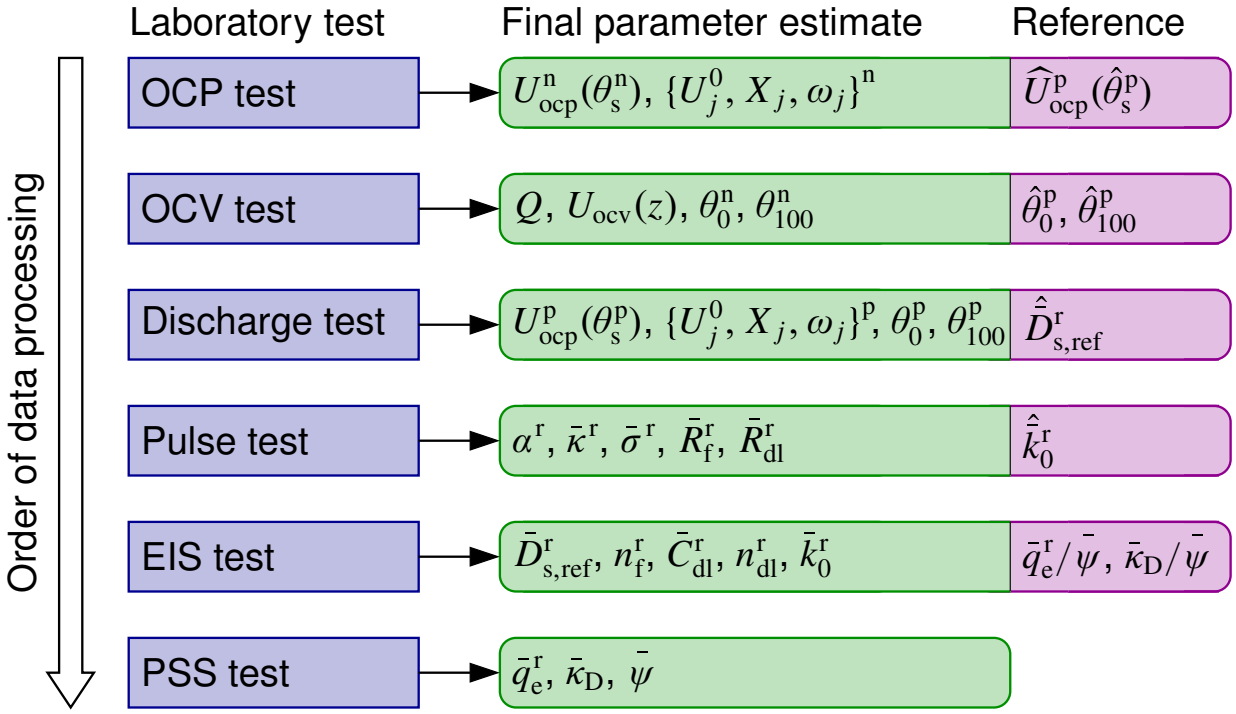

- Six tests collect data to regress to LMP-parameter subsets, reducing dimensionality of individual optimizations: faster and more accurate.
- This improves our chances of finding a good local minimum in the optimization cost function, resulting in good model parameterization.
- The OCP test estimates the negative-electrode OCP function and makes a preliminary estimate of the positive-electrode OCP function.
- OCV test finds capacity, OCV, negative-electrode operating boundaries; makes a preliminary estimate of positive-electrode boundaries.
- Discharge test calibrates positive-electrode OCP and boundaries; makes initial estimate of the solid diffusivities.
- The pulse test determines the values of all parameters used in the charge-conservation and interface-kinetics equations.
- The EIS test estimates all remaining parameter values except $\bar{\psi}$.
- Finally, the pseudo-steady-state (PSS) test estimates $\bar{\psi}$.

3.2: OCP testing and data analysis on a half cell

- Parameter-estimation process begins by finding $U^{\mathrm{r}}_{\mathrm{ocp}}(\theta^{\mathrm{r}}_{\mathrm{s}})$ (OCP vs. $\theta^{\mathrm{r}}_{\mathrm{s}}$) of both electrodes.
- Most accurate and direct approach requires opening the battery cell (teardown).
  - In some cases, it may be possible to avoid teardown; cf. App. 3.c.

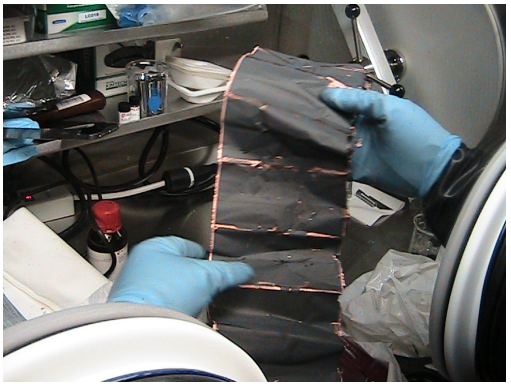

- Cell is opened in a glovebox, electrodes are extracted (negative electrode shown).
- To make a coin cell, a circular punch is used to make an electrode "active material" disc.

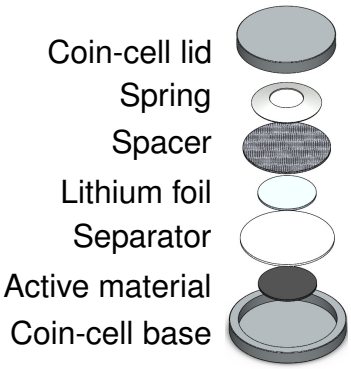

- Disc assembled in coin cell vs. Li metal foil (so can measure electrode OCP vs. $\mathrm{Li/Li^+}$).
- Once electrode and electrolyte sealed in cell, cell can be removed from glovebox.
- Single coin-cell capacity may be too small for reliable cycling using cell-test equipment.
- Wiring several cells in parallel helps by increasing total capacity and also by electrically averaging several samples together for more consistent results.

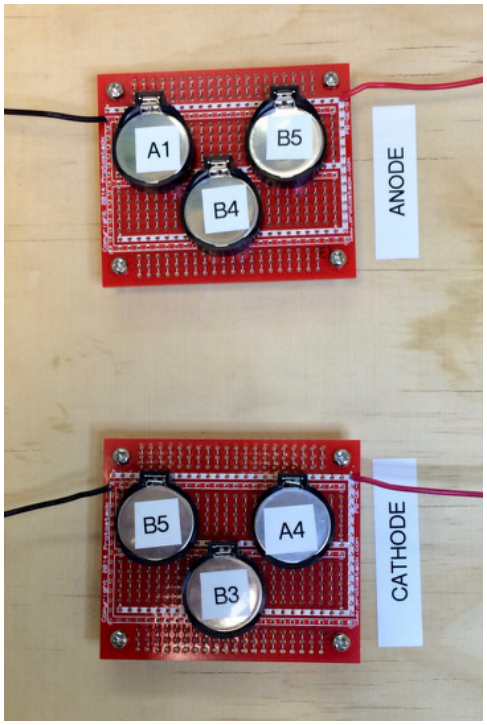

- Electrode OCP "measured" in same way as cell OCV "measured" in ECE5710.
- A brief review follows; cf. App. 3.a for test-procedure details.

Test procedure and data-analysis

- A coin cell is constructed as a single insertion electrode vs. metallic Li and not as two insertion electrodes; so, we refer to it as a half cell.
- Li metal has resting potential of 0 V vs. Li/Li^+, so resting half-cell voltage equals its insertion electrode's OCP at its present θ_s vs. Li/Li^+.
- We use four lab-test scripts, executed sequentially, to collect half-cell voltage across as much of its stoichiometry range as possible.
  - Script #1 (at test temp.): Starting at $U_{ocp} = v_{max}$, determines low-rate const.-current discharge voltage as function of Ah discharged.
  - Script #2 (at 25 °C): Calibrates cell to $U_{ocp} = v_{min}$ by dis/charging.
  - Script #3 (at test temp.): Starting at $U_{ocp} = v_{min}$, determines low-rate constant-current charge voltage as a function of Ah charged.
  - Script #4 (at 25 °C): Calibrates cell to $U_{ocp} = v_{max}$ by dis/charging.
- For every θ_s, OCP is between the discharge and charge voltages.
- Roughly speaking, we average voltages at every θ_s to find OCP.
- Tests run at several temperatures to determine temp.-dependence.

Initial data processing and the "missing-data problem"

- Measured data are processed to create calibrated discharge voltage vs. relative stoichiometry $\tilde{\theta}_s$ and calibrated charge voltage vs. $\tilde{\theta}_s$.[1]

[1] We will discuss the distinction between relative stoichiometry $\tilde{\theta}_s$ and absolute stoichiometry θ_s later in this chapter. The basic problem that we will need to solve is that we do not yet know the absolute level of lithiation $\theta_s = \theta_{min}$ at the beginning of the test or $\theta_s = \theta_{max}$ at the most lithiated point in the test. So, we temporarily define a relative stoichiometry $\tilde{\theta}_s = 0$ at the beginning of the test and $\tilde{\theta}_s = 1$ at the most lithiated point in the test and will later find a relationship to convert between $\tilde{\theta}_s$ and θ_s.

- Here are some lab-test results that show the outcome of the process as described so far for a graphite material and an NMC material.
- Plot insets highlight regions of the calibrated dis/charge curves that illustrate what we call the “missing-data problem.”

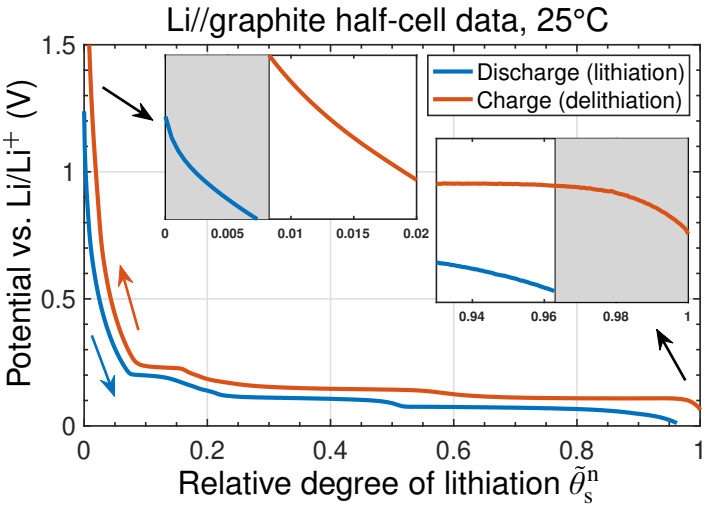

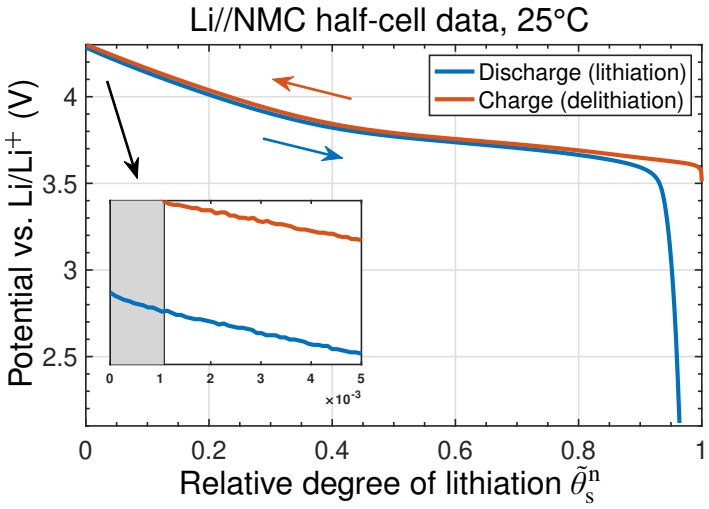

- Since our slow-cycling data are not collected in an equilibrium condition, the measurements contain voltage polarization.
- So, Script #1 never reaches $U_{\text{ocp}} = v_{\min}$ even though measured voltage reaches $v_{\min}$ and Script #3 never reaches $U_{\text{ocp}} = v_{\max}$ even though measured voltage reaches $v_{\max}$.
- The horizontal gaps between the blue and red lines at $v_{\min}$ and $v_{\max}$ is what we refer to as the “missing-data problem.”
- For $\tilde{\theta}_s \approx \{1, 0\}$ we don’t have discharge and charge data, respectively.
- So, we cannot perform a direct average of discharge and charge data to find OCP since we are missing voltage data for some values of $\tilde{\theta}_s$.

The inaccessible-lithium problem

- To understand a second problem, notice that we must select physically achievable values for $v_{\min}$ and $v_{\max}$ for the lab tests.

- Whatever values we choose, the electrode is never fully lithiated even when the half cell is discharged to $v_{\min}$ and is never completely delithiated even when the half cell is charged to $v_{\max}$.
- As illustrated in the figures, there are portions of active materials that are never accessed by the OCP tests since we cannot achieve either high-enough or low-enough voltages in a practical laboratory test.
  - We refer to this as the "inaccessible-lithium problem."

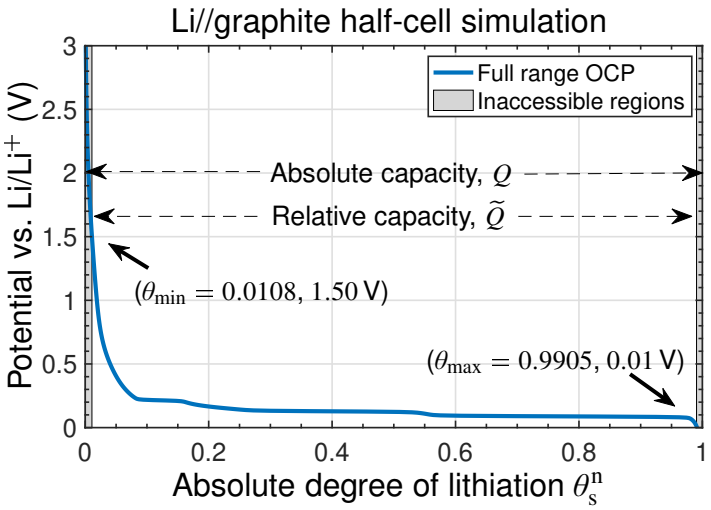

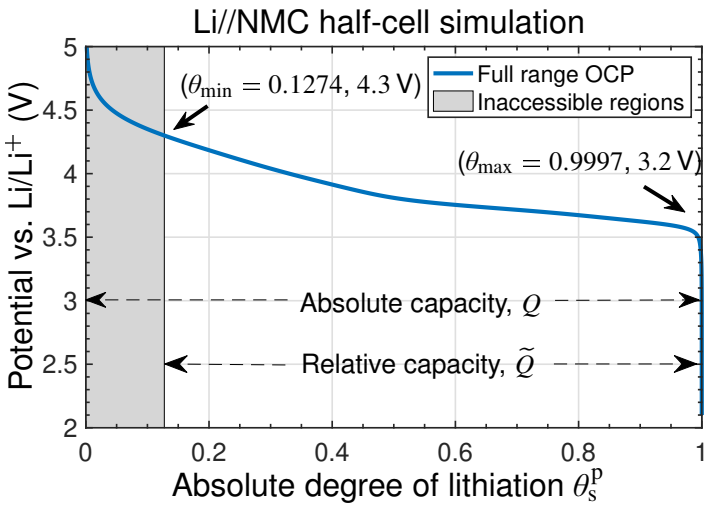

- This is why we make a distinction between $\tilde{\theta}_s$ and θ_s and between relative and absolute capacities $\tilde{Q}$ and Q.
  - If we were somehow able to use the entire range of lithiation and delithiation, we could achieve absolute capacity Q.
  - But, we cannot, and so the quantity confined between cutoff voltages $v_{\min}$ and $v_{\max}$ is then a relative capacity $\tilde{Q}$.
- The lab test measures only $\tilde{Q}$, not Q; so, the stoichiometric values computed from experimental data are also relative values, denoted $\tilde{\theta}_s$.
- The corresponding voltage//SOC relationships for the "absolute" and "relative" cases are written as $U_{\text{ocp}}(\theta_s)$ and $\tilde{U}_{\text{ocp}}(\tilde{\theta}_s)$, respectively.

- Recognizing this, finding OCP involves two steps:
  1. Estimate a relative $\widetilde{U}_{\rm ocp}(\tilde{\theta}_{\rm s})$ from the OCP-test data, then
  2. Estimate absolute $U_{\rm ocp}(\theta_{\rm s})$ by fitting $\widetilde{U}_{\rm ocp}(\tilde{\theta}_{\rm s})$ with an MSMR model.
- Skipping details for now, some form of averaging is performed between the dis/charge curves.
- Missing data are approximated by extrapolating voltage to $\tilde{\theta}_{\rm s} = 1$ and to $\tilde{\theta}_{\rm s} = 0$ before averaging.

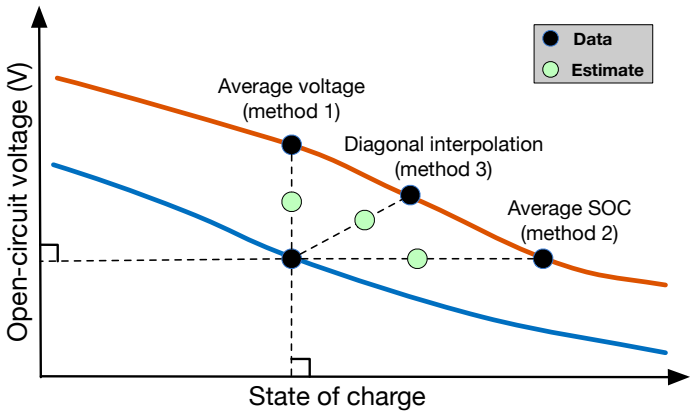

- The figures below display the simulation voltage outputs at 25 °C ("C/30 data"), along with the relative-stoichiometry OCP estimates:

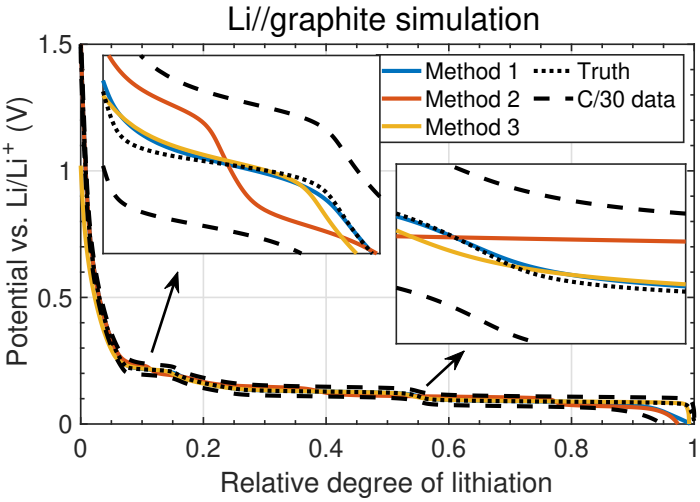

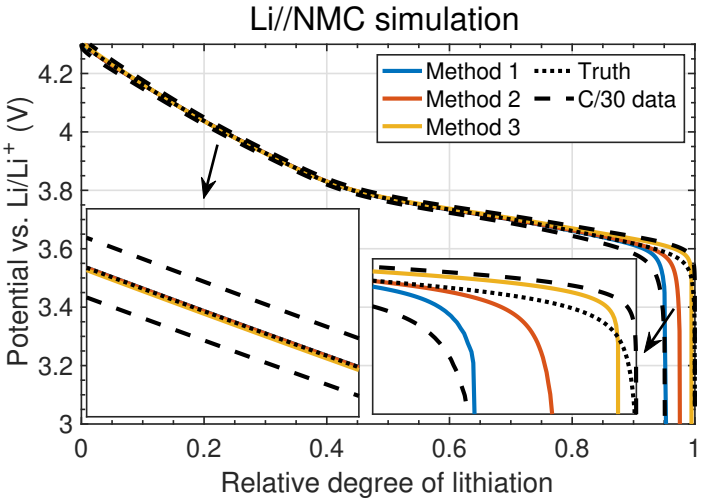

Temperature-dependence

- When applied to physical cells, we find that the MSMR values U_j, X_j and ω_j appear to be constant versus temperature.
- If this is true in general, then all temperature dependence is built into the $f = F/(RT)$ term in the model.
- This accelerates testing since we can get away with testing only a few temperatures to create an OCP model.

3.3: Converting dis/charge data to OCP estimate

- We now address the missing-data and inaccessible-lithium problems, estimating electrode OCP from available dis/charge data.
- For most methods presented, this involves two steps:
  1. Estimate a relative $\widetilde{U}_{\rm ocp}(\tilde{\theta}_{\rm s})$ from the OCP-test data, then
  2. Estimate absolute $U_{\rm ocp}(\theta_{\rm s})$ by fitting $\widetilde{U}_{\rm ocp}(\tilde{\theta}_{\rm s})$ with an MSMR model.
- We present four techniques: Methods 1–3 deal only with step 1, after which we need to implement step 2; Method 4 handles both steps.

Voltage averaging (method 1)

- Taking the average potential between the discharge and charge branches is the most commonly used method in the literature.
- The method assumes that deviations between true OCP and dis/charge curves have equal magnitude.
- OCP is approximated by averaging the two voltage curves at the same $\tilde{\theta}_{\rm s}$.

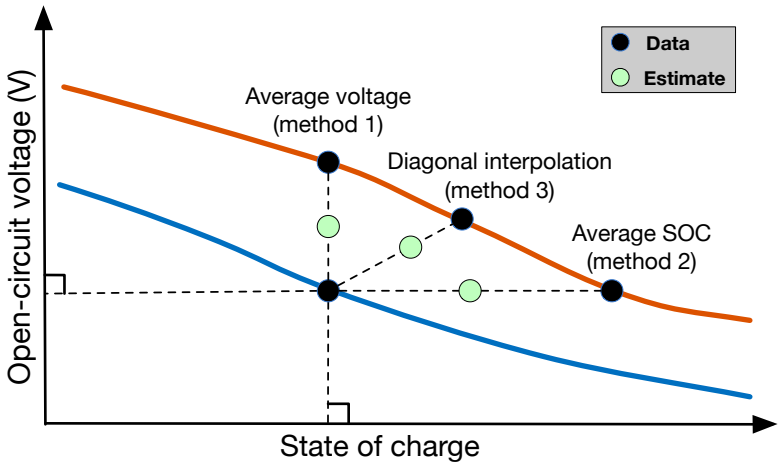

- Missing-data are approximated by linearly extrapolating lithiation voltage to $\tilde{\theta}_{\rm s} = 1$ and delithiation voltage to $\tilde{\theta}_{\rm s} = 0$ before averaging.
- The direct output of Method 1 is an estimate of OCP versus relative stoichiometry, which we denote as $\widehat{\widetilde{U}}_{\rm ocp}(\tilde{\theta}_{\rm s})$.
- An additional "step 2" must be taken later to convert this to the desired estimate versus absolute stoichiometry $\widehat{U}_{\rm ocp}(\theta_{\rm s})$.

SOC averaging (method 2)

- It is also possible to average $\tilde{\theta}_\mathrm{s}$ ("electrode SOC") of the lithiation and delithiation curves at points where their voltages are the same.
- Method 2 assumes that the deviation between true $\tilde{\theta}_\mathrm{s}$ and its experimental values for the dis/charge curves is equal in magnitude.
- Missing-data regions are linearly extrapolated to v_min and v_max.
- Again, the direct output of Method 2 is $\widehat{\widetilde{U}}_\mathrm{ocp}(\tilde{\theta}_\mathrm{s})$. "Step 2" must be taken later to convert this to the desired $\widehat{U}_\mathrm{ocp}(\theta_\mathrm{s})$.
- SOC averaging does not work well for materials having wide voltage plateaus (strong peaks in differential capacity, e.g., Li//graphite).

Diagonal interpolation (method 3)

- Method 3 seeks to interpolate the OCP in a diagonal sense.
  - For example, shift the discharge voltage curve "right and up" and the charge voltage "left and down" before averaging.
  - The shifts are determined by locations of peak in the cross-correlations between the dis/charge differential-capacity curves.[2]
- To visualize, plot dis/charge $\mathrm{d}\,\tilde{\theta}_\mathrm{s}/\mathrm{d}\,U_\mathrm{ocp}$ vs. both voltage and $\tilde{\theta}_\mathrm{s}$; also plot cross correlation between the dis/charge differential capacities.
- Location of peak in cross correlation is equal to shift of discharge curve that gives best agreement with respect to the charge curve.
- ΔU is half the voltage shift and $\Delta\tilde{\theta}_\mathrm{s}$ is half the SOC shift.
  - In following example, $\Delta U = 0.019$ and $\Delta\tilde{\theta}_\mathrm{s} = 0.0085$.

[2] cf. App. 3.b for a practical way to compute differential capacity from noisy data.

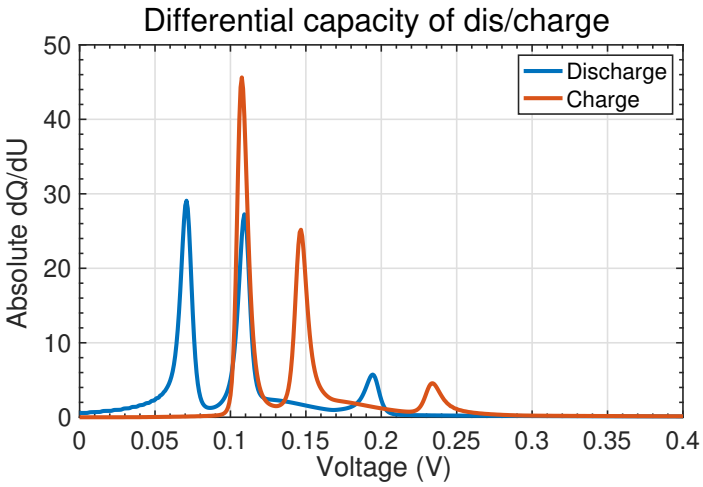

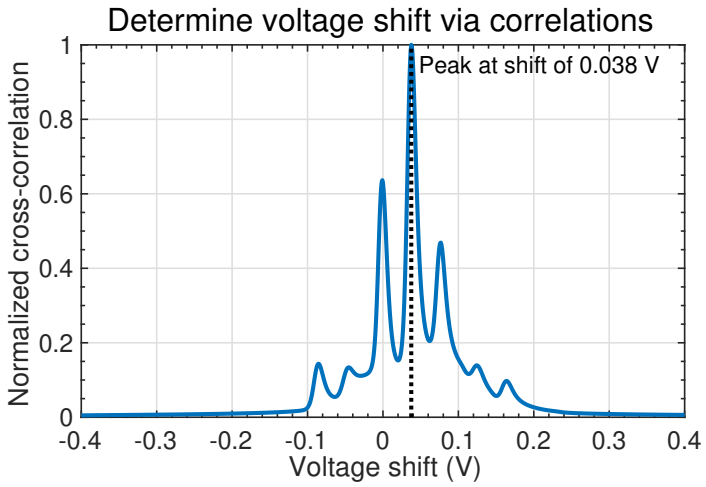

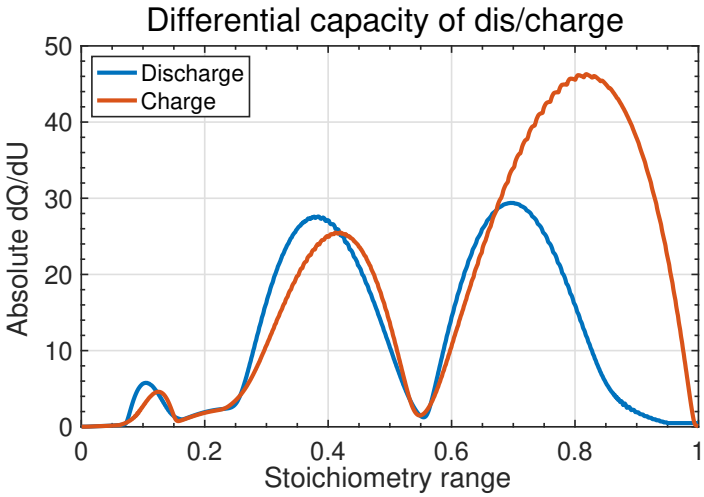

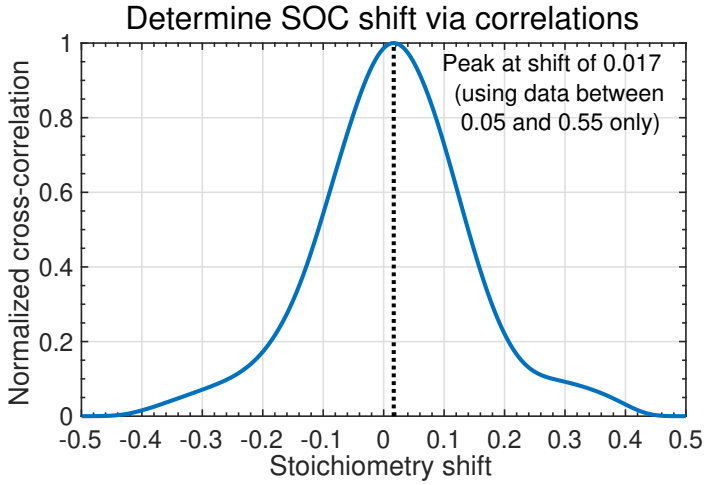

- We have a choice in how to use ΔU and $\Delta\tilde{\theta}_\mathrm{s}$ to make OCP estimate.
- We can shift discharge curve (producing $\widehat{\widetilde{U}}^{(\mathrm{d})}_{\mathrm{ocp}}(\tilde{\theta}_\mathrm{s})$), or charge curve (producing $\widehat{\widetilde{U}}^{(\mathrm{c})}_{\mathrm{ocp}}(\tilde{\theta}_\mathrm{s})$), or average both (producing $\widehat{\widetilde{U}}^{(\mathrm{a})}_{\mathrm{ocp}}(\tilde{\theta}_\mathrm{s})$):

$$\widehat{\widetilde{U}}^{(\mathrm{d})}_{\mathrm{ocp}}(\tilde{\theta}_\mathrm{s}) = U_{\mathrm{dis}}\left(\tilde{\theta}_\mathrm{s}^{\mathrm{dis}} - \Delta\tilde{\theta}_\mathrm{s}\right) + \Delta U; \quad \widehat{\widetilde{U}}^{(\mathrm{c})}_{\mathrm{ocp}}(\tilde{\theta}_\mathrm{s}) = U_{\mathrm{chg}}\left(\tilde{\theta}_\mathrm{s}^{\mathrm{chg}} + \Delta\tilde{\theta}_\mathrm{s}\right) - \Delta U;$$

$$\widehat{\widetilde{U}}^{(\mathrm{a})}_{\mathrm{ocp}}(\tilde{\theta}_\mathrm{s}) = \left(\widehat{\widetilde{U}}^{(\mathrm{d})}_{\mathrm{ocp}}(\tilde{\theta}_\mathrm{s}) + \widehat{\widetilde{U}}^{(\mathrm{c})}_{\mathrm{ocp}}(\tilde{\theta}_\mathrm{s})\right)/2.$$

- Can plot all three and choose the most reasonable-looking candidate. Without any other guidance, we recommend $\widehat{\widetilde{U}}^{(\mathrm{a})}_{\mathrm{ocp}}(\tilde{\theta}_\mathrm{s})$.
- The direct output of Method 3 is $\widehat{\widetilde{U}}_{\mathrm{ocp}}(\tilde{\theta}_\mathrm{s})$. "Step 2" (described next) must be taken later to convert this to the desired $\widehat{U}_{\mathrm{ocp}}(\theta_\mathrm{s})$.

Converting relative to absolute relationships for Methods 1–3

- Methods 1–3 address the "missing-data problem" by averaging the extrapolated dis/charge curves in different ways.
- But, none of these approaches determine OCP as a function of absolute stoichiometry to overcome "inaccessible-lithium problem."
- *An attempt* to do so extrapolates the estimates $\widehat{\widetilde{U}}_{\mathrm{ocp}}(\tilde{\theta}_{\mathrm{s}})$ made by Methods 1–3 beyond measured data; then, finds $\theta_{\min}$ and $\theta_{\max}$ in:

$$\theta_{\mathrm{s}} = \theta_{\min} + \tilde{\theta}_{\mathrm{s}}(\theta_{\max} - \theta_{\min}).$$

- We rely on the MSMR model, using nonlinear optimization to determine $\{\theta_{\min}, \theta_{\max}, U_j, X_j, \omega_j\}$ such that a MSMR model $\widehat{U}_{\mathrm{ocp}}(\theta_{\mathrm{s}})$ agrees with $\widehat{\widetilde{U}}_{\mathrm{ocp}}(\tilde{\theta}_{\mathrm{s}})$ as closely as possible.
- "Inaccessible-lithium problem" is addressed by MSMR model's ability to extrapolate in a physically reasonable way beyond measured data.
- *Can do so well as long as $\widehat{U}_{\mathrm{ocp}}(\tilde{\theta}_{\mathrm{s}})$ has a wide enough voltage range to include measurements from every gallery that physically exists.*
- Inside the optimization, $\widehat{U}^{\mathrm{data}}_{\mathrm{ocp}}(\theta_{\mathrm{s}})$ is computed from $\widehat{\widetilde{U}}_{\mathrm{ocp}}(\tilde{\theta}_{\mathrm{s}})$ by finding θ_{s} for every $\tilde{\theta}_{\mathrm{s}}$ for every data point using $\theta_{\min}$ and $\theta_{\max}$.
- U_j, X_j, and ω_j are used to create an MSMR estimate of $\widehat{U}^{\mathrm{mdl}}_{\mathrm{ocp}}(\theta_{\mathrm{s}})$.
- A nonlinear-optimization routine adjusts $\{\theta_{\min}, \theta_{\max}, U_j, X_j, \omega_j\}$ until $\widehat{U}^{\mathrm{mdl}}_{\mathrm{ocp}}(\theta_{\mathrm{s}})$ agrees with $\widehat{U}^{\mathrm{data}}_{\mathrm{ocp}}(\theta_{\mathrm{s}})$ as closely as possible. (Number of galleries J is a user-defined parameter, not optimized automatically.)
- Specifically, we seek parameter values p^*:

$$p^* = \arg\min_{p} \sum_{n=1}^{N} \left[\theta_{\mathrm{s},n}(\widehat{U}^{\mathrm{data}}_{\mathrm{ocp}}) - \theta_{\mathrm{s},n}(\widehat{U}^{\mathrm{mdl}}_{\mathrm{ocp}})\right]^2 + w \left[\frac{\mathrm{d}\theta_{\mathrm{s}}}{\widehat{U}^{\mathrm{data}}_{\mathrm{ocp}}(\theta_{\mathrm{s},n})} - \frac{\mathrm{d}\theta_{\mathrm{s}}}{\widehat{U}^{\mathrm{mdl}}_{\mathrm{ocp}}(\theta_{\mathrm{s},n})}\right]^2,$$

where ω is a weighting factor to blend modeling errors corresponding to raw OCP estimates and differential-capacity estimates.

- We use MATLAB's `fmincon.m` function to perform the regression.
- The output of this procedure is an MSMR model that fits measured data as closely as possible using absolute stoichiometries.
  - Uses Methods 1–3 to address "missing-data problem" and MSMR model fit to attempt to overcome "inaccessible-lithium problem."

Direct MSMR model fit (method 4)

- Final approach fits independent MSMR models directly to dis/charge curves; $\widehat{U}_{\text{ocp}}(\theta_{\text{s}})$ is then estimated by averaging parameters from both models (i.e., $\{\theta_{\min}, \theta_{\max}, U_j, X_j, \omega_j\}_{\text{dis}}$ and $\{\theta_{\min}, \theta_{\max}, U_j, X_j, \omega_j\}_{\text{chg}}$).
  - We assume that the true OCP MSMR parameters have equal distance to the discharge and charge MSMR-model parameters.
- Example fits to laboratory data are depicted below.
  - The data can be closely fit by the model, especially at warm temperatures, where voltage polarization is relatively smaller.

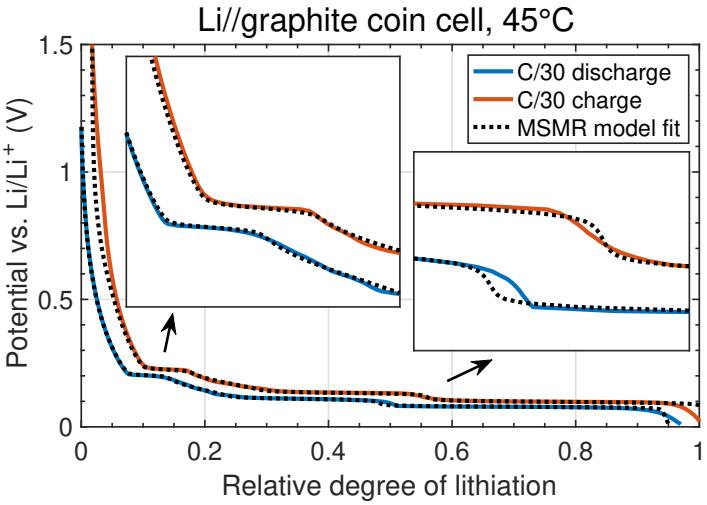

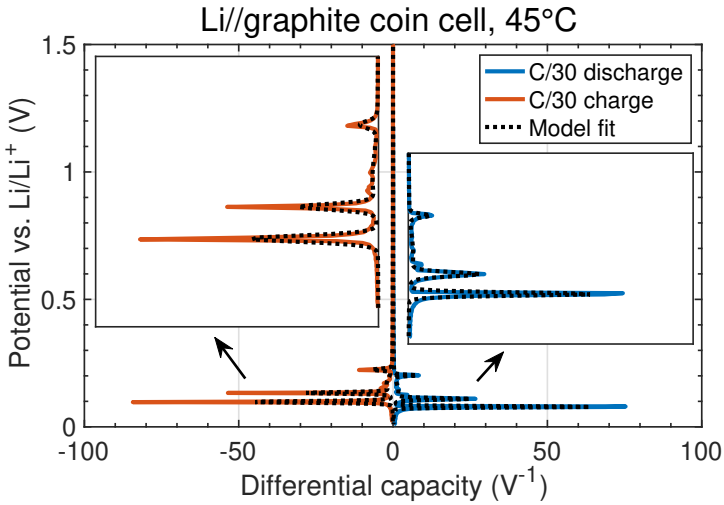

3.4: Examples of estimating OCP

Validation of methods using simulation

- It is impossible to judge accuracy of physical half-cell OCP estimates since there is strictly no known truth against which to compare.
- The only fact we can verify at this point is that $\widehat{\widetilde{U}}_{\mathrm{ocp}}(\tilde{\theta}_{\mathrm{s}})$ estimates should reside between the discharge and charge data curves.
- We can, however, validate the methods in simulation: We simulate dis/charge curves, then apply the methods to dis/charge voltages and compare estimated $\widehat{U}_{\mathrm{ocp}}(\theta_{\mathrm{s}})$ to true $U_{\mathrm{ocp}}(\theta_{\mathrm{s}})$ used in the simulations.
- In this section, a physics-based half-cell model was implemented in COMSOL and output data were processed with MATLAB scripts.
  - A Li//graphite half cell was lithiated from $\theta_{\mathrm{s}} = 0.0108$ to $v_{\min} = 0.01\,\mathrm{V}$, and delithiated from $\theta_{\mathrm{s}} = 0.9905$ to $v_{\max} = 1.5\,\mathrm{V}$.
  - A Li//NMC half cell was lithiated from $\theta_{\mathrm{s}} = 0.1274$ to $v_{\min} = 3.0\,\mathrm{V}$, and delithiated from $\theta_{\mathrm{s}} = 0.9992$ to $v_{\max} = 4.3\,\mathrm{V}$.
- The figures below display the simulation voltage outputs at 25 °C (“C/30 data”), along with the relative-stoichiometry OCP estimates:

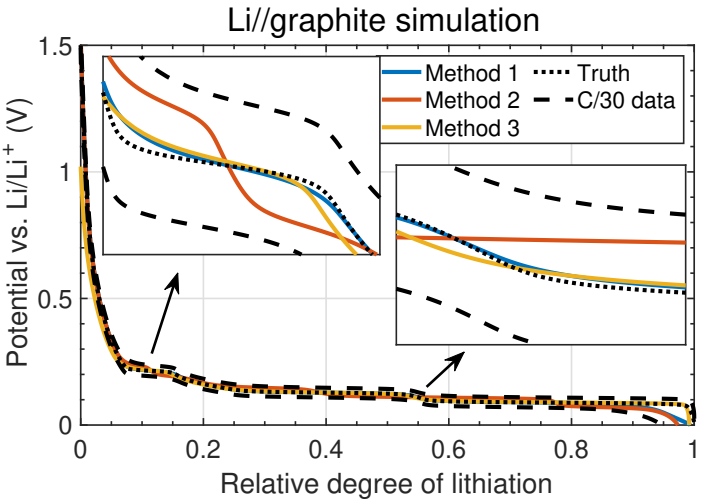

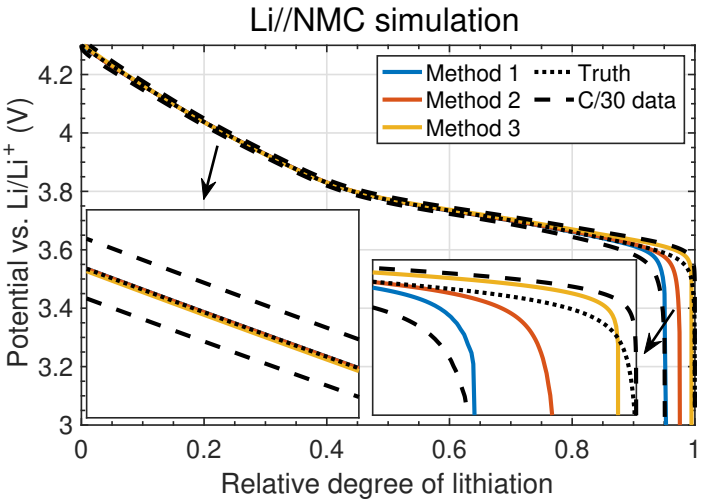

- The figures below show the conversion to absolute-stoichiometry OCP estimates, along with root-mean-squared error (RMSE):

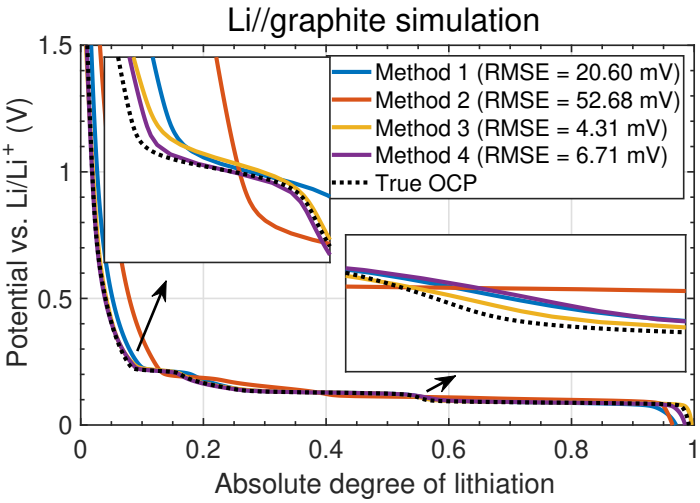

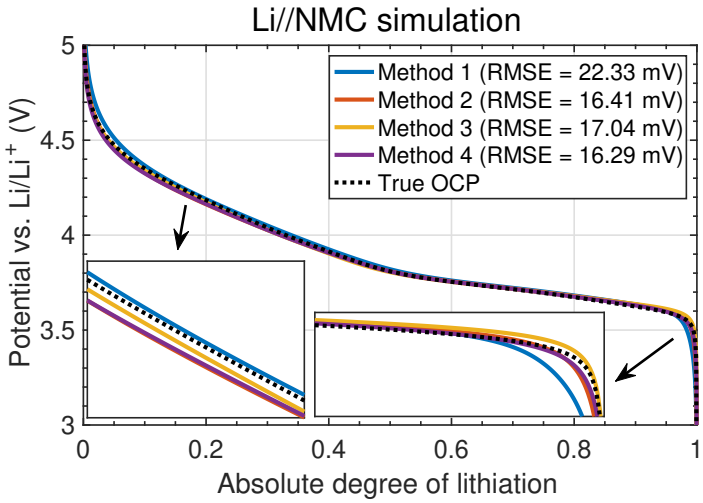

- RMSE was calculated over the range of $0.07 < \theta_s^n < 0.99$ (Li//graphite) and $0.1 < \theta_s^p < 1$ (Li//NMC), which should extend beyond the typical operating ranges used in commercial cells.
- Method 3 works well for the Li//graphite coin cell, which exhibits wide voltage plateaus; Method 4 also produces quite good results.
- Method 2 produces the best results for the Li//NMC coin cell, and Methods 3 and 4 also produce quite good results.
- We hesitate to recommend Method 2 in general as it does not work well for materials having wide, flat voltage plateaus (e.g., Li//graphite).
- Both Methods 1 and 2 tend to break down in high-curvature regions of OCP, especially at very high and very low levels of lithiation; while they are simple to implement, they do not predict OCV accurately when there is a significant level of “missing-data”.
- Methods 3 and 4 are the most accurate, but also the slowest. But, even Method 4 (the slowest) executes within about 3 s in MATLAB, which is not excessive for a one-time data-processing method.

- The figures below show the residuals (errors) of each estimate.

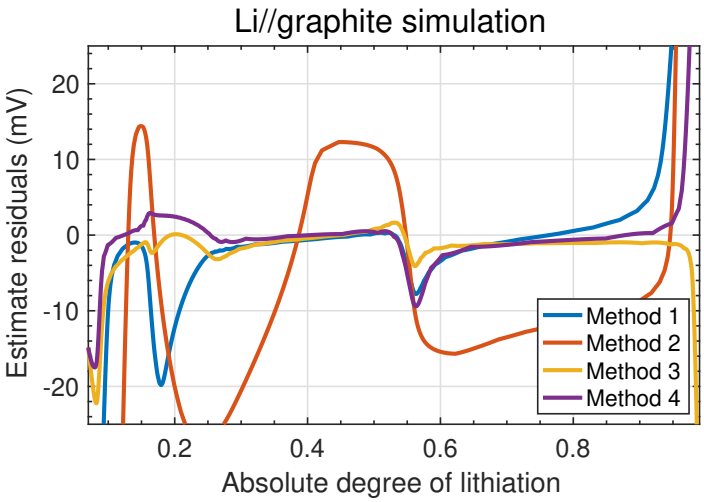

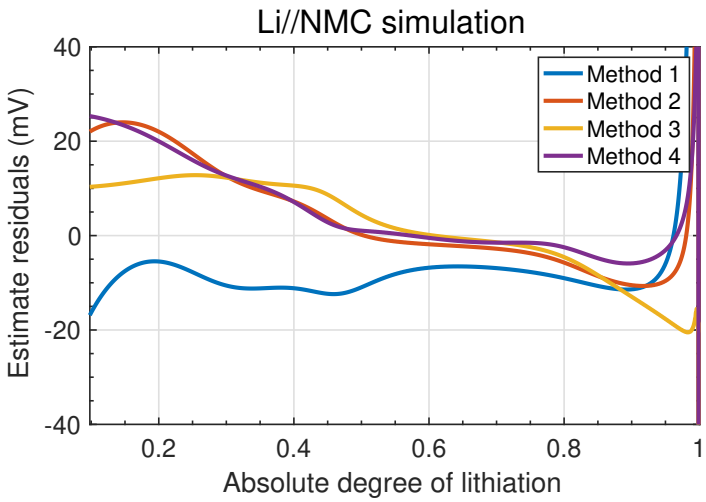

Application of methods to physical half cells

- We applied the four methods to data collected from physical coin cells where the test temperature was 25 °C.
  - Li//graphite was cycled between $v_{\min} = 0.01$ V and $v_{\max} = 1.5$ V and Li//NMC was cycled between $v_{\min} = 2.1$ V and 4.3 V.
- We cannot validate "correctness" beyond noticing whether OCP estimates lie between the discharge and charge curves.
- Figures present the results for physical Li//graphite coin cell:

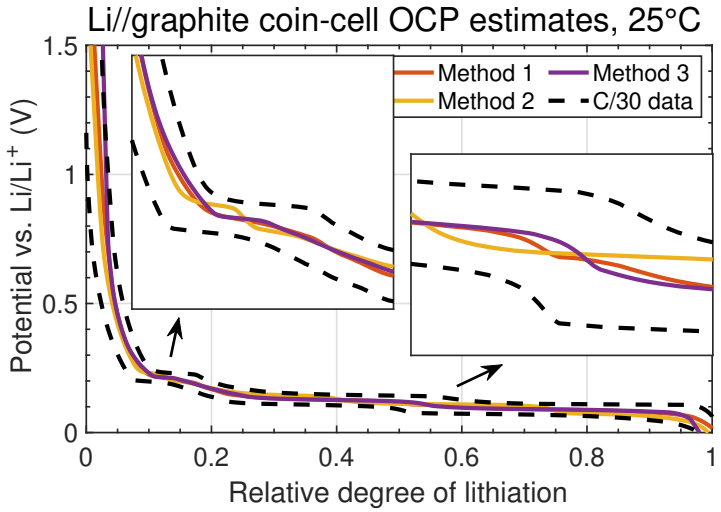

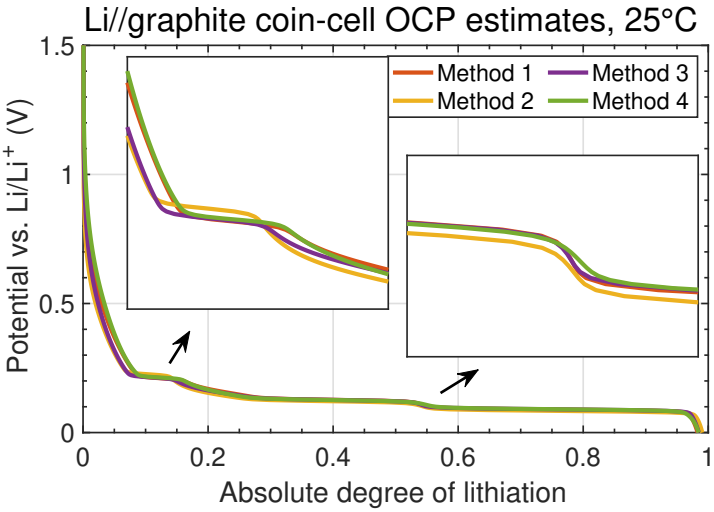

- Next figures present the results for physical Li//NMC coin cell:

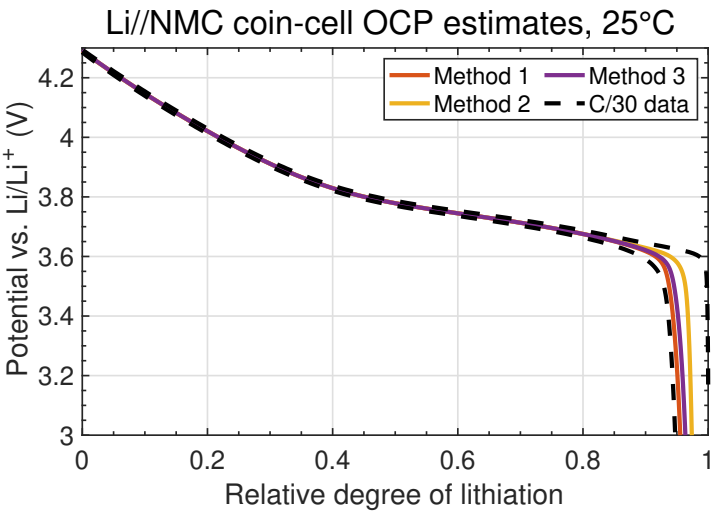

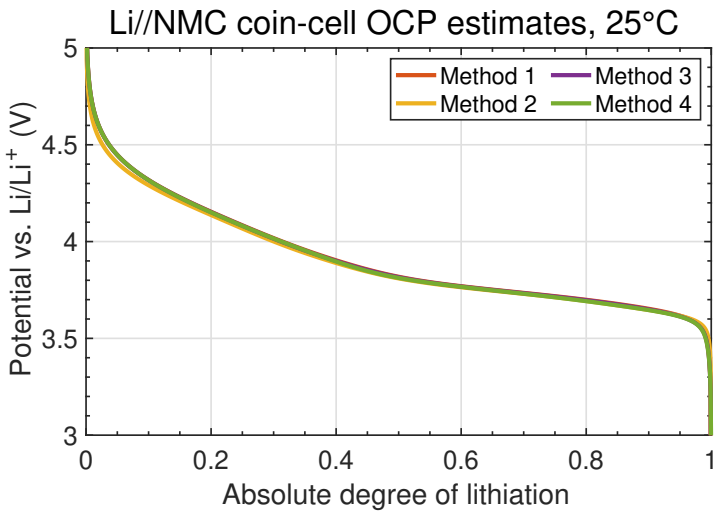

- The missing-data problem is more prominent at low levels of lithiation in the Li//graphite coin cell than it was in the simulations; in all other respects, simulation and lab results appear similar.
- We find less variation in the Method 4 results versus temperature than those produced by Method 3, so we believe it to be the better method.
- We also note that the step-1 results for Method 2 (and to a lesser extent for Method 1) are clearly biased, as shown in the zoom plots, but that fitting the MSMR model to these biased results in step 2 greatly improves the quality and reasonableness of the final OCP model produced by these methods.

3.5: OCV testing to find electrode operating windows

- We can find full-cell OCV vs. SOC using the same testing and data-processing methods used to find electrode OCP vs. stoichiometry.
- We use the OCV function to estimate electrode operating boundaries.
- That is, what are the values of θ_0^{n}, $\theta_{100}^{\mathrm{n}}$, θ_0^{p}, $\theta_{100}^{\mathrm{p}}$ between which the electrodes cycle as the cell is cycled between 0 % and 100 % SOC?
- We know that cell OCV equals positive-electrode OCP minus negative-electrode OCP:

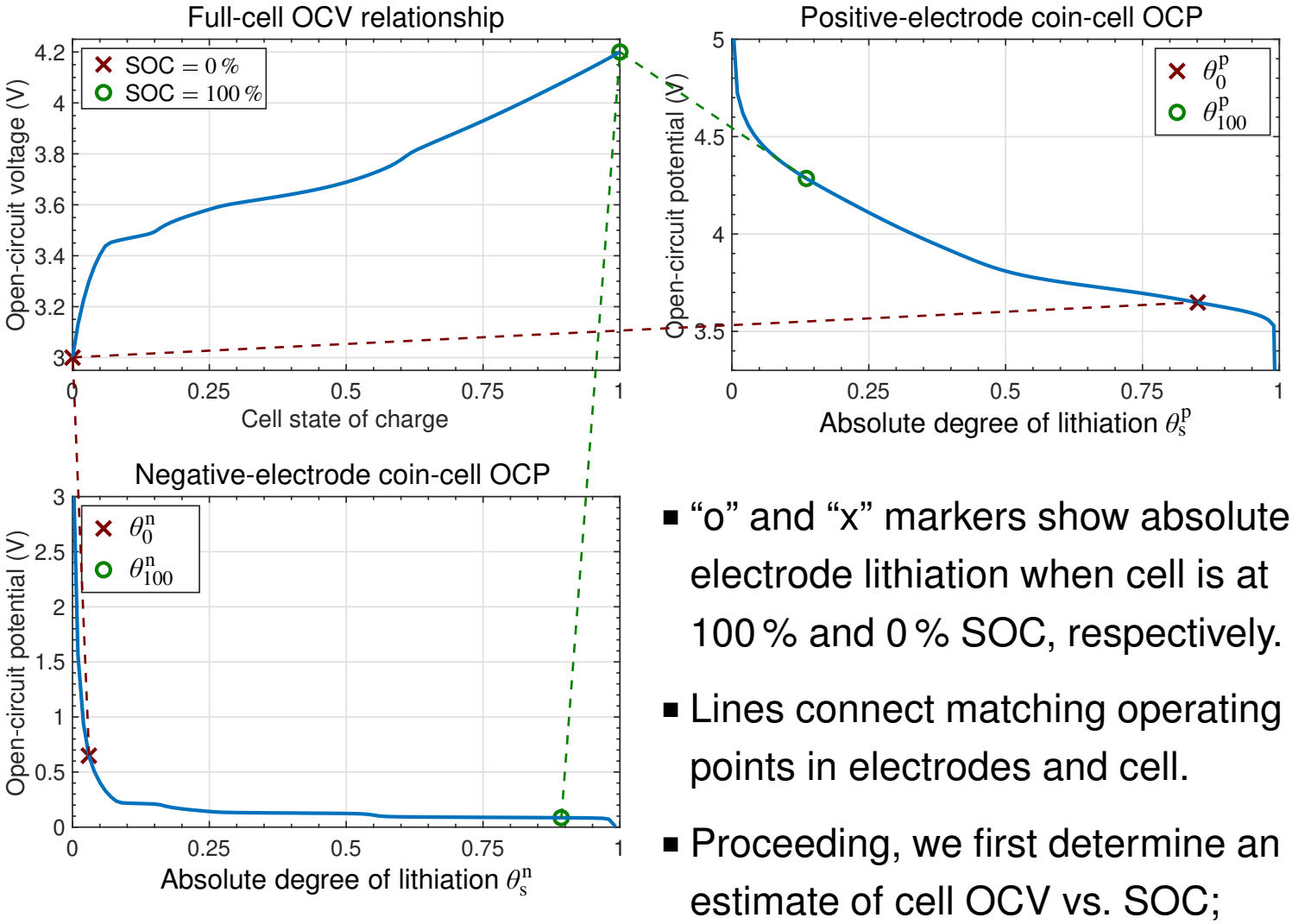

- "o" and "x" markers show absolute electrode lithiation when cell is at 100 % and 0 % SOC, respectively.
- Lines connect matching operating points in electrodes and cell.
- Proceeding, we first determine an estimate of cell OCV vs. SOC;
- Then, optimize estimates of θ_0^{n}, $\theta_{100}^{\mathrm{n}}$, θ_0^{p}, $\theta_{100}^{\mathrm{p}}$ boundaries to get best match between electrode OCP regions and cell OCV.

Step 1: Determining cell OCV versus SOC

- To find the OCV relationship, we use exactly the same procedure (at a cell level) as we used to find electrode OCP (at a half-cell level).
- We need to perform the lab test at 25 °C only since all temperature dependence is included in the OCP MSMR models; we simply need to correlate 25 °C cell OCV with 25 °C electrode OCPs.
- We can use the same four dis/charge voltage-processing methods to convert cell dis/charge data to an OCV vs. SOC estimate.
- We can also somewhat refine the final OCV model found this way:
  - We know $U_{\rm ocv}(0) = v_{\rm min}^{\rm cell}$ and $U_{\rm ocv}(1) = v_{\rm max}^{\rm cell}$ at ref. temperature.
  - However, after employing one of the four OCV-estimation methods, the resulting relationship will not meet these constraints exactly.
  - We can choose to perform additional steps to enforce these limits.
- A complete OCV-estimation process then involves the following steps:
  1. **Initial estimation**: One of the four OCV-estimation methods is used to provide an initial estimate $\widehat{U}_{\rm ocv}(\hat{z})$ of true $U_{\rm ocv}(z)$.
  2. **Extrapolation**: We linearly extrapolate $\widehat{U}_{\rm ocv}(\hat{z})$ over a "standard" voltage vector $U_{\rm std}$, assuring that $\widehat{U}_{\rm ocv}(\hat{z})$ spans $v_{\rm min}^{\rm cell}$ to $v_{\rm max}^{\rm cell}$.
  3. **Shift**: We shift the curve horizontally (adding a constant Δz to $\hat{z}$) to enforce $U_{\rm ocv} = v_{\rm min}^{\rm cell}$ at $z = 0\,\%$.
  4. **Stretch**: We stretch the curve horizontally (multiplying $\hat{z}$ by a constant k) to enforce $U_{\rm ocv} = v_{\rm max}^{\rm cell}$ at $z = 100\,\%$.
- This can be summarized by stating that we replace $\hat{z}$ with $k(\hat{z} + \Delta z)$.
- Process (using ECE5710 R_0 blending) is illustrated below:

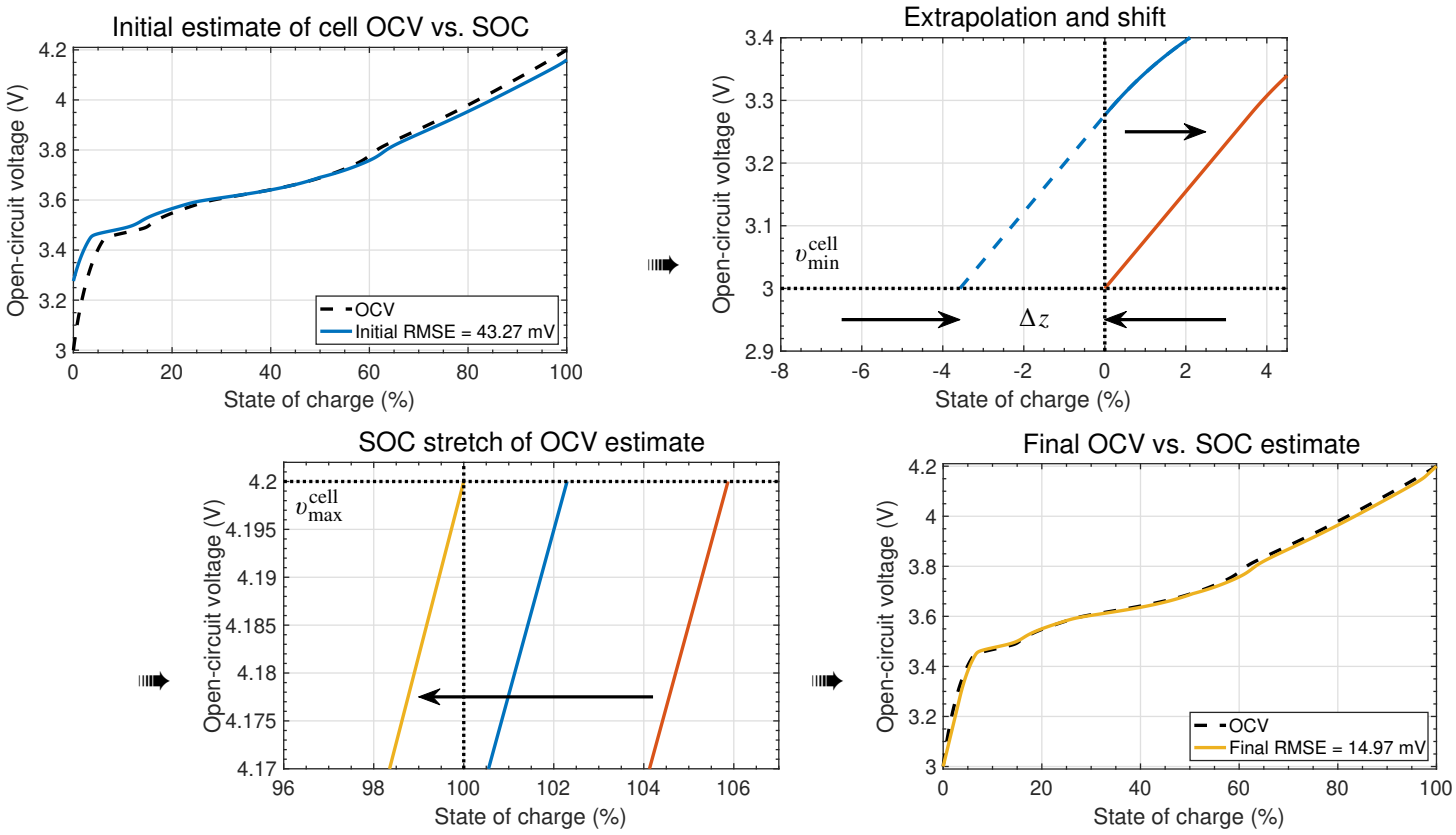

Example of estimating OCV

- Example simulation OCV fit and commercial-cell fits are shown below:

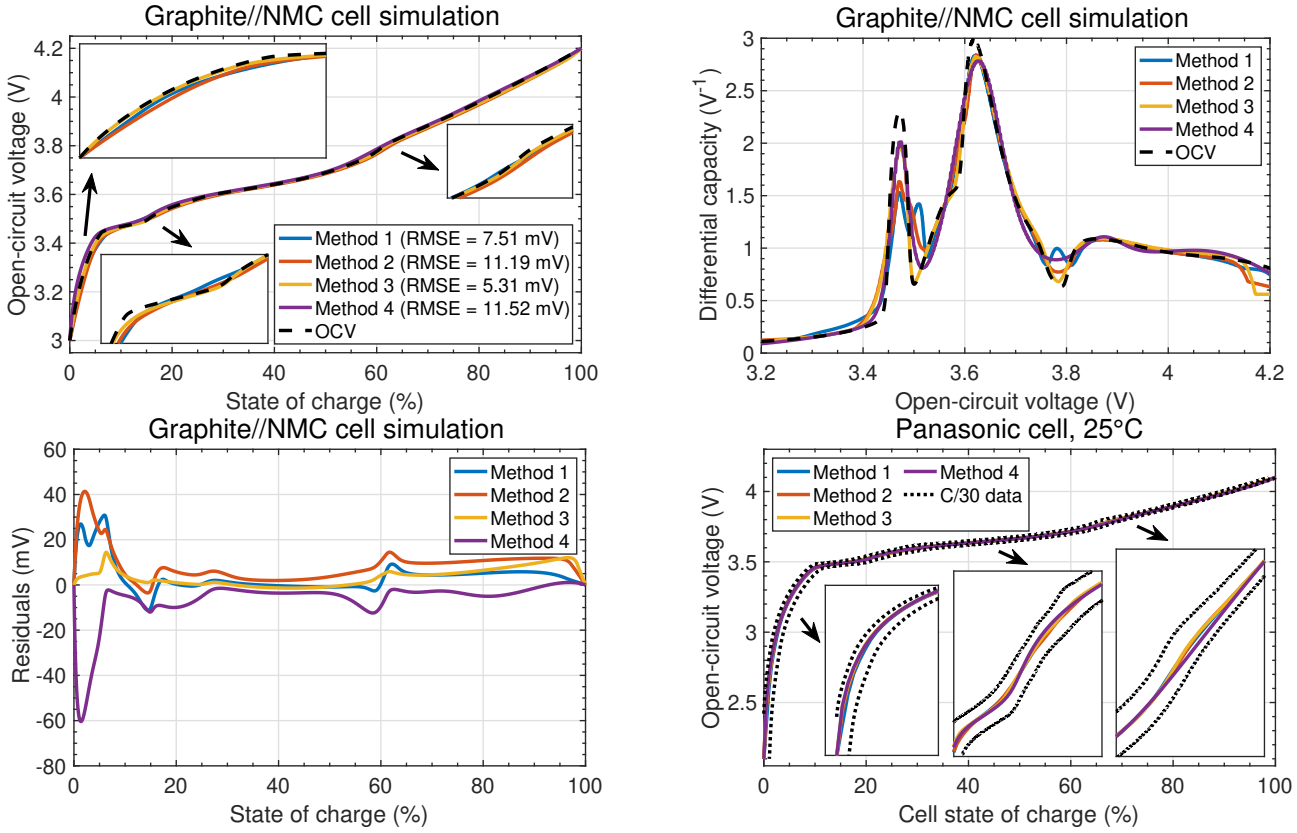

Step 2: Finding electrode operating windows

- Now, knowing cell-level OCV vs. SOC, we seek to estimate electrode operating boundaries $\{\theta_0^{\rm n}, \theta_{100}^{\rm n}, \theta_0^{\rm p}, \theta_{100}^{\rm p}\}$ that produce the best match between cell OCV $\widehat{U}_{\rm ocv}^{\rm cell}(z_k)$ and its electrode OCP functions $\widehat{U}_{\rm ocp}^{\rm r}(\theta_{\rm s}^{\rm r})$.
- Boundaries can be estimated by minimizing the cost function:

$$J = \sum_{k=1}^{N}\left[\left(\widehat{U}_{\rm ocv}^{\rm cell}(z_k) - \widehat{U}_{\rm ocv}^{\rm ocp}(z_k)\right)^2 + w\left(\frac{{\rm d}z}{{\rm d}\widehat{U}_{\rm ocv}^{\rm cell}(z_k)} - \frac{{\rm d}z}{{\rm d}\widehat{U}_{\rm ocv}^{\rm ocp}(z_k)}\right)^2\right],$$

  where

$$\widehat{U}_{\rm ocv}^{\rm ocp}(z) = \widehat{U}_{\rm ocp}^{\rm p}\left(\hat{\theta}_{\rm s}^{\rm p}(z)\right) - \widehat{U}_{\rm ocp}^{\rm n}\left(\hat{\theta}_{\rm s}^{\rm n}(z)\right)$$

$$\hat{\theta}_{\rm s}^{\rm r}(z) = \hat{\theta}_0^{\rm r} + z\left(\hat{\theta}_{100}^{\rm r} - \hat{\theta}_0^{\rm r}\right),$$

  and also

$$\frac{{\rm d}z}{{\rm d}\widehat{U}_{\rm ocv}^{\rm ocp}(z)} = \frac{1}{(\hat{\theta}_{100}^{\rm p} - \hat{\theta}_0^{\rm p})\frac{{\rm d}\widehat{U}_{\rm ocp}^{\rm p}(\hat{\theta}_{\rm s}^{\rm p})}{{\rm d}\hat{\theta}_{\rm s}^{\rm p}} - (\hat{\theta}_{100}^{\rm n} - \hat{\theta}_0^{\rm n})\frac{{\rm d}\widehat{U}_{\rm ocp}^{\rm n}(\hat{\theta}_{\rm s}^{\rm n})}{{\rm d}\hat{\theta}_{\rm s}^{\rm n}}}.$$

- During optimization, we can use the domain knowledge that $0 \le \theta_0^{\rm n} < \theta_{100}^{\rm n} \le 1$ and $0 \le \theta_{100}^{\rm p} < \theta_0^{\rm p} \le 1$ to constrain the solution.

Estimating operating boundaries using laboratory data

- We now seek estimates of $\{\theta_0^{\rm n}, \theta_{100}^{\rm n}, \theta_0^{\rm p}, \theta_{100}^{\rm p}\}$ using experimental data collected from a commercial cell, giving qualitative results.
- The table displays values for the optimized operating boundaries and the voltage RMSE from fitting the electrode OCP functions estimated from half-cell data to full-cell estimated OCV.

Method	RMSE (mV)	θ_0^{n}	$\theta_{100}^{\mathrm{n}}$	θ_0^{p}	$\theta_{100}^{\mathrm{p}}$
1	30.47	0.0010	0.8960	0.9990	0.1653
2	41.78	0.0009	0.8026	0.9990	0.1510
3	25.36	0.0008	0.8255	0.9284	0.1691
4	19.54	0.0007	0.8279	0.9089	0.1769

- Estimates having lower RMSE are expected to be better in PBMs because closer agreement between cell-level and electrode-level open-circuit functions can yield better model performance.
- It is also important to realize that the RMS errors calibrate only the voltage estimates within the operating windows.
- We are unable to evaluate the OCP models outside the operating boundaries (i.e., models where $\theta_{\mathrm{s}}^{\mathrm{n}} \notin \left[\theta_0^{\mathrm{n}}, \theta_{100}^{\mathrm{n}}\right]$ and $\theta_{\mathrm{s}}^{\mathrm{p}} \notin \left[\theta_{100}^{\mathrm{p}}, \theta_0^{\mathrm{p}}\right]$).
- But, MSMR-model constraints provide some confidence regarding reasonableness of OCP estimates outside normal operating regions.
- We comment that Methods 1–2 saturated θ_0^{p} to its maximum permitted value. This seems unreasonable for a physical cell since some positive-electrode lithium inventory will have been permanently consumed by SEI-layer growth in the negative electrode.
- Therefore, we believe that Methods 3 and 4 results are more physically meaningful.

3.6: Discharge testing to calibrate positive-electrode OCP

- By this point in the parameter-estimation process, we have:
  - Estimated $U^{\mathrm{n}}_{\mathrm{ocp}}(\theta^{\mathrm{n}}_{\mathrm{s}})$ and $\{U^0_j, X_j, \omega_j\}^{\mathrm{n}}$ from the OCP test. We have also created the preliminary result $\widetilde{U}^{\mathrm{p}}_{\mathrm{ocp}}(\tilde{\theta}^{\mathrm{p}}_{\mathrm{s}})$.
  - Estimated Q, $U_{\mathrm{ocv}}(z)$, θ^{n}_0, and $\theta^{\mathrm{n}}_{100}$ from the OCV test. We have also created the preliminary results $\tilde{\theta}^{\mathrm{p}}_0$ and $\tilde{\theta}^{\mathrm{p}}_{100}$.
- We don't yet have final $U^{\mathrm{p}}_{\mathrm{ocp}}(\theta^{\mathrm{p}}_{\mathrm{s}})$, θ^{p}_0, or $\theta^{\mathrm{p}}_{100}$. Why?
- The MSMR model leads us to expect that OCP relationships will have very steep slopes both near $\theta_{\mathrm{s}} = 0$ and $\theta_{\mathrm{s}} = 1$.
  - This was the case for $\widetilde{U}^{\mathrm{n}}_{\mathrm{ocp}}(\tilde{\theta}^{\mathrm{n}}_{\mathrm{s}})$ with graphite negative electrodes.
  - This is why we believe that the MSMR model $U^{\mathrm{n}}_{\mathrm{ocp}}(\theta^{\mathrm{n}}_{\mathrm{s}})$ is accurate, and hence why θ^{n}_0 and $\theta^{\mathrm{n}}_{100}$ are also accurate.
- However, we don't observe this for some positive-electrode materials such as NMC. The OCP test missed one or more low-θ_{s} galleries.
  - We do see a steep slope in $\widetilde{U}^{\mathrm{p}}_{\mathrm{ocp}}(\tilde{\theta}^{\mathrm{p}}_{\mathrm{s}})$ near $\tilde{\theta}^{\mathrm{p}}_{\mathrm{s}} = 1$ (so $\theta_{\mathrm{s}} \approx \tilde{\theta}_{\mathrm{s}}$ near $\tilde{\theta}_{\mathrm{s}} = 1$); however, we do not see a steep slope near $\tilde{\theta}^{\mathrm{p}}_{\mathrm{s}} = 0$.

- In the figure, the blue line shows $\widetilde{U}^{\mathrm{p}}_{\mathrm{ocp}}(\tilde{\theta}^{\mathrm{p}}_{\mathrm{s}})$ for an NMC electrode.
- It must be stretched via a scale factor "b" so the steep slope moves to $\tilde{\theta}^{\mathrm{p}}_{\mathrm{s}} \approx 1$.
- It may also need to be compressed by a second scale factor "m" to find absolute OCP.

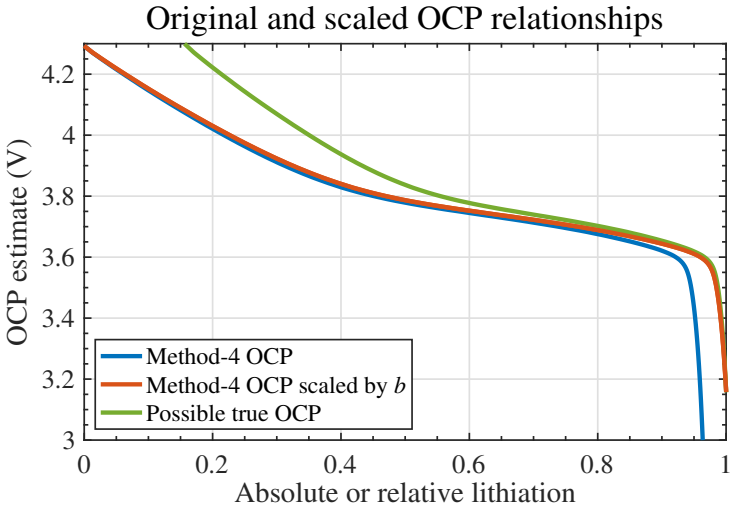

- One way to "solve" this would be to perform OCP testing over a wider voltage range, including higher voltages.
  - Unfortunately, this would cause electrode-material and electrolyte failure, so it is physically not possible to do.
- Alternately, we can seek a way to calibrate $\widetilde{U}^{\mathrm{p}}_{\mathrm{ocp}}(\tilde{\theta}^{\mathrm{p}}_{\mathrm{s}})$, allowing us to determine an MSMR model $U^{\mathrm{p}}_{\mathrm{ocp}}(\theta^{\mathrm{p}}_{\mathrm{s}})$ and $\{U^0_j, X_j, \omega_j\}^{\mathrm{p}}$ and boundaries θ^{p}_0, and $\theta^{\mathrm{p}}_{100}$. This is what we do here.

Why is this important?

- Some parts of the PBM require knowledge of $U^{\mathrm{r}}_{\mathrm{ocp}}(\theta^{\mathrm{r}}_{\mathrm{s}})$. However, we know that $U^{\mathrm{r}}_{\mathrm{ocp}}(\theta^{\mathrm{r}}_{\mathrm{s}}) = \widetilde{U}^{\mathrm{r}}_{\mathrm{ocp}}(\tilde{\theta}^{\mathrm{r}}_{\mathrm{s}})$.
  - So, we don't need to know either the absolute level of lithiation or the OCP function in terms of absolute lithiation in those places.
  - Instead, we can simply substitute $\widetilde{U}^{\mathrm{r}}_{\mathrm{ocp}}(\tilde{\theta}^{\mathrm{r}}_{\mathrm{s}})$.
- But, other parts of the PBM *do* require knowledge of absolute θ_{s}.
  - One example is the prefactor of the Butler–Volmer equation:

$$i^{\mathrm{r}}_0 = \bar{k}^{\mathrm{r}}_0\sqrt{\theta^{\mathrm{r}}_{\mathrm{s}}}\sqrt{1-\theta^{\mathrm{r}}_{\mathrm{s}}}\sqrt{\theta_{\mathrm{e}}} \neq \bar{k}^{\mathrm{r}}_0\sqrt{\tilde{\theta}^{\mathrm{r}}_{\mathrm{s}}}\sqrt{1-\tilde{\theta}^{\mathrm{r}}_{\mathrm{s}}}\sqrt{\theta_{\mathrm{e}}},$$

    remembering that $\theta_{\mathrm{s}} = \theta_{\min} + \tilde{\theta}_{\mathrm{s}}(\theta_{\max} - \theta_{\min})$.
    - We can find a similar result for the MSMR model.
  - Another example is in the expression for SOC-dependent $\bar{D}^{\mathrm{r}}_{\mathrm{s}}$:

$$\bar{D}^{\mathrm{r}}_{\mathrm{s}} = \bar{D}^{\mathrm{r}}_{\mathrm{s,ref}}\frac{F}{RT}\theta^{\mathrm{r}}_{\mathrm{s}}(\theta^{\mathrm{r}}_{\mathrm{s}}-1)\frac{\mathrm{d}U_{\mathrm{ocp}}(\theta_{\mathrm{s}})}{\mathrm{d}\theta_{\mathrm{s}}} \neq \bar{D}^{\mathrm{r}}_{\mathrm{s,ref}}\frac{F}{RT}\tilde{\theta}^{\mathrm{r}}_{\mathrm{s}}(\tilde{\theta}^{\mathrm{r}}_{\mathrm{s}}-1)\frac{\mathrm{d}\widetilde{U}_{\mathrm{ocp}}(\tilde{\theta}_{\mathrm{s}})}{\mathrm{d}\tilde{\theta}_{\mathrm{s}}}.$$

- Therefore, without a properly calibrated set of $U^{\mathrm{r}}_{\mathrm{ocp}}(\theta^{\mathrm{r}}_{\mathrm{s}})$ and $\theta^{\mathrm{r}}_{\mathrm{s}}$, the kinetic predictions of the PBM will be biased.

An idea to correct this

- The fact that solid diffusivity $\bar{D}_{\mathrm{s}}^{\mathrm{r}}$ is SOC-dependent gives us an opportunity to calibrate $\theta_{\mathrm{s}}^{\mathrm{p}}$, and therefore $U_{\mathrm{ocp}}^{\mathrm{p}}(\theta_{\mathrm{s}}^{\mathrm{p}})$.
- We rely on literature that shows that single-particle models (SPMs) can predict cell voltage well for low-rate constant-current profiles.
  - We collect constant-current data from the cell;
  - We then adjust the parameter values of an SPM to fit these data.
- In the SPM, we assume that our existing model of negative-electrode absolute $U_{\mathrm{ocp}}^{\mathrm{n}}(\theta_{\mathrm{s}}^{\mathrm{n}})$ and θ_0^{n} and $\theta_{100}^{\mathrm{n}}$ are accurate.
- We assume that relative $\widetilde{U}_{\mathrm{ocp}}^{\mathrm{p}}(\tilde{\theta}_{\mathrm{s}}^{\mathrm{p}})$, $\tilde{\theta}_0^{\mathrm{p}}$, and $\tilde{\theta}_{100}^{\mathrm{p}}$ are also accurate.
- We choose to model $(1-\theta_{\mathrm{s}}^{\mathrm{p}}) = m(1-\tilde{\theta}_{\mathrm{s}}^{\mathrm{p}}/b)$.
  - The factor "b" stretches the $\widetilde{U}_{\mathrm{ocp}}^{\mathrm{p}}(\tilde{\theta}_{\mathrm{s}}^{\mathrm{p}})$ relationship so that the steep slope moves to $\tilde{\theta}_{\mathrm{s}}^{\mathrm{p}} \approx 1$ (cf. figure on earlier page).
  - We can adjust b manually (e.g., with $m = 1$) to achieve this goal.
- The $\widetilde{U}_{\mathrm{ocp}}^{\mathrm{p}}(\tilde{\theta}_{\mathrm{s}}^{\mathrm{p}}/b)$ relationship then reflects a fully lithiated positive electrode when $\tilde{\theta}_{\mathrm{s}}^{\mathrm{p}}/b = 1$.
- The implications of m then are:
  - When $\tilde{\theta}_{\mathrm{s}}^{\mathrm{p}}/b = 1$, $\theta_{\mathrm{s}}^{\mathrm{p}} = 1$ also.
  - When $\tilde{\theta}_{\mathrm{s}}^{\mathrm{p}}/b = 0$, $\theta_{\mathrm{s}}^{\mathrm{p}} = 1-m$.

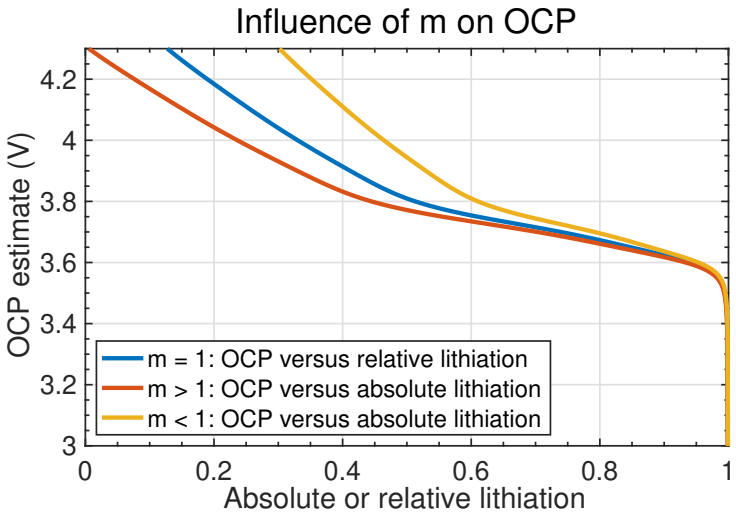

- So, m stretches or compresses $\widetilde{U}_{\mathrm{ocp}}^{\mathrm{p}}(\tilde{\theta}_{\mathrm{s}}^{\mathrm{p}}/b)$ to determine $U_{\mathrm{ocp}}^{\mathrm{p}}(\theta_{\mathrm{s}}^{\mathrm{p}})$.

SPM equations

- There are multiple SPM variations in the literature.[3]
- Here, we adopt a polynomial-based SPM, where the stoichiometry profile inside a particle is modeled as a fourth-order polynomial in r.[4]
- The "state variables" of this SPM are:
  - $\theta_{\text{avg}}(t)$ is the average stoichiometry of the particle.
  - $\nabla\theta_{\text{avg}}(t)$ is the average gradient of the stoichiometry of the particle.
- The "output variable" of the SPM is surface stoichiometry $\theta_{\text{ss}}(t)$.
- We define electrode absolute capacity as a function of cell total capacity Q to be: $Q^{\text{r}} = Q / \left|\theta^{\text{r}}_{100} - \theta^{\text{r}}_{0}\right|$.
- Then, the polynomial-based SPM can be expressed as:

$$\begin{bmatrix} \dot{\theta}^{\text{r}}_{\text{avg}}(t) \\ \nabla\dot{\theta}^{\text{r}}_{\text{avg}}(t) \end{bmatrix} = \begin{bmatrix} 0 & 0 \\ 0 & -30\bar{D}^{\text{r}}_{\text{s}}(\theta^{\text{r}}_{\text{ss}}(t^{-})) \end{bmatrix} \begin{bmatrix} \theta^{\text{r}}_{\text{avg}}(t) \\ \nabla\theta^{\text{r}}_{\text{avg}}(t) \end{bmatrix} + \begin{bmatrix} -\dfrac{1}{3600Q^{\text{r}}} \\ -\dfrac{1}{480Q^{\text{r}}} \end{bmatrix} i^{\text{r}}_{\text{f}}(t)$$

$$\left[\theta^{\text{r}}_{\text{ss}}(t)\right] = \begin{bmatrix} 1 & \dfrac{8}{35} \end{bmatrix} \begin{bmatrix} \theta^{\text{r}}_{\text{avg}}(t) \\ \nabla\theta^{\text{r}}_{\text{avg}}(t) \end{bmatrix} + \left[-\frac{(1/378\,000)}{Q^{\text{r}}\bar{D}^{\text{r}}_{\text{s}}(\theta^{\text{r}}_{\text{ss}}(t^{-}))}\right] i^{\text{r}}_{\text{f}}(t),$$

  where the factors of 3600 convert capacity in Ah to coulombs (or, As), and where we set $i^{\text{n}}_{\text{f}}(t) = i_{\text{app}}(t)$ and $i^{\text{p}}_{\text{f}}(t) = -i_{\text{app}}(t)$.
- Voltage is computed as: $v(t) = U^{\text{p}}_{\text{ocp}}(\theta^{\text{p}}_{\text{ss}}(t)) - U^{\text{n}}_{\text{ocp}}(\theta^{\text{n}}_{\text{ss}}(t)) - R_0 i_{\text{app}}(t)$.
- We can simulate the negative electrode using this SPM model without changes, where the only unknown parameter value is $\bar{D}^{\text{n}}_{\text{s,ref}}$.

[3] For example, you investigated an FVM-based version in ECE5710.

[4] The derivation details are in App. 3.d.

- However, when we seek to simulate the positive electrode, we know neither $\bar{D}^{\mathrm{p}}_{\mathrm{s,ref}}$ nor $U^{\mathrm{p}}_{\mathrm{ocp}}$ nor θ^{p}_{0} nor $\theta^{\mathrm{p}}_{100}$.
- To use the SPM to model the positive electrode, we must convert its expressions to be in terms of $\tilde{\theta}^{\mathrm{p}}_{\mathrm{s}}$, $\widetilde{U}^{\mathrm{p}}_{\mathrm{ocp}}(\tilde{\theta}^{\mathrm{p}}_{\mathrm{s}})$, m, and b.
- Then, we can optimize the parameter values $\bar{D}^{\mathrm{n}}_{\mathrm{s,ref}}$, $\bar{D}^{\mathrm{p}}_{\mathrm{s,ref}}$, and m until the SPM model matches the measured data as closely as possible.
  - Note that we have already chosen b manually, so we do not need to use optimization to find its value.
  - We will also need to optimize R_0, but since it is "linear in the parameters" this turns out to be a linear-optimization substep of the overall nonlinear optimization to find the three other values.
- The desired output of this overall procedure is the set of factors b and m, which calibrate the positive-electrode OCP function.
  - But, a further benefit of this process is that it gives initial estimates of $\bar{D}^{\mathrm{n}}_{\mathrm{s,ref}}$ and $\bar{D}^{\mathrm{p}}_{\mathrm{s,ref}}$ as well (further optimized by the EIS test).

3.7: Converting SPM to biased stoichiometry

- We seek to convert the positive-electrode SPM equations, which originally are functions of $\theta_{\mathrm{s}}^{\mathrm{p}}$, to be in terms of $\tilde{\theta}_{\mathrm{s}}^{\mathrm{p}}$, m, and b.
- Recall that we have defined $(1-\theta_{\mathrm{s}}^{\mathrm{p}}) = m(1-\tilde{\theta}_{\mathrm{s}}^{\mathrm{p}}/b)$. Therefore,

$$\theta_0^{\mathrm{p}} = 1 - \frac{m}{b}(b - \tilde{\theta}_0^{\mathrm{p}})$$

$$\theta_{100}^{\mathrm{p}} = 1 - \frac{m}{b}(b - \tilde{\theta}_{100}^{\mathrm{p}}).$$

- We start the conversion process with (where $\widetilde{Q}^{\mathrm{p}} = Q/\left|\tilde{\theta}_{100}^{\mathrm{p}} - \tilde{\theta}_0^{\mathrm{p}}\right|$):

$$Q^{\mathrm{p}} = \frac{Q}{\left|\theta_{100}^{\mathrm{p}} - \theta_0^{\mathrm{p}}\right|} = \frac{b}{m}\frac{Q}{\left|\tilde{\theta}_{100}^{\mathrm{p}} - \tilde{\theta}_0^{\mathrm{p}}\right|} = \frac{b}{m}\widetilde{Q}^{\mathrm{p}}.$$

- The SPM equation for electrode average stoichiometry is:

$$\frac{\mathrm{d}\theta_{\mathrm{avg}}^{\mathrm{p}}(t)}{\mathrm{d}t} = -\frac{1}{3600Q^{\mathrm{p}}} i_{\mathrm{f}}^{\mathrm{p}}(t).$$

- Substituting the relationships between $\theta_{\mathrm{s}}^{\mathrm{p}}$ and $\tilde{\theta}_{\mathrm{s}}^{\mathrm{p}}$:

$$\frac{m}{b}\frac{\mathrm{d}\tilde{\theta}_{\mathrm{avg}}^{\mathrm{p}}(t)}{\mathrm{d}t} = -\frac{m}{b}\frac{1}{3600\widetilde{Q}^{\mathrm{p}}} i_{\mathrm{f}}^{\mathrm{p}}(t)$$

$$\frac{\mathrm{d}\tilde{\theta}_{\mathrm{avg}}^{\mathrm{p}}(t)}{\mathrm{d}t} = -\frac{1}{3600\widetilde{Q}^{\mathrm{p}}} i_{\mathrm{f}}^{\mathrm{p}}(t),$$

  which has exactly the same form as before.

- The SPM equation for electrode average gradient of stoichiometry is:

$$\frac{\mathrm{d}\nabla\theta_{\mathrm{avg}}^{\mathrm{p}}(t)}{\mathrm{d}t} = -30\bar{D}_{\mathrm{s}}^{\mathrm{p}}(\theta_{\mathrm{ss}}^{\mathrm{r}}(t^-))\nabla\theta_{\mathrm{avg}}^{\mathrm{p}}(t) - \frac{1}{480Q^{\mathrm{p}}} i_{\mathrm{f}}^{\mathrm{p}}(t).$$

- Substituting the relationships between $\theta_{\mathrm{s}}^{\mathrm{p}}$ and $\tilde{\theta}_{\mathrm{s}}^{\mathrm{p}}$:

$$\frac{m}{b}\frac{\mathrm{d}\nabla\tilde{\theta}_{\mathrm{avg}}^{\mathrm{p}}(t)}{\mathrm{d}t} = -30\frac{m}{b}\bar{D}_{\mathrm{s}}^{\mathrm{p}}\left(1 - \frac{m}{b}(b - \tilde{\theta}_{\mathrm{ss}}^{\mathrm{r}}(t^-))\right)\nabla\tilde{\theta}_{\mathrm{avg}}^{\mathrm{p}}(t) - \frac{m}{b}\frac{1}{480\widetilde{Q}^{\mathrm{p}}} i_{\mathrm{f}}^{\mathrm{p}}(t)$$

$$\frac{\mathrm{d}\nabla\tilde{\theta}^{\mathrm{p}}_{\mathrm{avg}}(t)}{\mathrm{d}t} = -30\bar{D}^{\mathrm{p}}_{\mathrm{s}}\left(1-\frac{m}{b}(b-\tilde{\theta}^{\mathrm{r}}_{\mathrm{ss}}(t^{-}))\right)\nabla\tilde{\theta}^{\mathrm{p}}_{\mathrm{avg}}(t) - \frac{1}{480\widetilde{Q}^{\mathrm{p}}}i^{\mathrm{p}}_{\mathrm{f}}(t).$$

- This also has exactly the same form as before, except for the argument to the $\bar{D}^{\mathrm{p}}_{\mathrm{s}}$ function.
- The SOC-dependent solid diffusivity is:

$$\bar{D}^{\mathrm{p}}_{\mathrm{s}}(\theta^{\mathrm{p}}_{\mathrm{s}}) = \bar{D}^{\mathrm{p}}_{\mathrm{s,ref}}\frac{F}{RT}\theta^{\mathrm{p}}_{\mathrm{s}}(\theta^{\mathrm{p}}_{\mathrm{s}}-1)\left.\frac{\mathrm{d}U^{\mathrm{p}}_{\mathrm{ocp}}(\theta^{\mathrm{p}})}{\mathrm{d}\theta^{\mathrm{p}}}\right|_{\theta^{\mathrm{p}}=\theta^{\mathrm{p}}_{\mathrm{s}}}.$$

- Therefore,

$$\bar{D}^{\mathrm{p}}_{\mathrm{s}}\left(1-\frac{m}{b}(b-\tilde{\theta}^{\mathrm{p}}_{\mathrm{s}})\right) = \frac{m}{b}\bar{D}^{\mathrm{p}}_{\mathrm{s,ref}}\frac{F}{RT}\left(1-\frac{m}{b}(b-\tilde{\theta}^{\mathrm{p}}_{\mathrm{s}})\right)\left(\tilde{\theta}^{\mathrm{p}}_{\mathrm{s}}-b\right) \times \left.\frac{\mathrm{d}U^{\mathrm{p}}_{\mathrm{ocp}}(\theta^{\mathrm{p}})}{\mathrm{d}\theta^{\mathrm{p}}}\right|_{\theta^{\mathrm{p}}=1-m(1-\tilde{\theta}^{\mathrm{p}}_{\mathrm{s}}/b)}.$$

- But, $U^{\mathrm{p}}_{\mathrm{ocp}}(\theta^{\mathrm{p}}) = \widetilde{U}^{\mathrm{p}}_{\mathrm{ocp}}\left(b-\frac{b}{m}(1-\theta^{\mathrm{p}})\right)$, so:

$$\left.\frac{\mathrm{d}U^{\mathrm{p}}_{\mathrm{ocp}}(\theta^{\mathrm{p}})}{\mathrm{d}\theta^{\mathrm{p}}}\right|_{\theta^{\mathrm{p}}=1-\frac{m}{b}(b-\tilde{\theta}^{\mathrm{p}}_{\mathrm{s}})} = \left.\frac{\mathrm{d}\widetilde{U}^{\mathrm{p}}_{\mathrm{ocp}}\left(b-\frac{b}{m}(1-\theta^{\mathrm{p}})\right)}{\mathrm{d}\left(b-\frac{b}{m}(1-\theta^{\mathrm{p}})\right)}\frac{\mathrm{d}\left(b-\frac{b}{m}(1-\theta^{\mathrm{p}})\right)}{\mathrm{d}\theta^{\mathrm{p}}}\right|_{\theta^{\mathrm{p}}=1-\frac{m}{b}(b-\tilde{\theta}^{\mathrm{p}}_{\mathrm{s}})}$$

$$= \frac{b}{m}\left.\frac{\mathrm{d}\widetilde{U}^{\mathrm{p}}_{\mathrm{ocp}}(\tilde{\theta}^{\mathrm{p}})}{\mathrm{d}\tilde{\theta}^{\mathrm{p}}}\right|_{\tilde{\theta}^{\mathrm{p}}=\tilde{\theta}^{\mathrm{p}}_{\mathrm{s}}}.$$

- So, finally, redefining $\bar{D}^{\mathrm{p}}_{\mathrm{s}}(\cdot)$ to have input argument $\tilde{\theta}^{\mathrm{p}}_{\mathrm{s}}$:

$$\bar{D}^{\mathrm{p}}_{\mathrm{s}}\left(\tilde{\theta}^{\mathrm{p}}_{\mathrm{s}}\right) = \bar{D}^{\mathrm{p}}_{\mathrm{s,ref}}\frac{F}{RT}\left(1-\frac{m}{b}(b-\tilde{\theta}^{\mathrm{p}}_{\mathrm{s}})\right)\left(\tilde{\theta}^{\mathrm{p}}_{\mathrm{s}}-b\right)\left.\frac{\mathrm{d}\widetilde{U}^{\mathrm{p}}_{\mathrm{ocp}}(\tilde{\theta}^{\mathrm{p}})}{\mathrm{d}\tilde{\theta}^{\mathrm{p}}}\right|_{\tilde{\theta}^{\mathrm{p}}=\tilde{\theta}^{\mathrm{p}}_{\mathrm{s}}}.$$

- Putting everything together, we can simulate the true SPM using biased inputs via the following definitions in the positive electrode:

$$\widetilde{Q}^{\mathrm{p}} = Q/\left|\tilde{\theta}^{\mathrm{p}}_{100}-\tilde{\theta}^{\mathrm{p}}_{0}\right|$$

$$\begin{bmatrix} \dot{\tilde{\theta}}^{\mathrm{p}}_{\mathrm{avg}}(t) \\ \nabla\dot{\tilde{\theta}}^{\mathrm{p}}_{\mathrm{avg}}(t) \end{bmatrix} = \begin{bmatrix} 0 & 0 \\ 0 & -30\bar{D}^{\mathrm{p}}_{\mathrm{s}}(\tilde{\theta}^{\mathrm{p}}_{\mathrm{ss}}(t^-)) \end{bmatrix} \begin{bmatrix} \tilde{\theta}^{\mathrm{p}}_{\mathrm{avg}}(t) \\ \nabla\tilde{\theta}^{\mathrm{p}}_{\mathrm{avg}}(t) \end{bmatrix} + \begin{bmatrix} -\dfrac{1}{3600\widetilde{Q}^{\mathrm{p}}} \\ -\dfrac{1}{480\widetilde{Q}^{\mathrm{p}}} \end{bmatrix} i^{\mathrm{r}}_{\mathrm{f}}(t)$$

$$\left[\tilde{\theta}^{\mathrm{p}}_{\mathrm{ss}}(t)\right] = \begin{bmatrix} 1 & \dfrac{8}{35} \end{bmatrix} \begin{bmatrix} \tilde{\theta}^{\mathrm{p}}_{\mathrm{avg}}(t) \\ \nabla\tilde{\theta}^{\mathrm{p}}_{\mathrm{avg}}(t) \end{bmatrix} + \left[-\frac{(1/378\,000)}{\widetilde{Q}^{\mathrm{p}}\bar{D}^{\mathrm{p}}_{\mathrm{s}}(\tilde{\theta}^{\mathrm{p}}_{\mathrm{ss}}(t^-))}\right] i^{\mathrm{p}}_{\mathrm{f}}(t)$$

$$\bar{D}^{\mathrm{p}}_{\mathrm{s}}(\tilde{\theta}^{\mathrm{p}}_{\mathrm{s}}) = \bar{D}^{\mathrm{p}}_{\mathrm{s,ref}} \frac{F}{RT} \left(1 - \frac{m}{b}(b - \tilde{\theta}^{\mathrm{p}}_{\mathrm{s}})\right) \left(\tilde{\theta}^{\mathrm{p}}_{\mathrm{s}} - b\right) \left.\frac{\mathrm{d}\widetilde{U}^{\mathrm{p}}_{\mathrm{ocp}}(\tilde{\theta}^{\mathrm{p}})}{\mathrm{d}\tilde{\theta}^{\mathrm{p}}}\right|_{\tilde{\theta}^{\mathrm{p}}=\tilde{\theta}^{\mathrm{p}}_{\mathrm{s}}}.$$

- Optimization produces estimate of m which we use to convert:[5]

$$U^{\mathrm{p}}_{\mathrm{ocp}}(\theta^{\mathrm{p}}_{\mathrm{s}}) = \widetilde{U}^{\mathrm{p}}_{\mathrm{ocp}} \left(b - \frac{b}{m}\left(1 - \theta^{\mathrm{p}}_{\mathrm{s}}\right)\right)$$

$$\theta^{\mathrm{p}}_0 = 1 - \frac{m}{b}\left(b - \tilde{\theta}^{\mathrm{p}}_0\right)$$

$$\theta^{\mathrm{p}}_{100} = 1 - \frac{m}{b}\left(b - \tilde{\theta}^{\mathrm{p}}_{100}\right).$$

- Finally, we create an MSMR model $\{U^0_j, X_j, \omega_j\}^{\mathrm{p}}$ of $U^{\mathrm{p}}_{\mathrm{ocp}}(\theta^{\mathrm{p}}_{\mathrm{s}})$.

[5] When we use the SPM inside an optimization code, it is helpful to have bounds for m.

- Suppose that we "know" that the true $\theta^{\mathrm{p}}_{\mathrm{s}}$ for $U^{\mathrm{p}}_{\mathrm{ocp}} = 4.3\,\mathrm{V}$ is between 0.05 and 0.5.
- Also, suppose that from the OCP test we have that $\widetilde{U}^{\mathrm{p}}_{\mathrm{ocp}} = 4.3\,\mathrm{V}$ when $\tilde{\theta}^{\mathrm{p}}_{\mathrm{s}} = \tilde{\theta}_{4.3}$.
- Then, optimization bounds on m are:

$$\frac{1 - 0.5}{b - \tilde{\theta}^{\mathrm{p}}_{4.3}} < \frac{m}{b} < \frac{1 - 0.05}{b - \tilde{\theta}^{\mathrm{p}}_{4.3}}.$$

3.8: Setting up the SPM regression; results

- We need to design a lab test to use with SPM to estimate $\{\bar{D}^{\mathrm{r}}_{\mathrm{s,ref}}, m\}$.
  - Polynomial SPMs work best for constant-current tests.
  - To get the best estimates of $\bar{D}^{\mathrm{r}}_{\mathrm{s,ref}}$, we need to test a cell over as wide a range of SOC as possible.
  - If we use too low a C-rate, modeling error will be dominated by estimation errors in $U^{\mathrm{n}}_{\mathrm{ocp}}(\theta^{\mathrm{n}}_{\mathrm{s}})$ and $\widetilde{U}^{\mathrm{p}}_{\mathrm{ocp}}(\tilde{\theta}^{\mathrm{p}}_{\mathrm{s}})$ since cell polarization will be very low and measurements will be dominated by OCV.
  - If we use too high a C-rate, the SPM will not model cell voltage very well (the literature suggests that SPMs of the nature we are proposing work reasonably well up to about a 2C rate).
- We choose to implement a modified OCV test, with all steps executed at 25 °C, at around a 1C constant-current dis/charge rate.
- The discharge voltage and charge voltage versus SOC are calibrated in the same way as we calibrate OCV data.
- Discharge and/or charge voltages are regressed against $\bar{D}^{\mathrm{n}}_{\mathrm{s,ref}}$, $\bar{D}^{\mathrm{p}}_{\mathrm{s,ref}}$, and m using the SPM approach just presented.
- Then, m and b are used to convert $\widetilde{U}^{\mathrm{p}}_{\mathrm{ocp}}(\tilde{\theta}^{\mathrm{p}}_{\mathrm{s}})$ to $U^{\mathrm{p}}_{\mathrm{ocp}}(\theta^{\mathrm{p}}_{\mathrm{s}})$.
- Finally, we create an MSMR model $\{U^0_j, X_j, \omega_j\}^{\mathrm{p}}$ of $U^{\mathrm{p}}_{\mathrm{ocp}}(\theta^{\mathrm{p}}_{\mathrm{s}})$.

The problem of R_0 when regressing parameter values

- Cell voltage is estimated as: $U^{\mathrm{p}}_{\mathrm{ocp}}(\theta^{\mathrm{p}}_{\mathrm{ss}}(t)) - U^{\mathrm{n}}_{\mathrm{ocp}}(\theta^{\mathrm{n}}_{\mathrm{ss}}(t)) - R_0 i_{\mathrm{app}}(t)$.
- The $U^{\mathrm{r}}_{\mathrm{ocp}}(\theta^{\mathrm{r}}_{\mathrm{ss}}(t))$ terms can be computed if $\bar{D}^{\mathrm{r}}_{\mathrm{s,ref}}$ and m are given.
  - But, to predict voltage, we also need to know R_0.
- When optimizing a set of parameter values, one possibility would be:

  - Construct a cost function in terms of: $p_4 = \{\bar{D}^{\mathrm{n}}_{\mathrm{s,ref}}, \bar{D}^{\mathrm{p}}_{\mathrm{s,ref}}, m, R_0\}$.
  - Then, find the p_4^* that minimizes the difference between predicted cell voltage and true $v(t)$.

- However, this is a 4D nonlinear optimization; we can reduce it to a 3D nonlinear optimization plus a 1D linear optimization.
- Define values found by nonlinear optimization: $p_3 = \{\bar{D}^{\mathrm{n}}_{\mathrm{s,ref}}, \bar{D}^{\mathrm{p}}_{\mathrm{s,ref}}, m\}$.
- Then, every time the cost function is evaluated for a specific p_3:
  - Compute $U^{\mathrm{p}}_{\mathrm{ocp}}(\theta^{\mathrm{p}}_{\mathrm{ss}}(t))$ and $U^{\mathrm{n}}_{\mathrm{ocp}}(\theta^{\mathrm{n}}_{\mathrm{ss}}(t))$ using the SPM and p_3.
  - Construct the vector $e(t) = v(t) - \left(U^{\mathrm{p}}_{\mathrm{ocp}}(\theta^{\mathrm{p}}_{\mathrm{ss}}(t)) - U^{\mathrm{n}}_{\mathrm{ocp}}(\theta^{\mathrm{n}}_{\mathrm{ss}}(t))\right)$.
    - Ideally, this equals $-R_0 i_{\mathrm{app}}(t)$.
  - Solve the least-squares problem $\widehat{R}_0 = -\left[i_{\mathrm{app}}(t)\right]^{\dagger} e(t)$.
  - Define cost as: $\mathrm{rms}\left(v(t) - \left(U^{\mathrm{p}}_{\mathrm{ocp}}(\theta^{\mathrm{p}}_{\mathrm{ss}}(t)) - U^{\mathrm{n}}_{\mathrm{ocp}}(\theta^{\mathrm{n}}_{\mathrm{ss}}(t)) - \widehat{R}_0 i_{\mathrm{app}}(t)\right)\right)$.
- Minimizing this cost function over the three variables of p_3 will automatically choose the best value of $\widehat{R}_0$ as well.
  - Speeds up optimization and improves likelihood of converging to a good local-minimum solution for p_3.

Application to Panasonic-cell data

- We performed the modified OCV tests where scripts 1 and 3 used rates between 0.5C to 4C.
- Rates up to 2C give voltage spread of about 100–250 mV.
- We will use these data to find m.

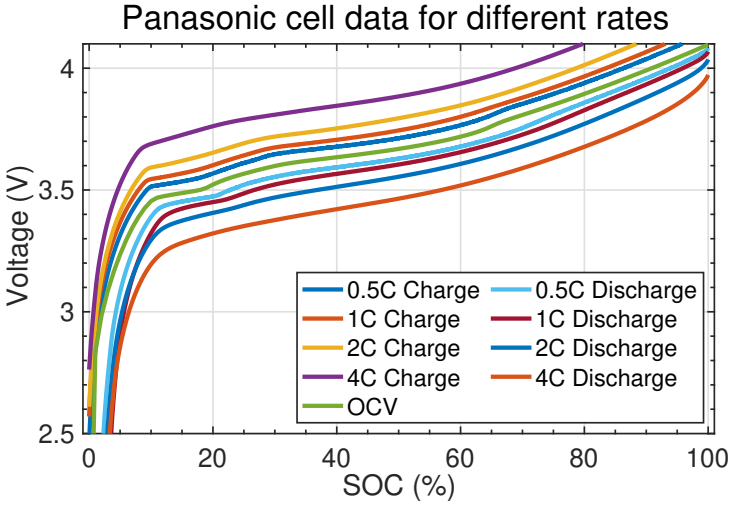

- When running the SPM on lab data, which $\widetilde{U}^{\mathrm{p}}_{\mathrm{ocp}}(\tilde{\theta}^{\mathrm{p}}_{\mathrm{s}})$ estimate to use?
  - From prior sections, Method-3 and Method-4 estimates were best.
  - Method-3 $\widetilde{U}^{\mathrm{p}}_{\mathrm{ocp}}(\tilde{\theta}^{\mathrm{p}}_{\mathrm{s}})$ required $b = 0.96$; but $b = 1$ for Method-4.
- We ran `particleswarm` 100 times on each discharge dataset for both OCP methods and cell serial numbers 41 and 42.
  - Datasets from two cells were used to assess cell-to-cell variation.

OCP method	Rate	$\bar{D}^{\mathrm{n}}_{\mathrm{s,ref}}$	Std. dev. $\bar{D}^{\mathrm{n}}_{\mathrm{s,ref}}$	$\bar{D}^{\mathrm{p}}_{\mathrm{s,ref}}$	Std. dev. $\bar{D}^{\mathrm{p}}_{\mathrm{s,ref}}$	m	Std. dev. m
Method 3, cell 41	C/2	7.45×10^{-5}	1.4×10^{-7}	1.15×10^{-3}	1.5×10^{-5}	0.84	1.5×10^{-3}
Method 3, cell 41	1C	1.02×10^{-4}	4.6×10^{-6}	1.23×10^{-3}	9.2×10^{-5}	0.86	2.1×10^{-2}
Method 3, cell 41	2C	2.61×10^{-4}	1.2×10^{-6}	1.14×10^{-3}	6.6×10^{-6}	0.84	1.9×10^{-3}
Method 3, cell 42	1C	9.67×10^{-5}	4.3×10^{-6}	1.21×10^{-3}	1.2×10^{-4}	0.85	3.1×10^{-2}
Method 4, cell 41	C/2	7.39×10^{-5}	1.5×10^{-7}	1.16×10^{-3}	5.0×10^{-6}	0.94	1.5×10^{-3}
Method 4, cell 41	1C	1.02×10^{-4}	5.1×10^{-6}	1.16×10^{-3}	1.0×10^{-4}	0.95	2.6×10^{-2}
Method 4, cell 41	2C	2.64×10^{-4}	5.8×10^{-12}	1.10×10^{-3}	4.8×10^{-10}	0.93	1.5×10^{-7}
Method 4, cell 42	1C	9.73×10^{-5}	4.3×10^{-6}	1.13×10^{-3}	1.1×10^{-4}	0.94	2.9×10^{-2}

- Very high consistency between estimates of m for these data.
- Using these data, we estimate $m = 0.8475$ for the Method-3 OCP function and $m = 0.94$ for the Method-4 OCP function.
- Figure shows Method-3 OCP scaled by b as the blue line; Method-4 OCP as yellow line.
  - Markers show $\tilde{\theta}^{\mathrm{p}}_{0}$ and $\tilde{\theta}^{\mathrm{p}}_{100}$.
- Versions scaled by both $\{b, m\}$ are shown as red and purple.
  - Markers show θ^{p}_{0} and $\theta^{\mathrm{p}}_{100}$.

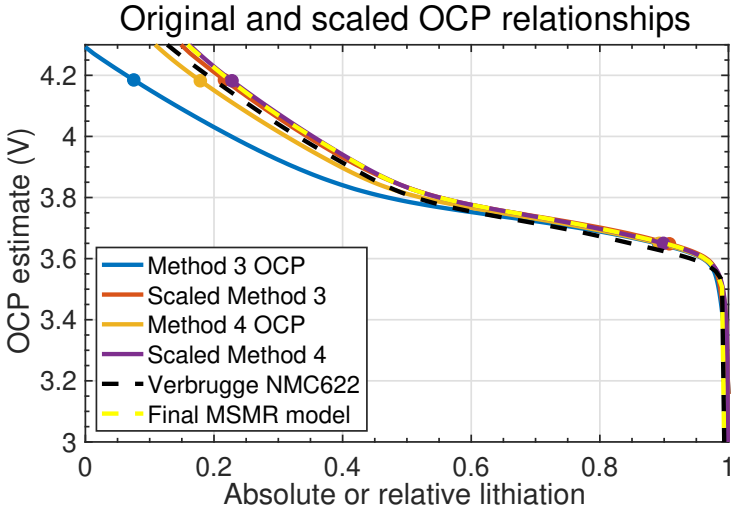

- The red and purple curves both estimate $U^{\mathrm{p}}_{\mathrm{ocp}}(\theta^{\mathrm{p}}_{\mathrm{s}})$ and agree very well.
  - Either can serve as $U^{\mathrm{p}}_{\mathrm{ocp}}(\theta^{\mathrm{p}}_{\mathrm{s}})$ in the steps going forward.

3.9: Pulse-resistance testing

- It remains to find all parameter values related to cell dynamic effects.
- We choose to design a lab test to eliminate the Li-concentration (θ_e and θ_s) equations from consideration when computing voltage.
- To do this, we recognize that these two PDEs involve time derivatives, and so their values cannot change instantly (in zero time).
- We begin with the cell at rest at some SOC, so $\theta_e = \theta_{e,0}$ and $\theta_s = \theta_{s,0}$.
- We apply a *very* short-duration pulse (a few μs) of current to the cell: θ_e and θ_s remain constant but ϕ_s, ϕ_e, and i_{f+dl} can change instantly.
- Change in cell voltage is a nonlinear function of about 13 model parameters, cell SOC, pulse magnitude, and temperature.[6]
- By conducting >13 experiments at different SOCs and magnitudes, we can optimize a fit between the nonlinear function and the changes in cell voltages to solve for the unknown model parameter values.
- To begin, we note that $v(t) = \phi_s^p(3,t) - \phi_s^n(0,t)$.
  - To find a change in voltage, we must find changes in ϕ_s^r.
  - But, since we are relying on the nonlinearity of this relationship, we cannot use our linear transfer functions.
- Instead, consider again simplified solid–electrolyte interphase model:

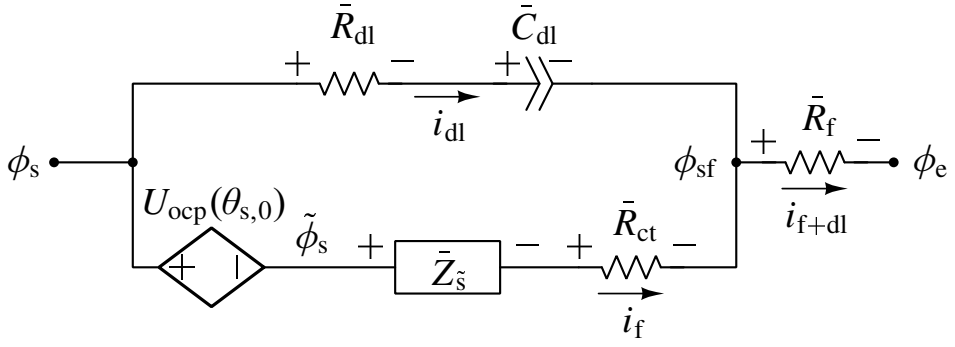

[6] Depends on MSMR model size. Remaining number of parameters $= 11 + J^n + J^p$.

- For very-short-duration current (infinite-frequency) pulses:[7]
  - $\bar{Z}_{\tilde{s}} = 0$ (since Li concentration in solid cannot change instantly).
  - Double-layer impedance of $\bar{C}_{\rm dl}$, $\bar{Z}_{\bar{C}_{\rm dl}} = ((j\omega)^{n_{\rm dl}}\bar{C}_{\rm dl})^{-1}$, is also zero (since Li concentration in electrolyte cannot change instantly).
  - $U_{\rm ocp}(\theta_{\rm s,0})$ is constant and we treat $\bar{R}_{\rm dl}$ and $\bar{R}_{\rm f}$ as linear resistances.
  - $\bar{R}_{\rm ct}$ is a nonlinear resistance, governed by Butler–Volmer equation[8]

$$
\begin{aligned}
i_{\rm f} &= \bar{i}_0 \left\{ \exp\left(\frac{(1-\alpha)F}{RT}\eta\right) - \exp\left(\frac{-\alpha F}{RT}\eta\right) \right\} \\
\bar{i}_0 &= \bar{k}_0 \left(\theta_{\rm e}\right)^{1-\alpha} \left(1-\theta_{\rm s,0}\right)^{1-\alpha} \left(\theta_{\rm s,0}\right)^{\alpha} \quad \text{(and } \theta_{\rm e} = 1\text{)} \\
\eta &= \tilde{\phi}_{\rm s\text{-}e} - \bar{R}_{\rm f} i_{\rm f+dl} \\
i_{\rm f+dl} &= i_{\rm f} + \frac{\eta}{\bar{R}_{\rm dl}}.
\end{aligned} \tag{3.1}
$$

- To seek connections between model parameter values and cell pulse impedance, we start by examining the cell voltage equation

$$
\begin{aligned}
v(t) &= \phi_{\rm s}^{\rm p}(3,t) - \phi_{\rm s}^{\rm n}(0,t) \\
&= \left[\phi_{\rm s\text{-}e}^{\rm p}(3,t) + \phi_{\rm e}^{\rm p}(3,t)\right] - \left[\phi_{\rm s\text{-}e}^{\rm n}(0,t) + \phi_{\rm e}^{\rm n}(0,t)\right] \\
&= \left[\phi_{\rm s\text{-}e}^{\rm p}(3,t) - \phi_{\rm s\text{-}e}^{\rm n}(0,t)\right] + \phi_{\rm e}^{\rm p}(3,t) - \phi_{\rm e}^{\rm n}(0,t).
\end{aligned}
$$

- Since the cell is in equilibrium before the current pulse is applied,

[7] Note that this analysis shows that $\bar{R}_{\rm dl}^{\rm r}$ and $\bar{R}_{\rm f}^{\rm r}$ cannot both be zero. If they are and a current pulse is applied when the cell is in equilibrium, then the instantaneous voltage drops over $\bar{R}_{\rm dl}^{\rm r}$ and $\bar{R}_{\rm f}^{\rm r}$ and $\bar{C}_{\rm dl}^{\rm r}$ are all zero, forcing $\tilde{\phi}_{\rm s\text{-}e}^{\rm r}(\tilde{x},0^+) = 0$ for all $\tilde{x}$ and hence also $\partial\tilde{\phi}_{\rm s\text{-}e}^{\rm r}(\tilde{x},0^+)/\partial\tilde{x} = 0$. However, this violates the boundary conditions for the $\tilde{\phi}_{\rm s\text{-}e}^{\rm r}$ PDE that will be presented in Eq. (3.6). Therefore, either $\bar{R}_{\rm dl}^{\rm r}$ or $\bar{R}_{\rm f}^{\rm r}$ or both must be nonzero for the interphase model to be physically realistic.

[8] We use the standard DFN Butler–Volmer kinetics model for now; lab data will motivate changing this to the MSMR model later.

$$\phi_{\mathrm{e}}^{\mathrm{p}}(3,0^-) = \phi_{\mathrm{e}}^{\mathrm{n}}(0,0^-) = \phi_{\mathrm{e},0} = -U_{\mathrm{ocp}}^{\mathrm{n}}(\theta_{\mathrm{s},0}^{\mathrm{n}})$$

$$\begin{aligned}\phi_{\mathrm{s\text{-}e}}^{\mathrm{p}}(3,0^-) &= \phi_{\mathrm{s}}^{\mathrm{p}}(3,0^-) - \phi_{\mathrm{e}}^{\mathrm{p}}(3,0^-) \\ &= \left[U_{\mathrm{ocp}}^{\mathrm{p}}(\theta_{\mathrm{s},0}^{\mathrm{p}}) - U_{\mathrm{ocp}}^{\mathrm{n}}(\theta_{\mathrm{s},0}^{\mathrm{n}})\right] - \left[-U_{\mathrm{ocp}}^{\mathrm{n}}(\theta_{\mathrm{s},0}^{\mathrm{n}})\right] = U_{\mathrm{ocp}}^{\mathrm{p}}(\theta_{\mathrm{s},0}^{\mathrm{p}})\end{aligned}$$

$$\begin{aligned}\phi_{\mathrm{s\text{-}e}}^{\mathrm{n}}(0,0^-) &= \phi_{\mathrm{s}}^{\mathrm{n}}(0,0^-) - \phi_{\mathrm{e}}^{\mathrm{n}}(0,0^-) \\ &= 0 + U_{\mathrm{ocp}}^{\mathrm{n}}(\theta_{\mathrm{s},0}^{\mathrm{n}}) = U_{\mathrm{ocp}}^{\mathrm{n}}(\theta_{\mathrm{s},0}^{\mathrm{n}}),\end{aligned}$$

due to initial conditions. Therefore, $v(0^-) = U_{\mathrm{ocp}}^{\mathrm{p}}(\theta_{\mathrm{s},0}^{\mathrm{p}}) - U_{\mathrm{ocp}}^{\mathrm{n}}(\theta_{\mathrm{s},0}^{\mathrm{n}})$.

- Then, the moment after a current pulse is applied,

$$v(0^+) = \left[\phi_{\mathrm{s\text{-}e}}^{\mathrm{p}}(3,0^+) - \phi_{\mathrm{s\text{-}e}}^{\mathrm{n}}(0,0^+)\right] + \tilde{\phi}_{\mathrm{e}}^{\mathrm{p}}(3,0^+),$$

where $\tilde{\phi}_{\mathrm{e}}^{\mathrm{r}}(\tilde{x},t) = \phi_{\mathrm{e}}^{\mathrm{r}}(\tilde{x},t) - \phi_{\mathrm{e}}^{\mathrm{n}}(0,t)$.

- Therefore, the change in cell voltage is now

$$\begin{aligned}\triangle v &= v(0^+) - v(0^-) \\ \triangle v &= \lim_{t\to 0^+}\left[\tilde{\phi}_{\mathrm{s\text{-}e}}^{\mathrm{p}}(3,t) - \tilde{\phi}_{\mathrm{s\text{-}e}}^{\mathrm{n}}(0,t) + \tilde{\phi}_{\mathrm{e}}^{\mathrm{p}}(3,t)\right], \qquad (3.2)\end{aligned}$$

where $\tilde{\phi}_{\mathrm{s\text{-}e}}^{\mathrm{r}} = \phi_{\mathrm{s\text{-}e}}^{\mathrm{r}} - U_{\mathrm{ocp}}^{\mathrm{r}}$.

MATLAB ODE solvers (a time-domain approach)

- Parameter values will be found by regressing lab pulse-test data against model equations: must refine model for test assumptions.
- Recall the PDEs for ϕ_{s} and ϕ_{e}:

$$\bar{\sigma}\frac{\partial^2\phi_{\mathrm{s}}}{\partial\tilde{x}^2} = i_{\mathrm{f+dl}} \qquad (3.3)$$

$$\frac{\partial}{\partial\tilde{x}}\left(\bar{\kappa}\left(\frac{\partial}{\partial\tilde{x}}\phi_{\mathrm{e}} + \bar{\kappa}_D T\frac{\partial\ln(\theta_{\mathrm{e}})}{\partial\tilde{x}}\right)\right) = -i_{\mathrm{f+dl}} \qquad (3.4)$$

having nonzero boundary conditions:

$$\bar{\sigma}^{\,\mathrm{n}}\frac{\partial}{\partial\tilde{x}}\phi_{\mathrm{s}}\bigg|_{\tilde{x}=0} = \bar{\sigma}^{\,\mathrm{p}}\frac{\partial}{\partial\tilde{x}}\phi_{\mathrm{s}}\bigg|_{\tilde{x}=3} = -i_{\mathrm{app}}$$

$$-\bar{\kappa}\left[\frac{\partial}{\partial\tilde{x}}\phi_{\mathrm{e}} + \bar{\kappa}_D T\frac{\partial\ln(\theta_{\mathrm{e}})}{\partial\tilde{x}}\right]_{\tilde{x}=1,2} = i_{\mathrm{app}}$$

and initial values $\phi^{\mathrm{n}}_{\mathrm{s},0} = 0$, $\phi^{\mathrm{p}}_{\mathrm{s},0} = U^{\mathrm{p}}_{\mathrm{ocp}}(\theta^{\mathrm{p}}_{\mathrm{s},0}) - U^{\mathrm{n}}_{\mathrm{ocp}}(\theta^{\mathrm{n}}_{\mathrm{s},0})$, $\phi_{\mathrm{e},0} = -U^{\mathrm{n}}_{\mathrm{ocp}}(\theta^{\mathrm{n}}_{\mathrm{s},0})$.

- For the pulse test, θ_{e} remains uniform: the gradient of $\ln(\theta_{\mathrm{e}})$ is zero.
- Combining Eqs. (3.3) and (3.4) gives a debiased solid–electrolyte potential-difference expression

$$\frac{\partial^2\tilde{\phi}_{\text{s-e}}(\tilde{x},t)}{\partial\tilde{x}^2} = \left(\frac{1}{\bar{\sigma}} + \frac{1}{\bar{\kappa}}\right) i_{\text{f+dl}}(\tilde{x},t). \tag{3.5}$$

- Boundary conditions on the potential equations are also combined

$$\bar{\sigma}^{\,\mathrm{n}}\frac{\partial\tilde{\phi}_{\text{s-e}}}{\partial\tilde{x}}\bigg|_{\tilde{x}=0} = -\bar{\kappa}^{\mathrm{n}}\frac{\partial\tilde{\phi}_{\text{s-e}}}{\partial\tilde{x}}\bigg|_{\tilde{x}=1} = -\bar{\kappa}^{\mathrm{p}}\frac{\partial\tilde{\phi}_{\text{s-e}}}{\partial\tilde{x}}\bigg|_{\tilde{x}=2} = \bar{\sigma}^{\,\mathrm{p}}\frac{\partial\tilde{\phi}_{\text{s-e}}}{\partial\tilde{x}}\bigg|_{\tilde{x}=3} = -i_{\mathrm{app}}. \tag{3.6}$$

- The initial conditions for the debiased potentials are:

$$\tilde{\phi}^{\mathrm{n}}_{\text{s-e},0} = \phi^{\mathrm{n}}_{\mathrm{s},0} - \phi^{\mathrm{n}}_{\mathrm{e},0} - U^{\mathrm{n}}_{\mathrm{ocp}}\left(\theta^{\mathrm{n}}_{\mathrm{s},0}\right) = 0$$

$$\tilde{\phi}^{\mathrm{p}}_{\text{s-e},0} = \phi^{\mathrm{p}}_{\mathrm{s},0} - \phi^{\mathrm{p}}_{\mathrm{e},0} - U^{\mathrm{p}}_{\mathrm{ocp}}\left(\theta^{\mathrm{p}}_{\mathrm{s},0}\right) = 0. \tag{3.7}$$

- For the pulse-test assumptions, the PDE for $\tilde{\phi}_{\text{s-e}}$ is reduced to an ODE, Eq. (3.5), together with the interfacial flux Eq. (3.1), and subject to boundary conditions Eq. (3.6) and initial conditions Eq. (3.7).
- If all parameter values are fixed, can solve for $\tilde{\phi}_{\text{s-e}}$ in both electrodes directly in MATLAB by using boundary-value ODE solvers. Then, optimize parameter values by regressing data against ODE solutions.

3.10: Solving for pulse-test math factors

Determine $\tilde{\phi}^{\mathrm{p}}_{\mathrm{s\text{-}e}}(3,t)$ and $\tilde{\phi}^{\mathrm{n}}_{\mathrm{s\text{-}e}}(0,t)$

- To use MATLAB BV-ODE solver (e.g., `bvp5c`), we must provide the ODE to be solved (in standard first-order form), boundary conditions, and an initial guess for the solution, all in a prescribed format.
- The ODE being solved is assumed to be of the form

$$\frac{\partial y}{\partial x} = y' = f(x, y).$$

- To convert our problem to this form, we substitute $y_1 = \tilde{\phi}_{\mathrm{s\text{-}e}}$ and $y_2 = \partial\tilde{\phi}_{\mathrm{s\text{-}e}}/\partial\tilde{x}$ to rewrite the equations as vector of first-order equations, that is,

$$y_1^{'} = \frac{\partial\tilde{\phi}_{\mathrm{s\text{-}e}}}{\partial\tilde{x}} = y_2, \qquad \text{and} \qquad y_2' = \frac{\partial^2\tilde{\phi}_{\mathrm{s\text{-}e}}}{\partial\tilde{x}^2}.$$

- The boundary conditions are coded in the form $g(y(a), y(b)) = 0$: Eqs. (3.6) are translated to:

$$\frac{\partial\tilde{\phi}_{\mathrm{s\text{-}e}}(0,t)}{\partial\tilde{x}} + \frac{i_{\mathrm{app}}}{\bar{\sigma}^{\mathrm{n}}} = 0 \qquad \frac{\partial\tilde{\phi}_{\mathrm{s\text{-}e}}(2,t)}{\partial\tilde{x}} - \frac{i_{\mathrm{app}}}{\bar{\kappa}^{\mathrm{p}}} = 0$$

$$\frac{\partial\tilde{\phi}_{\mathrm{s\text{-}e}}(1,t)}{\partial\tilde{x}} - \frac{i_{\mathrm{app}}}{\bar{\kappa}^{\mathrm{n}}} = 0 \qquad \frac{\partial\tilde{\phi}_{\mathrm{s\text{-}e}}(3,t)}{\partial\tilde{x}} + \frac{i_{\mathrm{app}}}{\bar{\sigma}^{\mathrm{p}}} = 0.$$

- Finally, we use the MATLAB function "`bvpinit`" to create an initial guess for the solution to the equations.
  - Solver is robust to this guess, works even with a zero initialization.
- `bvp5c` executes more quickly if $\tilde{\phi}_{\mathrm{s\text{-}e}}$ initialized closer to final solution.
  - In the negative electrode, we assume a quadratic form: $\tilde{\phi}_{\mathrm{s\text{-}e}}(\tilde{x}, 0^+) \approx a\tilde{x}^2 + b\tilde{x} + c$, for $0 \le \tilde{x} \le 1$.

- The derivative at $\tilde{x} = 0$ is $\partial\tilde{\phi}_{\text{s-e}}/\partial\tilde{x}\Big|_{\tilde{x}=0} = b$. So, $b = -i_{\text{app}}/\bar{\sigma}^{\text{n}}$.
- Similarly, $\partial\tilde{\phi}_{\text{s-e}}/\partial\tilde{x}\Big|_{\tilde{x}=1} = 2a + b$. So, $a = (i_{\text{app}}/\bar{\kappa}^{\text{n}} - b)/2$.
- The mean across $0 \le \tilde{x} \le 1$ is $\bar{\tilde{\phi}}_{\text{s-e}} = a/3 + b/2 + c$. So, $c = \bar{\tilde{\phi}}_{\text{s-e}} - a/3 - b/2$.
- To approximate the true mean of $\tilde{\phi}_{\text{s-e}}$, we assume uniform $i_{\text{f+dl}}(\tilde{x}, 0^+) = i_{\text{app}}$ across the entire electrode.
  - Solve nonlinear equations for mean of $\tilde{\phi}_{\text{s-e}}$ using `fzero`:

```
negMean = @(x,i) i0n.*(exp(K1n.*x)-exp(K2n.*x))+x/Rdln-i; % x = etan
if Rdln == 0
  phisemean = Rfn*i;
else
  phisemean = fzero(negMean,0,[],i) + Rfn*i;
end
```

- The solution in the positive electrode is similar, except we approximate $\tilde{\phi}_{\text{s-e}}(\tilde{x}, 0^+) \approx a(3-\tilde{x})^2 + b(3-\tilde{x}) + c$ for $2 \le \tilde{x} \le 3$.
- Computation time $\lesssim$ 5 ms per (SOC,rate) pair.
- An example solution (evaluated using `deval` based on structure returned by `bvp5c`) when the cell is at 80% SOC and subjected to a 4C-rate short-duration pulse current is displayed below.

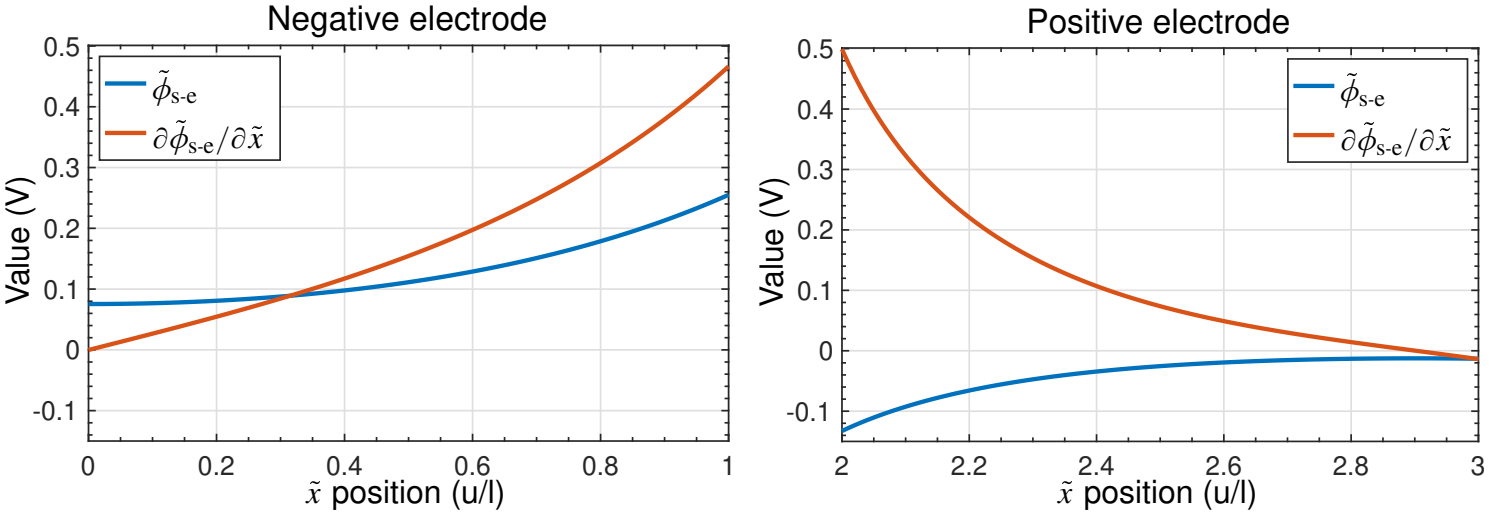

Determine $\tilde{\phi}_{\mathrm{e}}^{\mathrm{p}}(3,t)$ and $\Delta v(t)$

- To compute $\Delta v(t)$ we also need to be able to find $\tilde{\phi}_{\mathrm{e}}^{\mathrm{p}}(3,0^+)$.
- App. 3.e shows (after a lengthy but straightforward derivation):

$$\tilde{\phi}_{\mathrm{e}}^{\mathrm{p}}(3,0^+) = -\frac{i_{\mathrm{app}}}{\bar{\kappa}^{\mathrm{n}}+\bar{\sigma}^{\mathrm{n}}} - \frac{i_{\mathrm{app}}}{\bar{\kappa}^{\mathrm{s}}} - \frac{i_{\mathrm{app}}}{\bar{\kappa}^{\mathrm{p}}+\bar{\sigma}^{\mathrm{p}}} - \frac{\bar{\sigma}^{\mathrm{n}}}{\bar{\kappa}^{\mathrm{n}}+\bar{\sigma}^{\mathrm{n}}}\left(\tilde{\phi}_{\mathrm{s\text{-}e}}^{\mathrm{n}}(1,0^+) - \tilde{\phi}_{\mathrm{s\text{-}e}}^{\mathrm{n}}(0,0^+)\right) - \frac{\bar{\sigma}^{\mathrm{p}}}{\bar{\kappa}^{\mathrm{p}}+\bar{\sigma}^{\mathrm{p}}}\left(\tilde{\phi}_{\mathrm{s\text{-}e}}^{\mathrm{p}}(3,0^+) - \tilde{\phi}_{\mathrm{s\text{-}e}}^{\mathrm{p}}(2,0^+)\right),$$

  which is readily calculated given the `bvp5c` solution for $\tilde{\phi}_{\mathrm{s\text{-}e}}^{\mathrm{r}}(\tilde{x},0^+)$.

- We can now compute the change in voltage due to the current pulse:

$$\begin{aligned}\Delta v &= \tilde{\phi}_{\mathrm{s\text{-}e}}^{\mathrm{p}}(3,0^+) - \tilde{\phi}_{\mathrm{s\text{-}e}}^{\mathrm{n}}(0,0^+) + \tilde{\phi}_{\mathrm{e}}^{\mathrm{p}}(3,0^+) \\ &= -\frac{i_{\mathrm{app}}}{\bar{\kappa}^{\mathrm{n}}+\bar{\sigma}^{\mathrm{n}}} - \frac{i_{\mathrm{app}}}{\bar{\kappa}^{\mathrm{s}}} - \frac{i_{\mathrm{app}}}{\bar{\kappa}^{\mathrm{p}}+\bar{\sigma}^{\mathrm{p}}} - \frac{\bar{\sigma}^{\mathrm{n}}}{\bar{\kappa}^{\mathrm{n}}+\bar{\sigma}^{\mathrm{n}}}\tilde{\phi}_{\mathrm{s\text{-}e}}^{\mathrm{n}}(1,0^+) \\ &\quad - \frac{\bar{\kappa}^{\mathrm{n}}}{\bar{\kappa}^{\mathrm{n}}+\bar{\sigma}^{\mathrm{n}}}\tilde{\phi}_{\mathrm{s\text{-}e}}^{\mathrm{n}}(0,0^+) + \frac{\bar{\kappa}^{\mathrm{p}}}{\bar{\kappa}^{\mathrm{p}}+\bar{\sigma}^{\mathrm{p}}}\tilde{\phi}_{\mathrm{s\text{-}e}}^{\mathrm{p}}(3,0^+) + \frac{\bar{\sigma}^{\mathrm{p}}}{\bar{\kappa}^{\mathrm{p}}+\bar{\sigma}^{\mathrm{p}}}\tilde{\phi}_{\mathrm{s\text{-}e}}^{\mathrm{p}}(2,0^+).\end{aligned}$$

- Interestingly, this can be represented by an equivalent circuit:

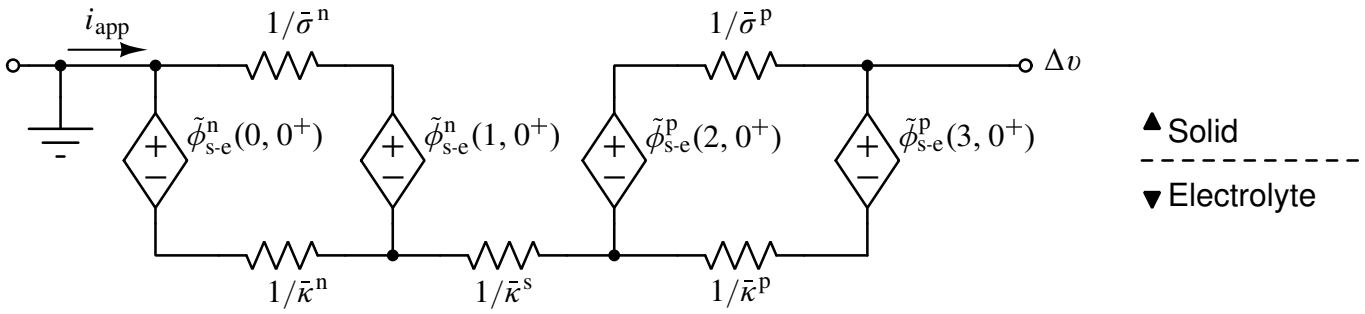

- If we normalize voltage change by the value of applied current, we define a nonlinear pulse resistance $R_0 = -\Delta v / i_{\mathrm{app}}$:

$$R_0 = \frac{1}{\bar{\kappa}^{\mathrm{n}}+\bar{\sigma}^{\mathrm{n}}} + \frac{1}{\bar{\kappa}^{\mathrm{s}}} + \frac{1}{\bar{\kappa}^{\mathrm{p}}+\bar{\sigma}^{\mathrm{p}}} + \frac{\bar{\kappa}^{\mathrm{n}}}{\bar{\kappa}^{\mathrm{n}}+\bar{\sigma}^{\mathrm{n}}}\frac{\tilde{\phi}_{\mathrm{s\text{-}e}}^{\mathrm{n}}(0,0^+)}{i_{\mathrm{app}}} + \frac{\bar{\sigma}^{\mathrm{n}}}{\bar{\kappa}^{\mathrm{n}}+\bar{\sigma}^{\mathrm{n}}}\frac{\tilde{\phi}_{\mathrm{s\text{-}e}}^{\mathrm{n}}(1,0^+)}{i_{\mathrm{app}}} - \frac{\bar{\sigma}^{\mathrm{p}}}{\bar{\kappa}^{\mathrm{p}}+\bar{\sigma}^{\mathrm{p}}}\frac{\tilde{\phi}_{\mathrm{s\text{-}e}}^{\mathrm{p}}(2,0^+)}{i_{\mathrm{app}}} - \frac{\bar{\kappa}^{\mathrm{p}}}{\bar{\kappa}^{\mathrm{p}}+\bar{\sigma}^{\mathrm{p}}}\frac{\tilde{\phi}_{\mathrm{s\text{-}e}}^{\mathrm{p}}(3,0^+)}{i_{\mathrm{app}}}.$$

- The figure below summarizes the ODE simulation method.

FOM equations

θ_s
θ_e
ϕ_s
ϕ_e
i_{f+dl}

Boundary conditions

θ_s
θ_e
ϕ_s
ϕ_e

ODE solver: Determine $\tilde{\phi}^n_{s\text{-}e}$ and $\tilde{\phi}^p_{s\text{-}e}$

[1] $$\frac{\partial^2 \tilde{\phi}^r_{s\text{-}e}}{\partial \tilde{x}^2} = \left(\frac{1}{\bar{\sigma}^r} + \frac{1}{\bar{\kappa}^r}\right) i^r_{f+dl}$$

[2] Initialize solution with parabolic form.

[3] $$i^r_{f+dl} = \bar{i}^r_0 \left[\exp\left(\frac{(1-\alpha)F}{RT}\eta^r\right) - \exp\left(\frac{-\alpha F}{RT}\eta\right)\right] + \frac{\eta^r}{R^r_{dl}}$$

$$\bar{i}^r_0 = \bar{k}^r_0 \left(1-\theta^r_{s,0}\right)^{1-\alpha} \left(\theta^r_{s,0}\right)^{\alpha}$$

$$\eta^r = \tilde{\phi}^r_{s\text{-}e} - \bar{R}^r_f i^r_{f+dl}$$

(solve for i_{f+dl} using nonlinear solver)

[4] $$\bar{\sigma}^r \frac{\partial \tilde{\phi}^r_{s\text{-}e}}{\partial \tilde{x}}\bigg|_{\tilde{x}=0,3} = -\bar{\kappa}^r \frac{\partial \tilde{\phi}^r_{s\text{-}e}}{\partial \tilde{x}}\bigg|_{\tilde{x}=1,2} = -i_{app}$$

Calculate resistance

$$R = \frac{1}{\bar{\kappa}^n + \bar{\sigma}^n} + \frac{1}{\bar{\kappa}^s} + \frac{1}{\bar{\kappa}^p + \bar{\sigma}^p}$$
$$+ \frac{\bar{\kappa}^n}{\bar{\kappa}^n + \bar{\sigma}^n} \frac{\tilde{\phi}^n_{s\text{-}e}(0,0^+)}{i_{app}}$$
$$+ \frac{\bar{\sigma}^n}{\bar{\kappa}^n + \bar{\sigma}^n} \frac{\tilde{\phi}^n_{s\text{-}e}(1,0^+)}{i_{app}}$$
$$- \frac{\bar{\sigma}^p}{\bar{\kappa}^p + \bar{\sigma}^p} \frac{\tilde{\phi}^p_{s\text{-}e}(2,0^+)}{i_{app}}$$
$$- \frac{\bar{\kappa}^p}{\bar{\kappa}^p + \bar{\sigma}^p} \frac{\tilde{\phi}^p_{s\text{-}e}(3,0^+)}{i_{app}}$$

- Some representative examples are shown below:

Doyle cell (no double layer, $\bar{R}^r_{dl} = \infty$)

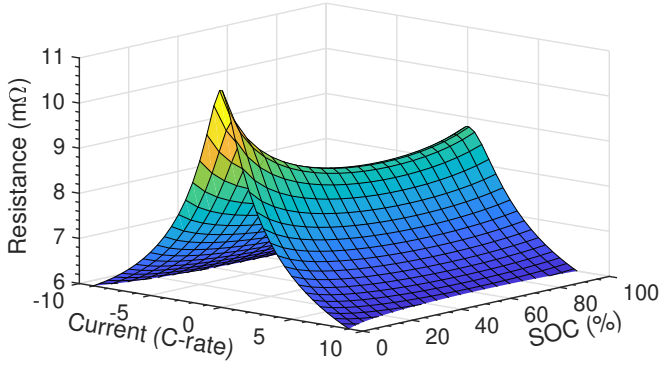

Doyle cell with double layer ($\bar{R}^r_{dl} < \infty$)

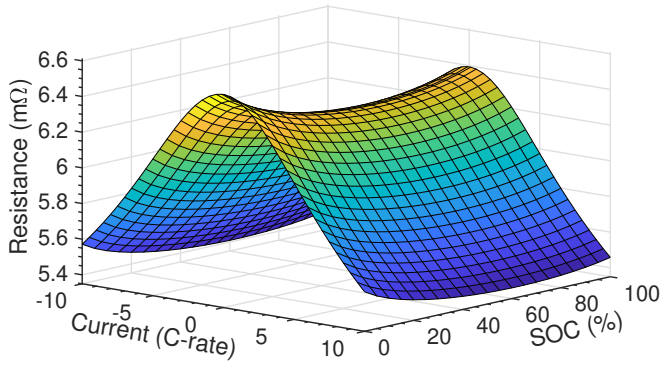

Doyle cell with double layer and $\alpha^r \neq 0.5$

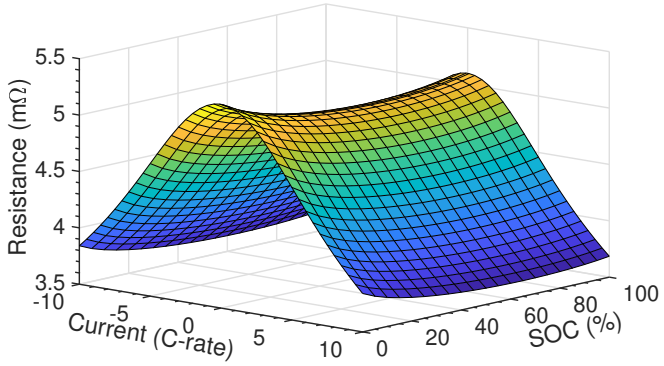

Doyle with double layer but $\bar{R}^r_{dl} = 0$

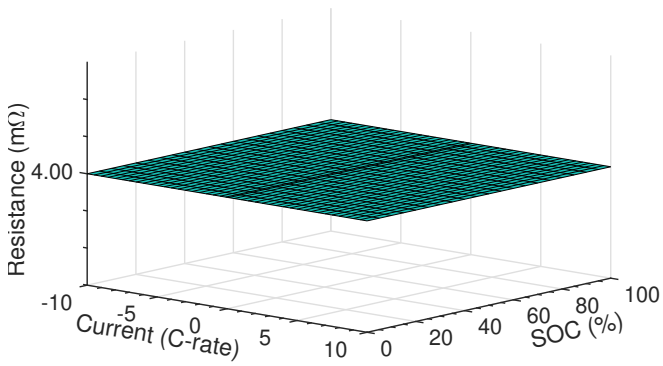

- In physical cell, would expect something in-between the top-left and bottom-right extreme cases.

3.11: Estimating cell-model parameter values using synthetic data

- R_0 is a nonlinear function of 13 model parameter values, and a further function of cell SOC and pulse magnitude (and also temperature).[9]
- Therefore, by collecting at least 13 data points at different SOCs and pulse magnitudes, we can fit the nonlinear model function to R_0 and optimize the 13 parameter values.
- The underlying optimization task aims to find a set of parameter values that can make the model predictions agree as closely as possible to the processed R_0 at all setpoints.
- If we define a vector of M input magnitudes and N SOC points, we can state the objective as seeking to minimize the following root-mean-squared error (RMSE) cost function:

$$p^* = \arg\min_p \sqrt{\frac{1}{MN}\sum_{m=1}^{M}\sum_{n=1}^{N}\left[R_0\left(i_m, z_n\right) - \hat{R}_0\left(i_m, z_n, p\right)\right]^2},$$

  where p is the set of 13 model parameters to identify.
- In this section, we seek to estimate cell-model parameter values using $\widehat{R}_0$ estimates found by time-domain simulation of a noisy PBM for $M = 30$ and $N = 4$.
- Parameters were initially chosen randomly around the true values.
- Graphical results are plotted below, evaluated at many more SOC and magnitude points than were included in the data used to estimate the model parameter values.

[9] Electrolyte intrinsic conductivity κ is a function of electrolyte concentration. However, we are estimating lumped parameters $\bar{\kappa}^{\mathrm{n}}$, $\bar{\kappa}^{\mathrm{s}}$, and $\bar{\kappa}^{\mathrm{p}}$ (based on κ) around the cell's equilibrium electrolyte lithium concentration, $\theta_{\mathrm{e}} = \theta_{\mathrm{e},0} = 1$. Therefore, κ is a constant for all of the pulse tests and $\bar{\kappa}^{\mathrm{n}}$, $\bar{\kappa}^{\mathrm{s}}$, and $\bar{\kappa}^{\mathrm{p}}$ are also constants.

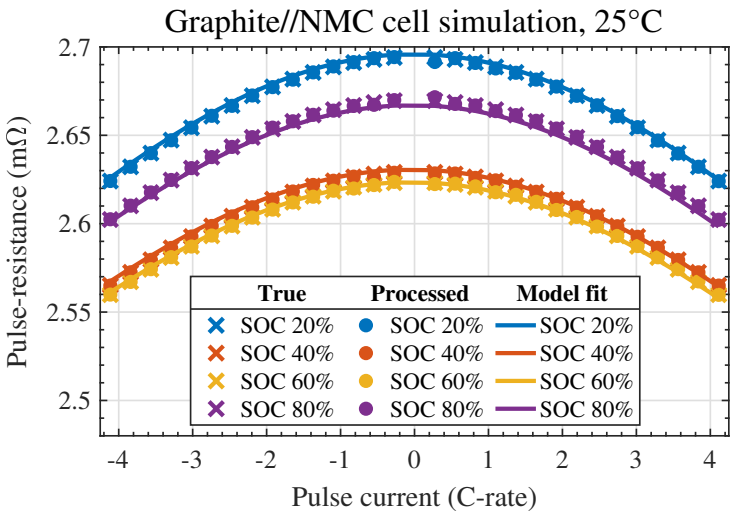

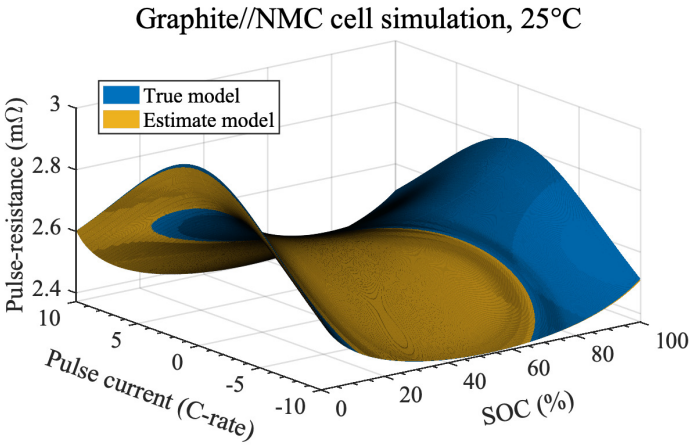

- Overall, the physics-based pulse-resistance model has excellent agreement to the processed R_0. The model generalizes well.
- Numeric results are shown below:

Lumped Parameter	Lower Limit	Upper Limit	Initial Value	Optimized Estimate	True Value	Relative Error
α^{n} [u/l]	0.37	0.68	0.53	0.52	0.50	5 %
α^{p} [u/l]	0.41	0.77	0.59	0.52	0.50	4 %
$\bar{k}_0^{\mathrm{n}}$ [mol s^{-1}]	4.34×10^{-4}	8.06×10^{-4}	6.20×10^{-4}	6.69×10^{-4}	8.01×10^{-4}	16 %
$\bar{k}_0^{\mathrm{p}}$ [mol s^{-1}]	2.06×10^{-4}	3.83×10^{-4}	2.94×10^{-4}	2.62×10^{-4}	2.71×10^{-4}	3 %
$\bar{\sigma}^{\mathrm{n}}$ [S]	315914	947743	631829	625975	612311	2 %
$\bar{\sigma}^{\mathrm{p}}$ [S]	12585	37755	25170	21918	28957	24 %
$\bar{\kappa}^{\mathrm{n}}$ [S]	646	1937	1291	1838	1350	36 %
$\bar{\kappa}^{\mathrm{s}}$ [S]	2977	8933	5955	5563	5758	3 %
$\bar{\kappa}^{\mathrm{p}}$ [S]	1655	4965	3310	3116	2438	28 %
$\bar{R}_{\mathrm{dl}}^{\mathrm{n}}$ [Ω]	8.94×10^{-4}	1.67×10^{-3}	1.28×10^{-3}	9.59×10^{-4}	1×10^{-3}	4 %
$\bar{R}_{\mathrm{dl}}^{\mathrm{p}}$ [Ω]	6.06×10^{-4}	1.12×10^{-3}	8.65×10^{-4}	9.83×10^{-4}	1×10^{-3}	2 %
$\bar{R}_{\mathrm{f}}^{\mathrm{n}}$ [Ω]	9.12×10^{-4}	1.69×10^{-3}	1.30×10^{-3}	1.04×10^{-3}	1×10^{-3}	4 %
$\bar{R}_{\mathrm{f}}^{\mathrm{p}}$ [Ω]	7.51×10^{-7}	1.39×10^{-6}	1.07×10^{-6}	1.07×10^{-6}	1×10^{-6}	7 %

- Traces of parameter values over time during the optimization process are shown below:

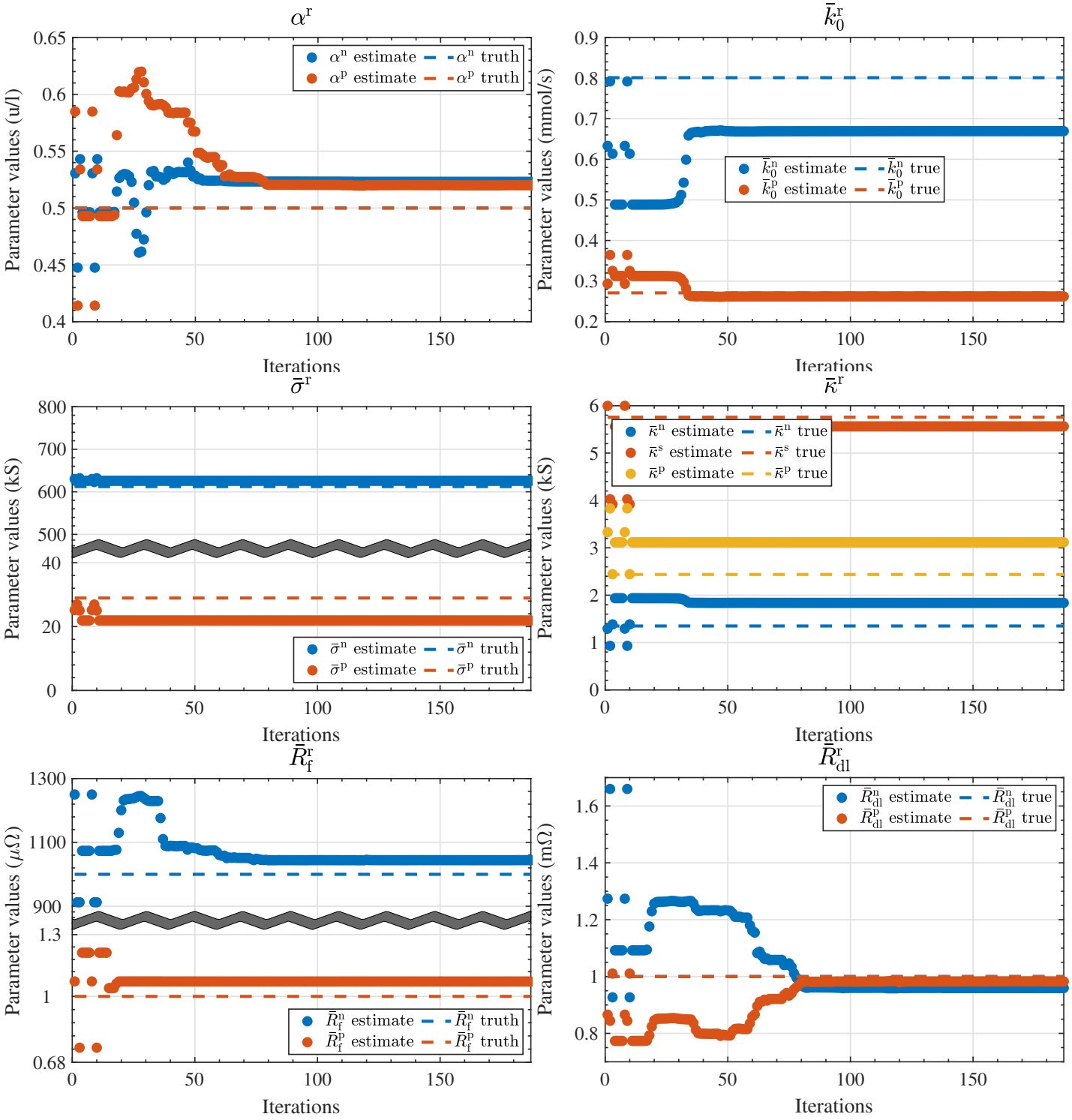

- We see that parameters converge to the correct neighborhoods. Further, the optimization is not confusing corresponding parameters in negative and positive-electrode regions.[10]

[10] This is due to the $\theta_{\mathrm{ss}}^{\mathrm{r}}$ influence in the Butler–Volmer equations of both electrodes varying in opposition to one another as a function of cell SOC.

- We make the following summary observations:
  - Estimates of charge-transfer coefficients α^{r} have good accuracies as they exhibit the highest nonlinear influences on R_0 responses.
  - $\bar{k}_0^{\mathrm{p}}$ is estimated well, while $\bar{k}_0^{\mathrm{n}}$ still has some offset to its true value.
    - We see slight but noticeable nonlinearities at low C-rates in a sensitivity-study (cf. textbook) that might aid in estimating these values well.
    - However, the processed R_0 are noisy and biased at low-input-magnitude setpoints. Therefore, we are more likely to compute inaccurate $\bar{k}_0^{\mathrm{r}}$ values if the data quality is not guaranteed.
  - R_0 is a very weak function of $\bar{\sigma}^{\mathrm{n}}$, so it is difficult to identify a high-accuracy estimate for $\bar{\sigma}^{\mathrm{n}}$.
    - However, even large-magnitude absolute error produces small relative estimation error due to the large magnitude of $\bar{\sigma}^{\mathrm{n}}$.
    - The value of $\bar{\sigma}^{\mathrm{p}}$ is relatively well estimated in the study.
  - Electrolyte conductances $\bar{\kappa}^{\mathrm{r}}$ have large relative errors because they are coupled with large-valued $\bar{\sigma}^{\mathrm{r}}$ in the model: small relative errors in identifying $\bar{\sigma}^{\mathrm{r}}$ will require large errors in $\bar{\kappa}^{\mathrm{r}}$ to compensate.
  - Estimates of lumped film resistance $\bar{R}_{\mathrm{f}}^{\mathrm{r}}$ and lumped double-layer resistance $\bar{R}_{\mathrm{dl}}^{\mathrm{r}}$ are highly accurate.

3.12: Application to a physical cell

- We now show summary pulse-test results for the Panasonic cell.
  - I have omitted a lot of detail (see text) on finding $\widehat{R}_0$ from raw data.
- MATLAB's `particleswarm` optimizes PBM parameter values to fit $\widehat{R}_0$ estimates. Fits of resistance model to $\widehat{R}_0$ data are plotted:

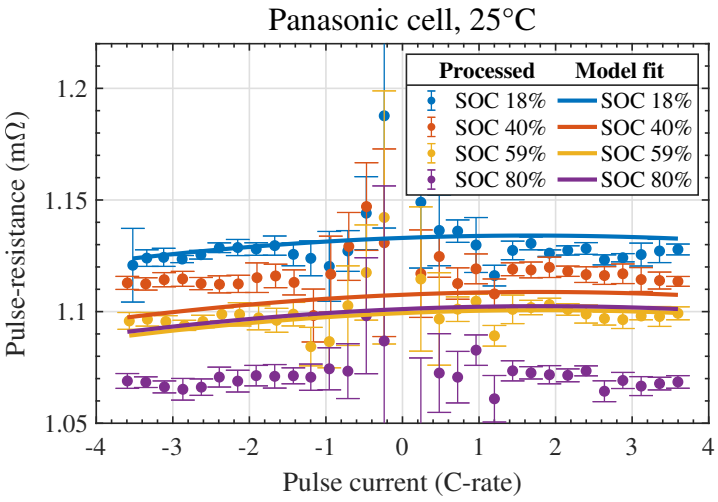

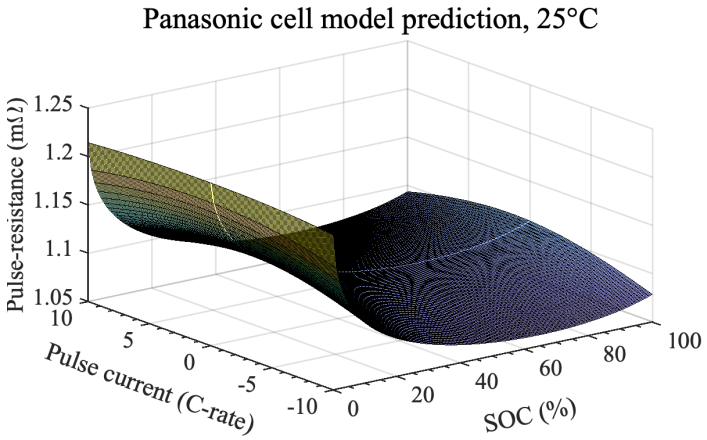

- We make two key observations:
  1. The apparent "bump" in the $\widehat{R}_0$ measured data between ± 1C is not reproduced by the model.
     - This fact, combined with the wide error bars for $\widehat{R}_0$ estimates in this operating region, leads us to believe that the bump is an artifact caused by voltage-measurement noise.
  2. Modeled average resistance at different SOC levels does not agree with actual average level of resistance as a function of SOC.
     - The collected data show monotonically decreasing resistance as SOC increases; however, the model predicts that resistances for 80 % SOC must be higher than for 60 % SOC.
- Fundamentally, this mismatch demonstrates that the model we have used does not have sufficient SOC degrees of freedom to describe the observed changes in resistance as a function of SOC.

- The only occurrence of SOC in the model is in the pre-factor to the Butler–Volmer equation. Therefore, this pre-factor is somehow too simple to describe the data we have measured.
- We believe that the solution to this problem is to replace the standard DFN (Butler–Volmer) kinetics model with the MSMR kinetics model.
- We conducted a simple simulation study where we replaced the DFN kinetics with the MSMR model.
- Results plotted below: more SOC degrees of freedom are enabled.

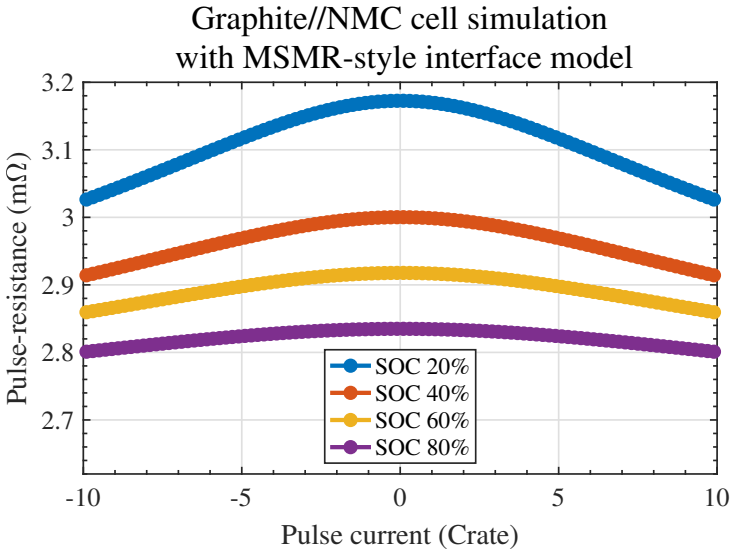

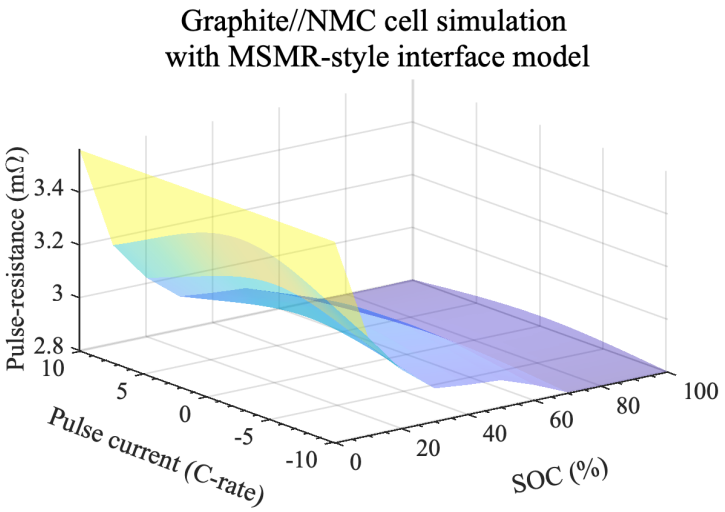

- MSMR model R_0 fits to the data are shown below.

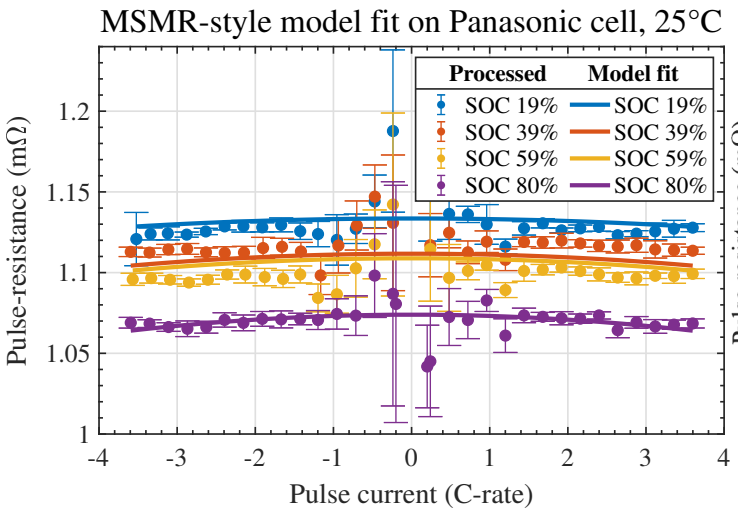

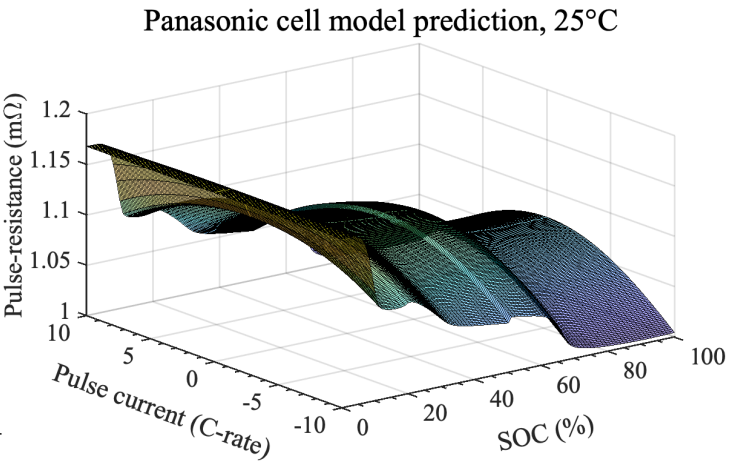

- At this point, we don't believe we've collected data at sufficient SOC setpoints to determine all MSMR $\bar{k}_0^{\mathrm{n}}$ and $\bar{k}_0^{\mathrm{p}}$ without ambiguity, which we hypothesize is one reason for the bumpiness of the 3D surface.
- However, the 2D fit to all R_0 data that have been measured to this point is greatly improved over the fit using the non-MSMR model.

Summary of pulse testing

- Use very-short-duration (a few μs) current pulses to excite cell: concentration variables cannot change in zero time and hence parameters of concentration equations are eliminated from model.
- There are about 26 parameters in the lumped-parameter model remaining to estimate: The pulse-resistance model eliminates 13 from consideration and so we are able to focus on estimating the others.
- In principle, this should make it easier to find accurate values reliably.
- Simulation studies show we are likely to make poor pulse-resistance estimates for low input currents due to measurement noise.
- After optimization, despite the fact that some model parameters do not have high-accuracy estimates (e.g., conductances), predicted pulse resistance still agrees well with the true data.
- This is because voltage is insensitive to some parameters. Perhaps better estimates could be made if more data from more setpoints were collected in order to reduce the impact of measurement noise.
- Nevertheless, the majority of the parameter estimates yield less than 30 % relative errors, which we consider to be reasonable with respect to the number of SOC/C-rate setpoints we emulated.

- Methods for data-processing and optimization were also applied to a commercial 25 Ah Panasonic graphite//NMC cell.
- In doing so, our lab equipment was pushed to its performance limits.
- This, combined with voltage-measurement noise, makes finding reliable estimates of $\widehat{R}_0$ difficult.
- However, we could still make several observations such noting the clear variation in pulse resistance versus cell SOC and temperature.
- We were not able to find a set of parameter values using DFN kinetics that accurately represented the SOC dependence of the lab data.
  - This appears to indicate that the SOC dependence of the kinetics in the DFN model is too simple.
- As proof-of-concept, we replaced the standard DFN interface kinetics with those of an MSMR model, and found that this new approach can explain the SOC dependence of $\widehat{R}_0$ observed in the lab data.
- This is a very promising result, hinting that perhaps the pulse test can find the set of kinetics parameter values for a full MSMR model. A detailed investigation remains as the topic of future work.

- In principle, pulse tests estimate all parameters in the table.
  - We might assume $\alpha_j^{\mathrm{r}} = 0.5$ to reduce count further.
- Remaining parameter values found using the EIS and PSS tests.

Negative Electrode	Separator	Positive Electrode
α_j^{n}		α_j^{p}
$\bar{\kappa}^{\mathrm{n}}$	$\bar{\kappa}^{\mathrm{s}}$	$\bar{\kappa}^{\mathrm{p}}$
$\bar{\sigma}^{\mathrm{n}}$		$\bar{\sigma}^{\mathrm{p}}$
$\bar{k}_{0,j}^{\mathrm{n}}$		$\bar{k}_{0,j}^{\mathrm{p}}$
$\bar{R}_{\mathrm{f}}^{\mathrm{n}}$		$\bar{R}_{\mathrm{f}}^{\mathrm{p}}$
$\bar{R}_{\mathrm{dl}}^{\mathrm{n}}$		$\bar{R}_{\mathrm{dl}}^{\mathrm{p}}$

3.13: Frequency-response testing: concept and complications

- Ch. 2 developed closed-form TFs for all electrochemical variables, which can be combined to form a closed-form cell impedance model.
- In principle, measured EIS data can be regressed against this model to find (most of) the remaining 13 parameter values.
- But, since so many parameters remain to be found, the cost function has many local minima.

Negative electrode	Separator	Positive electrode
$\bar{D}^{\mathrm{n}}_{\mathrm{s,ref}}$		$\bar{D}^{\mathrm{p}}_{\mathrm{s,ref}}$
$\bar{q}^{\mathrm{n}}_{\mathrm{e}}$	$\bar{q}^{\mathrm{s}}_{\mathrm{e}}$	$\bar{q}^{\mathrm{p}}_{\mathrm{e}}$
$\bar{C}^{\mathrm{n}}_{\mathrm{dl}}$		$\bar{C}^{\mathrm{p}}_{\mathrm{dl}}$
$n^{\mathrm{n}}_{\mathrm{f}}$		$n^{\mathrm{p}}_{\mathrm{f}}$
$n^{\mathrm{n}}_{\mathrm{dl}}$		$n^{\mathrm{p}}_{\mathrm{dl}}$
$\bar{\kappa}_D$ and $\bar{\psi}$ span all regions		

- We find that the quality of results is improved by:
  - Optimizing both the impedance match and the "distribution of relaxation times" (DRT) match together.
  - Using as tight parameter optimization bounds as possible, and initializing to physically reasonable values.
  - Using a powerful optimization tool such as `particleswarm`.
  - Preprocessing lab data to remove inductance from the test setup.
- But first, an unexpected complication.

TF model is not linearly identifiable

- Ideally, we seek to estimate—from EIS data—the parameter values:

$$p_{\mathrm{EIS}} = \{\bar{D}^{\mathrm{r}}_{\mathrm{s,ref}}, \bar{q}^{\mathrm{r}}_{\mathrm{e}}, \bar{C}^{\mathrm{r}}_{\mathrm{dl}}, n^{\mathrm{r}}_{\mathrm{f}}, n^{\mathrm{r}}_{\mathrm{dl}}, \bar{\kappa}_{\mathrm{D}}, \bar{\psi}\}.$$

- We begin by assuming all other model kinetics parameter values:

$$p_{\mathrm{pulse}} = \{\alpha^{\mathrm{r}}, \bar{k}^{\mathrm{r}}_{0,j}, \bar{\kappa}^{\mathrm{r}}, \bar{\sigma}^{\mathrm{r}}, \bar{R}^{\mathrm{r}}_{\mathrm{f}}, \bar{R}^{\mathrm{r}}_{\mathrm{dl}}\}$$

  have already been estimated by the pulse-resistance test.

- However, we encounter an identifiability problem when doing so.
- We know from Ch. 1 that all the parameters of the PDE LPM model are identifiable; but, not all parameters of the linearized TF model are.
  - We say that the LPM is "nonlinearly identifiable" but the TF impedance model is "not linearly identifiable."
- To illustrate, consider a simple model, $y(x) = ax + b\sin(x)$.
- If we collect (x, y) data for a variety of x, we can estimate both a and b accurately. We conclude that this model is nonlinearly identifiable.
- Linearizing the model (via a Taylor-series expansion around $x = 0$ and deleting nonlinear terms) gives $y(x) = (a + b)x$.
- In the linearized model, we can identify the sum $a + b$, but not the individual values of a and b.

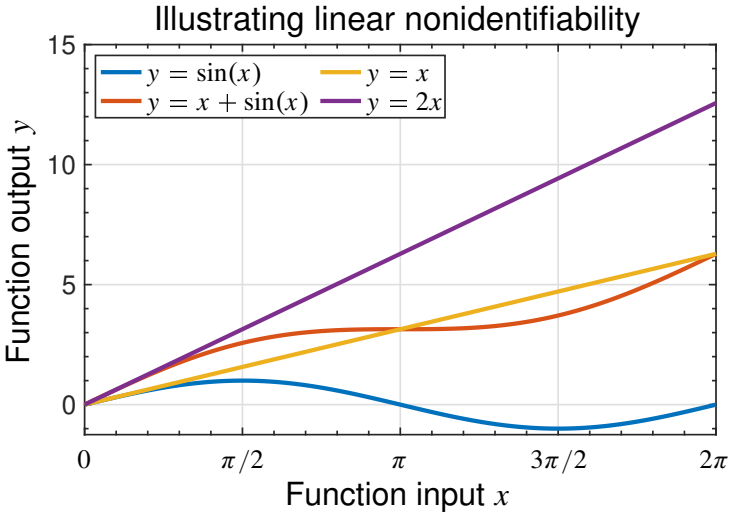

- It is not at all obvious from a casual glance at the TF equations that there is a redundancy such as this in the TF cell-impedance model.
- However, some detailed analysis shows that the model never has $\bar{\psi}$, $\bar{q}^{\mathrm{r}}_{\mathrm{e}}$, and $\bar{\kappa}_{\mathrm{D}}$ alone; they always occur as ratios of $\bar{q}^{\mathrm{r}}_{\mathrm{e}}/\bar{\psi}$ and $\bar{\kappa}_{\mathrm{D}}/\bar{\psi}$.
- So, the EIS test cannot identify all parameters in the desired set; rather, it can identify (by temporarily forcing $\bar{\psi} = 1$):

$$p^{\mathrm{lin}}_{\mathrm{EIS}} = \{\bar{D}^{\mathrm{r}}_{\mathrm{s,ref}}, \bar{q}^{\mathrm{r}}_{\mathrm{e}}/\bar{\psi}, \bar{C}^{\mathrm{r}}_{\mathrm{dl}}, n^{\mathrm{r}}_{\mathrm{f}}, n^{\mathrm{r}}_{\mathrm{dl}}, \bar{\kappa}_{\mathrm{D}}/\bar{\psi}\}.$$

- We rely on the pseudo-steady-state test, presented later in this chapter, to identify $\bar{\psi}$, which allows us to recover $\bar{q}^{\mathrm{r}}_{\mathrm{e}}$ and $\bar{\kappa}_{\mathrm{D}}$ also.

Distribution of relaxation times

- With the identifiability issue sorted out, we find that there are still challenges finding physically consistent parameter values, $p_{\text{EIS}}^{\text{lin}}$.
- The Nyquist-impedance "bump" is often roughly semi-circular.
- Recall, from Topic 2.9, that a semi-circular impedance signature can be modeled by a parallel R–C circuit having time constant $\tau = RC$.
- But, impedances having multiple similar R–C time constants will have overlapping "bumps" that visually appear to be a single semi-circle.
  - Large errors in time-constant estimates can result in small errors in impedance. Optimizing impedance matches alone is insufficient.
- "Distribution of relaxation times" (DRT) method seeks to deconvolve indistinct or "blurred" impedance into individual time constants.
- May help separate time constants for negative- and positive-electrode double layers, electrolyte- and solid-diffusion processes, and so forth.
- This might improve estimates of $p_{\text{EIS}}^{\text{lin}}$ in a similar way to how differential-capacity methods improved estimates of U_{ocp}.
- To introduce the DRT, consider the circuit to the right.

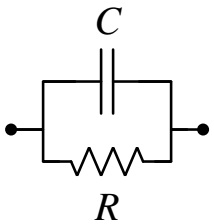

- We can determine this circuit's impedance readily via ac steady-state analysis:

$$Z(f) = \frac{1}{\frac{1}{R} + j2\pi f C} = \frac{R}{1 + j2\pi f(RC)} = \frac{R}{1 + j2\pi f \tau}.$$

- If there is a series resistance R_0 plus multiple R–C filters in series,

$$Z(f) = R_0 + \sum_{k=1}^{N} \frac{R_k}{1 + j2\pi f \tau_j}.$$

- Now, consider the nonideal case, where the Nyquist impedance "bump", even from a single process, can arise from a range of time constants rather than a single time constant.
  - Nonhomogeneous particle surfaces and porous materials are providing many different circuit pathways for charge storage in parallel, each having a different relaxation time.
  - This is the ZARC (R–CPE) case we have encountered before.
- In this case, we suppose we have total polarization resistance R_{pol} and some differential amount:

$$\frac{g(\tau)}{1 + j2\pi f\tau}$$

of the resistance between time constant τ and $\tau + \mathrm{d}\tau$. Therefore,

$$Z(f) = R_0 + R_{\text{pol}} \int_0^\infty \frac{g(\tau)}{1 + j2\pi f\tau}\,\mathrm{d}\tau.$$

- More generally, for a possibility of multiple ZARC elements, we have:

$$Z(f) = R_0 + \int_0^\infty \frac{\gamma\left(\ln\tau\right)}{1 + j2\pi f\tau}\,\mathrm{d}\tau,$$

where $\gamma\left(\ln\tau\right)$ is a "distribution of relaxation times" function describing the time-relaxation characteristics of the cell.

- We would like to deconvolve $Z(f)$ to solve for $\gamma\left(\ln\tau\right)$ directly from impedance data, but there are numeric challenges.
- We have had some success using the "DRT Toolbox" which approximates $\gamma\left(\ln\tau\right)$ using radial basis functions (RBFs).[11]

[11] T.H. Wan, M. Saccoccio, C. Chen, and F. Ciucci, "Influence of the Discretization Methods on the Distribution of Relaxation Times Deconvolution: Implementing Radial Basis Functions with DRTtools," *Electrochimica Acta*, vol. 184, pp. 483–499, Dec. 2015.

- Consider the example of a circuit having a series resistance and two R–C pairs.
- We wish to deconvolve the overall impedance using DRT to find circuit-element values.

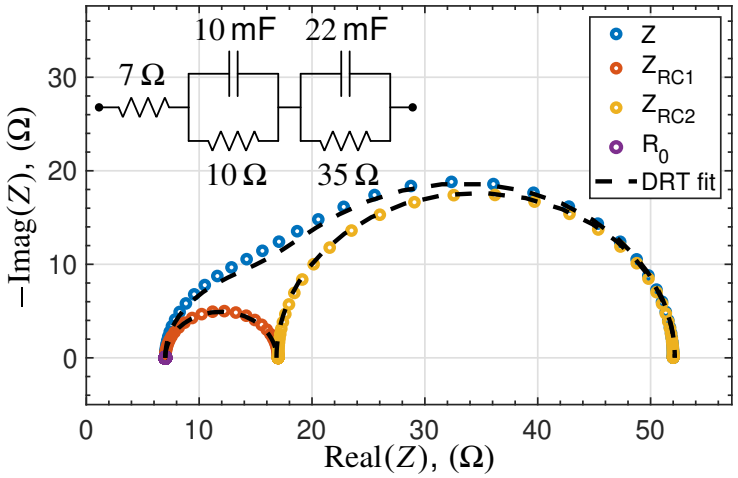

- Using the DRT toolbox, we find the RBF-approximation to the distribution function $\gamma(\ln \tau)$.
- We see two distinct peaks τ_k corresponding to the two R–C time constants.

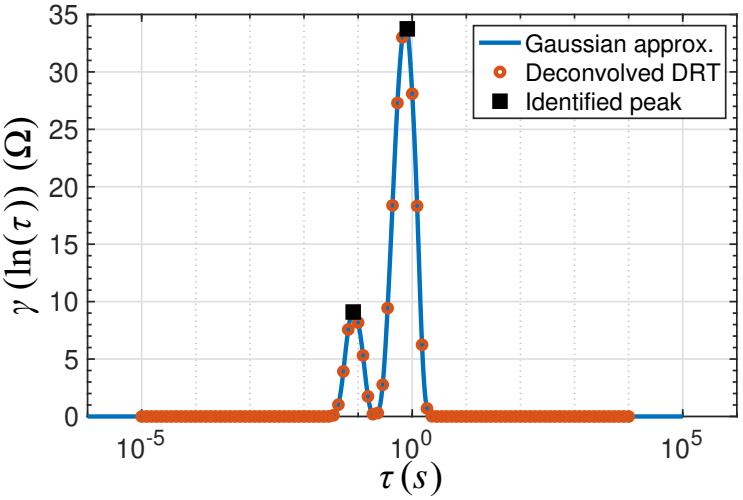

- Having identified τ_k, we then fit resistance values R_k by minimizing

$$\{R_1^*, R_2^*\} = \arg \min_{\{R_1, R_2\}} \sum_f \| Z_{\text{true}}(f) - Z_{\text{est}}(f) \|^2 .$$

- We then compute capacitance as $C_k = \tau_k / R_k$.
- Results tabulated:

	R_1 [Ω]	R_2 [Ω]	C_1 [mF]	C_2 [mF]
Truth	10	35	10	22
Estimate	9.85	35.29	8.23	22.98
Relative error	1.5%	0.83%	17.7%	4.45%

- Note that since the DRT provides a discrete solution, the values for τ_k will be (at least) somewhat wrong.
- An additional optimization of the overall impedance using the identified R–C values as initializations might improve final results.

3.14: Frequency-response testing: Results

- Recall that cell impedance can be expressed as:

$$Z(s) = -\left[\frac{\tilde{\Phi}^{\mathrm{p}}_{\mathrm{s\text{-}e}}(3,s)}{I_{\mathrm{app}}(s)} + \frac{\tilde{\Phi}^{\mathrm{p}}_{\mathrm{e}}(3,s)}{I_{\mathrm{app}}(s)} - \frac{\tilde{\Phi}^{\mathrm{n}}_{\mathrm{s\text{-}e}}(0,s)}{I_{\mathrm{app}}(s)}\right].$$

- Visualize using Doyle-cell parameters (plus double layer).

- Plots show individual impedance components.
- Color is function of frequency, helps show overlapping segments.
- Expect at least two time constants per electrode, three for electrolyte.

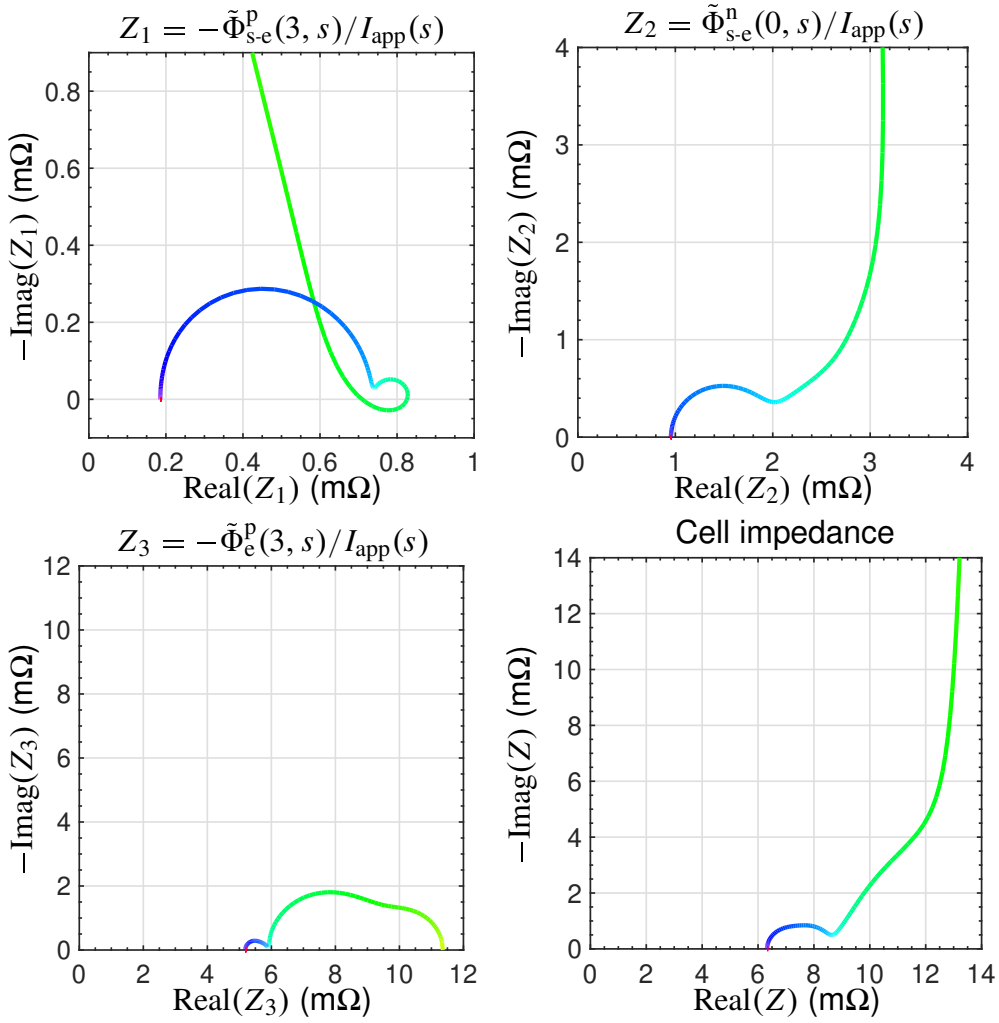

- Note that none of the impedances extend below the real axis, which is different from what we see in measured EIS data.
- Real measurements include inductive behavior, which is not a part of our cell models and should be removed from the data before optimization so that parameter estimates are not biased.

- We use the “generalized DRT” (GDRT) to help with this: It identifies R–L time constants in addition to R–C time constants.
- We then subtract the impedance contribution of the R–L time constants from the impedance data before optimizations.

Data-process performance, 25 °C

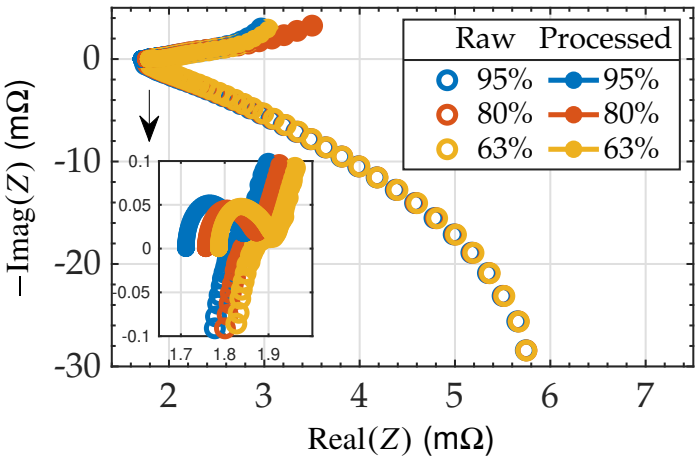

Panasonic sample GDRT, 25 °C, 90 % SOC

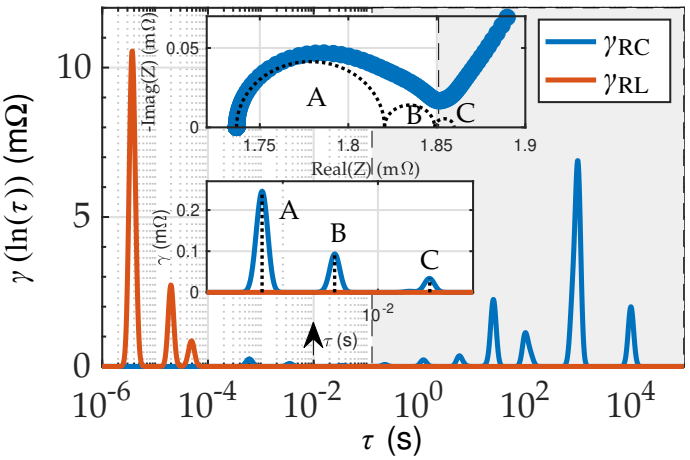

- Repeating for multiple SOCs, we have:

Processed Panasonic cell, 25 °C

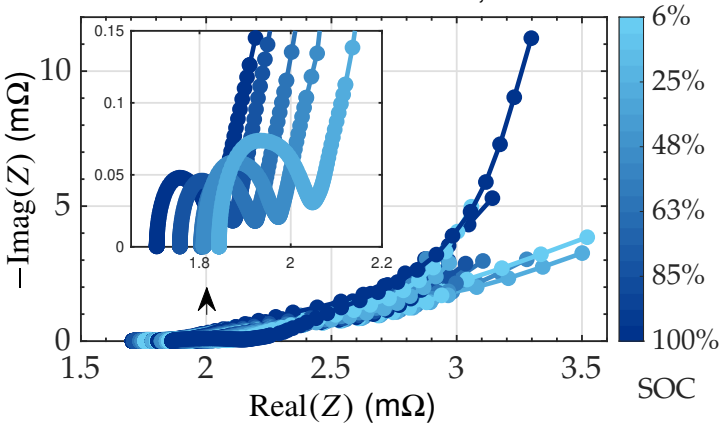

Panasonic cell GDRT, 25 °C

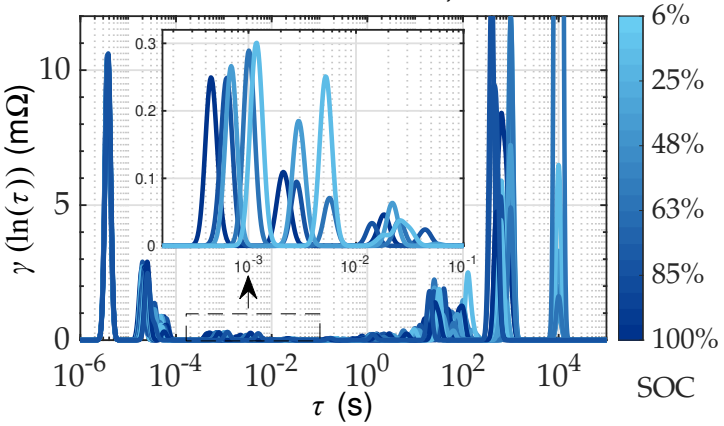

- Then, regress processed impedance data (optionally DRT peaks also) to TF parameters.
- The fit is quite good over a wide SOC and frequency range.
- (cf. text for details on data processing and optimizations.)

Model fit to measured data

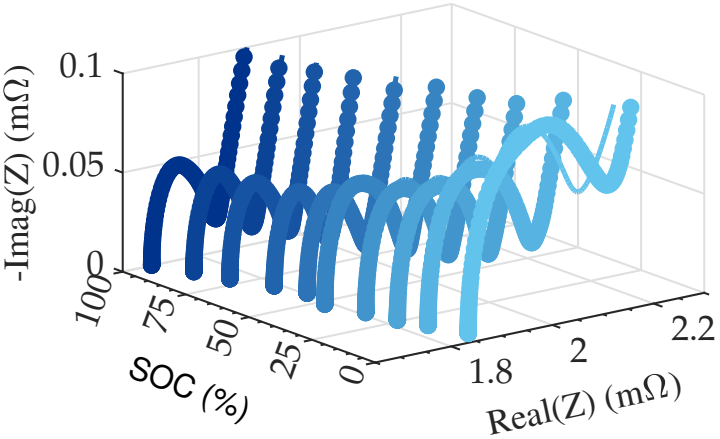

- We can choose to fit individual models to each SOC measurement setpoint (“Strategy 2”) or a single global model (“Strategy 1”).
- If we have physically correct models of how parameters vary with SOC, then Strategy 1 is best; otherwise, Strategy 2 captures true parameter variation that otherwise would have been masked.
- Using Strategy 2, we do discover parameter variations.

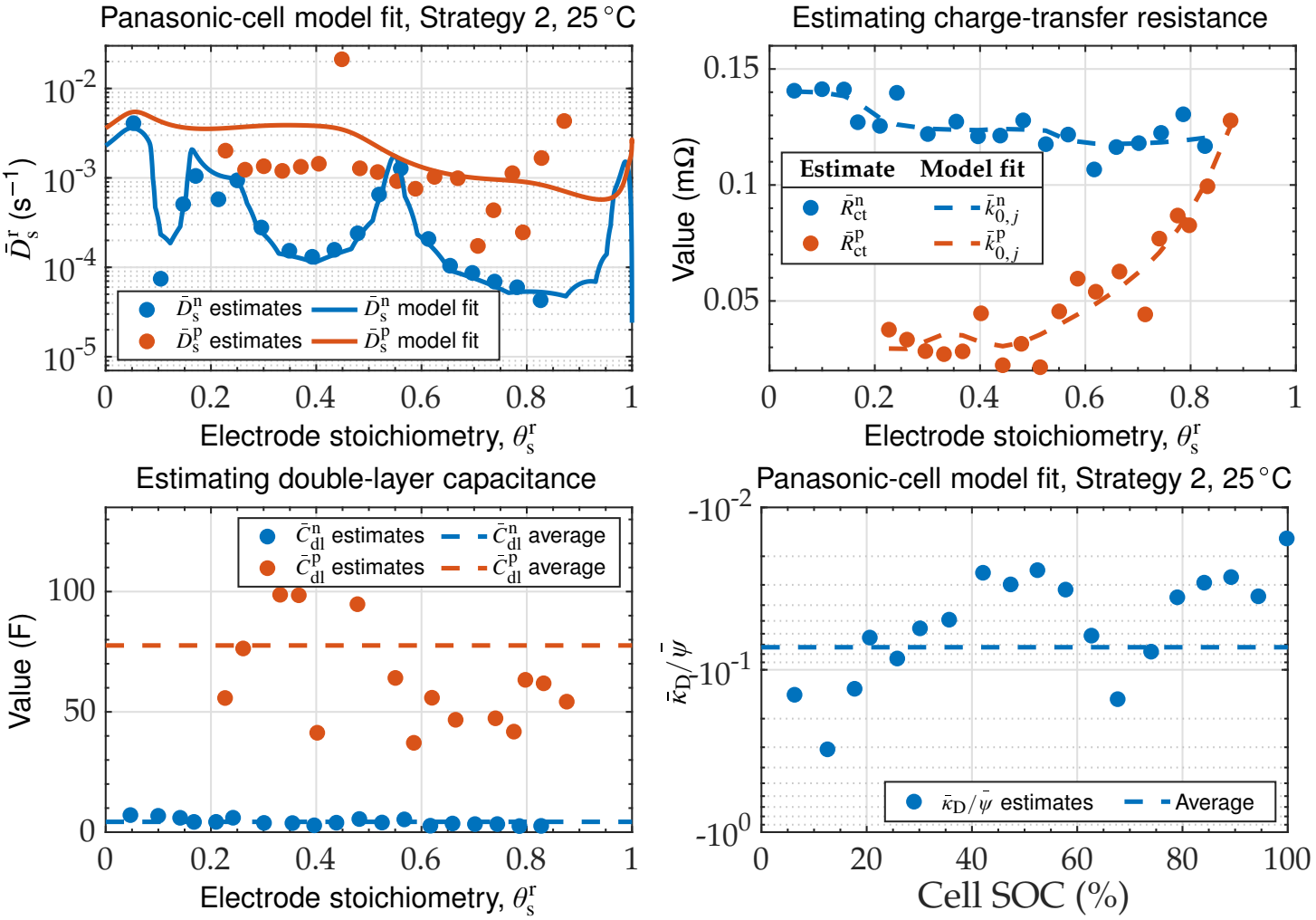

- The Baker–Verbrugge SOC-dependent solid-diffusion model appears to work well for the negative electrode, but perhaps less well for the positive (we don’t know why; perhaps θ_s^p is still poorly calibrated).
- The MSMR model for SOC-dependent charge-transfer resistance appears to work well for both electrodes.

- The data are inconclusive regarding whether $\bar{C}_{\mathrm{dl}}$ and $\bar{\kappa}_{\mathrm{D}}/\bar{\psi}$ are SOC-dependent (or, voltage-dependent).

Temperature dependence

- Many parameters are temperature-dependent: use Arrhenius reln.:

$$\bar{\Psi}(T) = \bar{\Psi}_{\mathrm{ref}} \underbrace{\exp\left(\frac{E_{\bar{\Psi}}}{R}\left(\frac{1}{T_{\mathrm{ref}}} - \frac{1}{T}\right)\right)}_{\text{temperature-dependent factor}},$$

  where $\bar{\Psi}_{\mathrm{ref}}$ is parameters's value at reference temperature T_{ref} (e.g., $T_{\mathrm{ref}} = 298.15\,\mathrm{K}$) and $E_{\bar{\Psi}}$ is its activation energy [$\mathrm{J\,mol^{-1}}$].

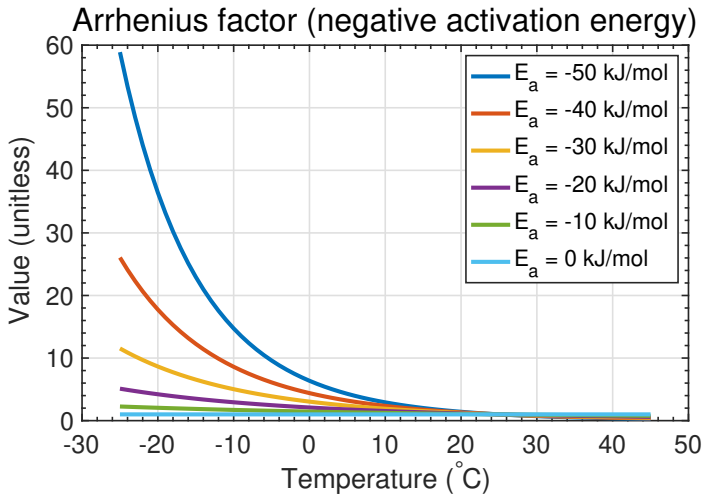

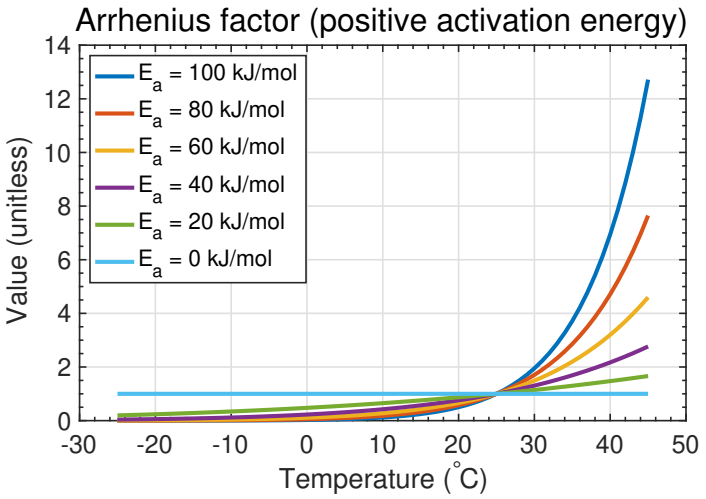

- Conductivities, diffusivities, and reaction-rate constants increase as temperature increases.
- Resistances decrease as temperature increases; use same equation, but activation energies are negative.
- Activation energies that must be found are tabulated to right.

Negative electrode	Separator	Positive electrode
$E^{\mathrm{n}}_{\bar{\sigma}}$		$E^{\mathrm{p}}_{\bar{\sigma}}$
$E^{\mathrm{n}}_{\bar{k}_0}$		$E^{\mathrm{p}}_{\bar{k}_0}$
$E^{\mathrm{n}}_{\bar{D}_{\mathrm{s}}}$		$E^{\mathrm{p}}_{\bar{D}_{\mathrm{s}}}$
$E^{\mathrm{n}}_{\bar{R}_{\mathrm{f}}}$		$E^{\mathrm{p}}_{\bar{R}_{\mathrm{f}}}$
$E^{\mathrm{n}}_{\bar{R}^{\mathrm{sf}}_{\mathrm{dl}}}$		$E^{\mathrm{p}}_{\bar{R}^{\mathrm{sf}}_{\mathrm{dl}}}$
$E^{\mathrm{n}}_{\bar{C}^{\mathrm{sf}}_{\mathrm{dl}}}$		$E^{\mathrm{p}}_{\bar{C}^{\mathrm{sf}}_{\mathrm{dl}}}$
$E_{\bar{\kappa}}$, $E_{\bar{\psi}}$ span all regions		

3.15: Pseudo-steady-state testing

- We are now at the final step of the parameter-estimation process.
- By this point, we have found values for all parameters except $\bar{\psi}$.
  - It turns out that $\bar{q}_{\mathrm{e}}^{\mathrm{r}}$ and κ_D cannot be separated from $\bar{\psi}$ using a linear test (e.g., EIS) so we must perform one final optimization.
- To estimate $\bar{\psi}$, we will reuse the constant-current discharge data collected for the discharge test and will regress those data against an enhanced single-particle model that includes electrolyte effects and is optimized to predict pseudo-steady-state behaviors of a cell.
  - We call this model the pseudo-steady-state or PSS model.
- The PSS approximation relies on the observation that when a constant current is applied to a lithium-ion cell, two things will happen after an initial transient:
  - All cell electrochemical variables described by stable TFs will approach steady-state values.
  - Cell electrochemical variables whose TFs have integration dynamics will continue to evolve over time, but their integrator-removed TFs will approach steady-state values.
- Therefore, while some variables continuously change, there is still an aspect of steady-state behavior that applies to all cell variables.[12]
- The PSS model takes advantage of this observation to build an enhanced SPM of the cell that can be used inside an optimization routine to determine $\bar{\psi}$.

[12] Since not all variables achieve steady state, we refer to the overall model as the *pseudo*-steady-state model.

- The flowchart below illustrates the interactions between the different components of the PSS reduced-order model (PSS-ROM):

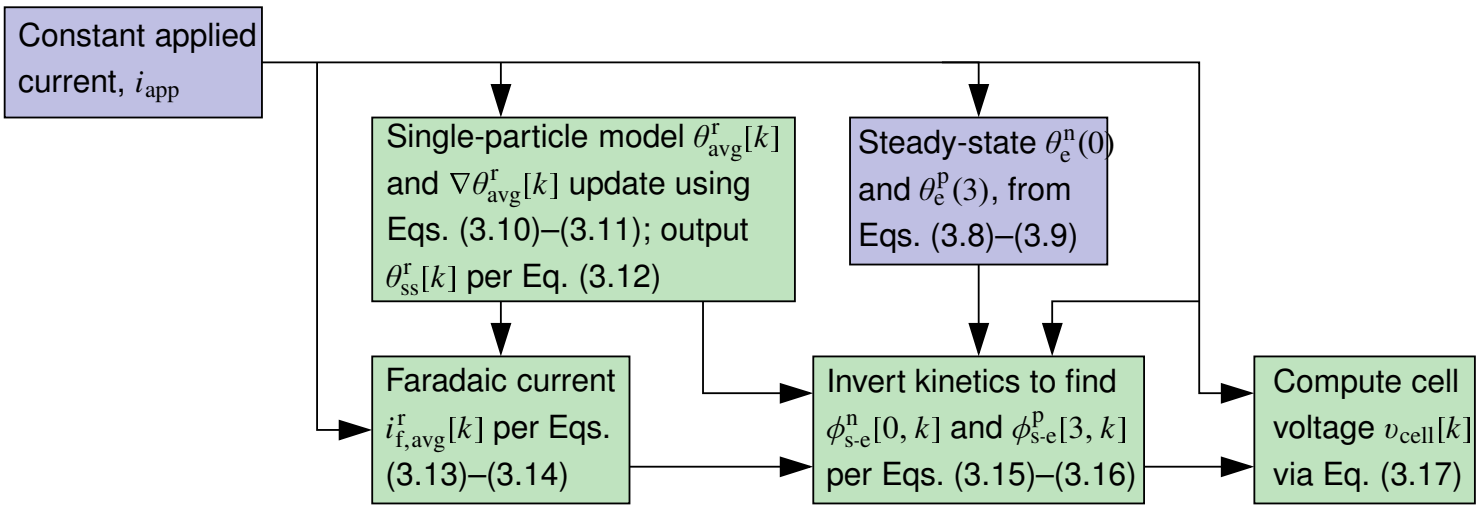

- It calculates voltage derived from:

$$\begin{aligned} v(t) &= \left[\phi^{\text{p}}_{\text{s-e}}(3,t) - \phi^{\text{n}}_{\text{s-e}}(0,t)\right] + \phi^{\text{p}}_{\text{e}}(3,t) - \phi^{\text{n}}_{\text{e}}(0,t) \\ &= \left[\phi^{\text{p}}_{\text{s-e}}(3,t) - \phi^{\text{n}}_{\text{s-e}}(0,t)\right] + \tilde{\phi}^{\text{p}}_{\text{e}}(3,t). \end{aligned}$$

- To find $\phi^{\text{r}}_{\text{s-e}}(\tilde{x},t)$, we recognize that it exists in the overpotential term:

$$\eta^{\text{r}}(\tilde{x},t) = \phi^{\text{r}}_{\text{s-e}}(\tilde{x},t) - U^{\text{r}}_{\text{ocp}}(\theta^{\text{r}}_{\text{ss}}(\tilde{x},t)).$$

- We solve for its values by inverting the kinetics equation, which further requires knowledge of $\theta^{\text{r}}_{\text{e}}(\tilde{x},t)$ and $\theta^{\text{r}}_{\text{ss}}(\tilde{x},t)$ at $\tilde{x} \in \{0,3\}$.
- The electrolyte profiles are assumed to attain steady state quickly during the discharge test, so we solve for their values using TF limits.
- The time-varying average (across electrode thickness) solid surface stoichiometries are calculated using an SPM for each electrode.
- We use an SPM with the same form as that used for discharge test.
- The solid/electrolyte potential differences are found by calculating cell overpotential, which is done by inverting the kinetics equations.

- Finally, electrolyte potential and solid/electrolyte potential difference are summed at $\tilde{x} = 3$ to form the cell voltage.
- The components of this process are described in the following.

PSS electrolyte approximation

- The PSS model assumes that the electrolyte variables can be adequately described by their steady-state values.
- These, in turn, are computed by evaluating their corresponding TFs in the limit as $s \to 0$.
- These low-frequency limits have already been calculated, and are listed in App. 2.d. For reference, we will need:
  - The low-frequency gain for debiased potential of the electrolyte, $\widetilde{\Phi}_{\rm e}^{\rm r}(\tilde{x},0)/I_{\rm app}(0)$ at $\tilde{x}=3$, which is:

$$\frac{\widetilde{\Phi}_{\rm e}^{\rm r}(3,0)}{I_{\rm app}(0)} = \left(\frac{\bar{\kappa}_{\rm D}}{\bar{\psi}} - 1\right)\left(\frac{1}{2\bar{\kappa}^{\rm n}} + \frac{1}{2\bar{\kappa}^{\rm p}} + \frac{1}{\bar{\kappa}^{\rm s}}\right).$$

    - Notice that the $\bar{\kappa}_{\rm D}/\bar{\psi}$ term is not decoupled in this expression.
    - Therefore, its contribution to cell voltage will not assist us in distinguishing $\bar{\kappa}_{\rm D}$ versus $\bar{\psi}$.
  - The low-frequency gains for debiased concentration of lithium in the electrolyte, $\widetilde{\Theta}_{\rm e}^{\rm r}(\tilde{x},0)/I_{\rm app}(0)$ at $\tilde{x} \in \{0,3\}$, which are:

$$\frac{\widetilde{\Theta}_{\rm e}^{\rm n}(0,0)}{I_{\rm app}(0)} = \frac{\bar{q}_{\rm e}^{\rm n}\bar{\kappa}^{\rm s}\bar{\kappa}^{\rm p} + 3\bar{q}_{\rm e}^{\rm s}(\bar{\kappa}^{\rm s}\bar{\kappa}^{\rm p} + \bar{\kappa}^{\rm n}\bar{\kappa}^{\rm p}) + \bar{q}_{\rm e}^{\rm p}(2\bar{\kappa}^{\rm n}\bar{\kappa}^{\rm s} + 3\bar{\kappa}^{\rm s}\bar{\kappa}^{\rm p} + 6\bar{\kappa}^{\rm n}\bar{\kappa}^{\rm p})}{6\bar{\kappa}^{\rm n}\bar{\kappa}^{\rm s}\bar{\kappa}^{\rm p}\bar{\psi}T(\bar{q}_{\rm e}^{\rm n} + \bar{q}_{\rm e}^{\rm s} + \bar{q}_{\rm e}^{\rm p})} \tag{3.8}$$

$$\frac{\widetilde{\Theta}_{\rm e}^{\rm p}(3,0)}{I_{\rm app}(0)} = \frac{-\bar{q}_{\rm e}^{\rm n}(2\bar{\kappa}^{\rm s}\bar{\kappa}^{\rm p}+3\bar{\kappa}^{\rm n}\bar{\kappa}^{\rm s}+6\bar{\kappa}^{\rm n}\bar{\kappa}^{\rm p}) - 3\bar{q}_{\rm e}^{\rm s}(\bar{\kappa}^{\rm n}\bar{\kappa}^{\rm s}+\bar{\kappa}^{\rm n}\bar{\kappa}^{\rm p}) - \bar{q}_{\rm e}^{\rm p}\bar{\kappa}^{\rm n}\bar{\kappa}^{\rm s}}{6\bar{\kappa}^{\rm n}\bar{\kappa}^{\rm s}\bar{\kappa}^{\rm p}\bar{\psi}T(\bar{q}_{\rm e}^{\rm n} + \bar{q}_{\rm e}^{\rm s} + \bar{q}_{\rm e}^{\rm p})}. \tag{3.9}$$

- In these equations, note that we can divide numerator and denominator by $\bar{\psi}$ to achieve:

$$\frac{\widetilde{\Theta}_{\mathrm{e}}^{\mathrm{n}}(0,0)}{I_{\mathrm{app}}(0)} = \frac{\frac{\bar{q}_{\mathrm{e}}^{\mathrm{n}}}{\bar{\psi}}\bar{\kappa}^{\mathrm{s}}\bar{\kappa}^{\mathrm{p}} + 3\frac{\bar{q}_{\mathrm{e}}^{\mathrm{s}}}{\bar{\psi}}(\bar{\kappa}^{\mathrm{s}}\bar{\kappa}^{\mathrm{p}} + \bar{\kappa}^{\mathrm{n}}\bar{\kappa}^{\mathrm{p}}) + \frac{\bar{q}_{\mathrm{e}}^{\mathrm{p}}}{\bar{\psi}}(2\bar{\kappa}^{\mathrm{n}}\bar{\kappa}^{\mathrm{s}} + 3\bar{\kappa}^{\mathrm{s}}\bar{\kappa}^{\mathrm{p}} + 6\bar{\kappa}^{\mathrm{n}}\bar{\kappa}^{\mathrm{p}})}{6\bar{\kappa}^{\mathrm{n}}\bar{\kappa}^{\mathrm{s}}\bar{\kappa}^{\mathrm{p}}[\bar{\boldsymbol{\psi}}]T\frac{\bar{q}_{\mathrm{e}}^{\mathrm{n}}+\bar{q}_{\mathrm{e}}^{\mathrm{s}}+\bar{q}_{\mathrm{e}}^{\mathrm{p}}}{\bar{\psi}}}$$

$$\frac{\widetilde{\Theta}_{\mathrm{e}}^{\mathrm{p}}(3,0)}{I_{\mathrm{app}}(0)} = \frac{-\frac{\bar{q}_{\mathrm{e}}^{\mathrm{n}}}{\bar{\psi}}(2\bar{\kappa}^{\mathrm{s}}\bar{\kappa}^{\mathrm{p}}+3\bar{\kappa}^{\mathrm{n}}\bar{\kappa}^{\mathrm{s}}+6\bar{\kappa}^{\mathrm{n}}\bar{\kappa}^{\mathrm{p}}) - 3\frac{\bar{q}_{\mathrm{e}}^{\mathrm{s}}}{\bar{\psi}}(\bar{\kappa}^{\mathrm{n}}\bar{\kappa}^{\mathrm{s}}+\bar{\kappa}^{\mathrm{n}}\bar{\kappa}^{\mathrm{p}}) - \frac{\bar{q}_{\mathrm{e}}^{\mathrm{p}}}{\bar{\psi}}\bar{\kappa}^{\mathrm{n}}\bar{\kappa}^{\mathrm{s}}}{6\bar{\kappa}^{\mathrm{n}}\bar{\kappa}^{\mathrm{s}}\bar{\kappa}^{\mathrm{p}}[\bar{\boldsymbol{\psi}}]T\frac{\bar{q}_{\mathrm{e}}^{\mathrm{n}}+\bar{q}_{\mathrm{e}}^{\mathrm{s}}+\bar{q}_{\mathrm{e}}^{\mathrm{p}}}{\bar{\psi}}}.$$

  - In both expressions, we retain coupled $\bar{q}_{\mathrm{e}}^{\mathrm{r}}/\bar{\psi}$ terms.
  - But, they also have a decoupled $\bar{\psi}$ term in the denominators (typeset in boldface with brackets as $[\bar{\boldsymbol{\psi}}]$ for emphasis).
  - It is the presence of this decoupled $\bar{\psi}$ term that allows us to use the PSS test to estimate $\bar{\psi}$ independently of $\bar{\kappa}_{\mathrm{D}}$ and $\bar{q}_{\mathrm{e}}^{\mathrm{r}}$.

PSS average solid-surface approximation

- To compute the time-varying average solid-surface stoichiometry, we adopt the SPM of the discharge test.
- But, it is expressed as a continuous-time state-space model and we desire to convert it to a discrete-time model for efficient computation.
- That is, we wish to convert a generic single-variable state-space form,

$$\dot{x}(t) = ax(t) + bu(t)$$

$$y(t) = cx(t) + du(t),$$

  to a model that is equivalent at the sample points:

$$x[k] = a_{\mathrm{d}}x[k-1] + b_{\mathrm{d}}u[k-1]$$

$$y[k] = cx[k] + du[k].$$

- We employed a zero-order-hold approach to perform this conversion in Ch. 2 of ECE5710, where the result was found to be:[13]

$$x[k] = \underbrace{e^{aT_\mathrm{s}}}_{a_\mathrm{d}} x[k-1] + \frac{1}{a}\left(e^{aT_\mathrm{s}} - 1\right) bu[k-1].$$

- Applying this to the SPM, we achieve discrete-time recurrences for the two SPM states (where: $a_\mathrm{d}^\mathrm{r} = \exp\left(-30T_\mathrm{s}\bar{D}_\mathrm{s}^\mathrm{r}(\theta_\mathrm{ss}^\mathrm{r}[k-1])\right)$):

$$\theta_\mathrm{avg}^\mathrm{r}[k] = \theta_\mathrm{avg}^\mathrm{r}[k-1] - \frac{T_\mathrm{s}}{3600Q^\mathrm{r}} i_\mathrm{f,avg}^\mathrm{r}[k-1] \tag{3.10}$$

$$\nabla\theta_\mathrm{avg}^\mathrm{r}[k] = a_\mathrm{d}^\mathrm{r}\nabla\theta_\mathrm{avg}^\mathrm{r}[k-1] + \frac{a_\mathrm{d}^\mathrm{r} - 1}{14400Q^\mathrm{r}\bar{D}_\mathrm{s}^\mathrm{r}(\theta_\mathrm{ss}^\mathrm{r}[k-1])} i_\mathrm{f,avg}^\mathrm{r}[k-1]. \tag{3.11}$$

- The output average surface concentration is computed as:

$$\theta_\mathrm{ss}^\mathrm{r}[k] = \theta_\mathrm{avg}^\mathrm{r}[k] + \frac{8}{35}\nabla\theta_\mathrm{avg}^\mathrm{r}[k] + \frac{-1/378\,000}{Q^\mathrm{r}\bar{D}_\mathrm{s}^\mathrm{r}(\theta_\mathrm{ss}^\mathrm{r}[k-1])} i_\mathrm{f,avg}^\mathrm{r}[k]. \tag{3.12}$$

- The average faradaic current for these equations is computed via the dc gains:

$$i_\mathrm{f,avg}^\mathrm{n}[k] = \frac{3600Q}{3600Q - \bar{C}_\mathrm{dl,eff}^\mathrm{n}\left|\theta_{100}^\mathrm{n} - \theta_0^\mathrm{n}\right|\left[U_\mathrm{ocp}^\mathrm{n}\right]'} i_\mathrm{app} \tag{3.13}$$

$$i_\mathrm{f,avg}^\mathrm{p}[k] = \frac{-3600Q}{3600Q - \bar{C}_\mathrm{dl,eff}^\mathrm{p}\left|\theta_{100}^\mathrm{p} - \theta_0^\mathrm{p}\right|\left[U_\mathrm{ocp}^\mathrm{p}\right]'} i_\mathrm{app}. \tag{3.14}$$

- Note that these values are time-varying, since the input to the OCP derivative function is $\theta_\mathrm{ss}^\mathrm{r}$, which is also time-varying.

Kinetics inversion

- Solid/electrolyte potential difference is found by inverting the kinetics.

[13] This applies only when $a \neq 0$. When $a = 0$, we simply integrate over one time step, so: $x[k] = x[k-1] + bT_s u[k-1]$.

- In general, this can be done using a nonlinear optimization.

- For simplicity, we consider a simplified MSMR model where $\alpha_j^{\mathrm{r}} = 0.5$.
  - In this case, we can solve in closed form.

- We start with the faradaic current, which can be written as:

$$i_{\mathrm{f}} = 2\left(\sum_{j=1}^{J} i_{0,j}\right)\sinh\left(\frac{f}{2}\eta\right),$$

where $\eta = \phi_{\text{s-e}} - U_{\mathrm{ocp}}(\theta_{\mathrm{ss}}) - \bar{R}_{\mathrm{f}} i_{\mathrm{f+dl}}$, and:

$$i_{0,j} = \bar{k}_{0,j}\sqrt{(\theta_{\mathrm{e}})(X_j - x_j)^{\omega_j}(x_j)^{\omega_j}}$$

$$x_j = \frac{X_j}{1 + \exp(f(U_{\mathrm{ocp}}(\theta_{\mathrm{ss}}) - U_j^0)/\omega_j)}.$$

- The interfacial potential difference is then approximated as:

$$\phi_{\text{s-e}}[\tilde{x}, k] = \frac{2}{f}\mathrm{asinh}\left(\frac{i_{\mathrm{f,avg}}[\tilde{x}, k]}{2\sum_{j=1}^{J} i_{0,j}}\right) + U_{\mathrm{ocp}}(\theta_{\mathrm{ss}}[\tilde{x}, k]) + \bar{R}_{\mathrm{f}} i_{\mathrm{f+dl,avg}}.$$

- The interfacial potential differences at each current collector are required to compute the cell's voltage. They are:

$$\phi_{\text{s-e}}^{\mathrm{n}}[0, k] = \frac{2}{f}\mathrm{asinh}\left(\frac{i_{\mathrm{f,avg}}^{\mathrm{n}}[k]}{2\sum_{j=1}^{J}\bar{k}_{0,j}^{\mathrm{n}}\sqrt{\theta_{\mathrm{e}}^{\mathrm{n}}(0)(X_j^{\mathrm{n}} - x_j^{\mathrm{n}}[k])^{\omega_j^{\mathrm{n}}}(x_j^{\mathrm{n}}[k])^{\omega_j^{\mathrm{n}}}}}\right)$$
$$+ U_{\mathrm{ocp}}^{\mathrm{n}}(\theta_{\mathrm{ss}}^{\mathrm{n}}[k]) + \bar{R}_{\mathrm{f}}^{\mathrm{n}} i_{\mathrm{app}}, \tag{3.15}$$

which appears in the expression for $\phi_{\mathrm{e}}^{\mathrm{p}}[3, k]$, and,

$$\phi_{\text{s-e}}^{\mathrm{p}}[3, k] = \frac{2}{f}\mathrm{asinh}\left(-\frac{i_{\mathrm{f,avg}}^{\mathrm{p}}[k]}{2\sum_{j=1}^{J}\bar{k}_{0,j}^{\mathrm{p}}\sqrt{\theta_{\mathrm{e}}^{\mathrm{p}}(3)(X_j^{\mathrm{p}} - x_j^{\mathrm{p}}[k])^{\omega_j^{\mathrm{p}}}(x_j^{\mathrm{p}}[k])^{\omega_j^{\mathrm{p}}}}}\right)$$
$$+ U_{\mathrm{ocp}}^{\mathrm{p}}(\theta_{\mathrm{ss}}^{\mathrm{p}}[k]) - \bar{R}_{\mathrm{f}}^{\mathrm{p}} i_{\mathrm{app}}. \tag{3.16}$$

Cell voltage

- The cell voltage is synthesized from the potential difference between the current collectors.
- Using the profile calculated previously for the electrolyte potential, the expression becomes:

$$v_{\text{cell}}[k] = \phi^{\text{p}}_{\text{s-e}}[3,k] - \phi^{\text{n}}_{\text{s-e}}[0,k] + \left(\frac{\bar{\kappa}_D}{\bar{\psi}} - 1\right)\left(\frac{1}{2\bar{\kappa}^{\text{n}}} + \frac{1}{\bar{\kappa}^{\text{s}}} + \frac{1}{2\bar{\kappa}^{\text{p}}}\right) i_{\text{app}}. \tag{3.17}$$

Summary of the PSS-ROM

- The entire PSS-ROM has now been derived.
- Here is a quick summary of what is necessary to compute cell voltage for a constant-current discharge simulation:
- At the beginning of the simulation, we must initialize variables.
  - We initialize $\theta^{\text{r}}_{\text{avg}}[0] = \theta^{\text{r}}_{\text{s},0}$ and $\nabla\theta^{\text{r}}_{\text{avg}}[0] = 0$.
- During the simulation, every time step:
  - We update $\theta^{\text{r}}_{\text{avg}}[k]$ using Eq. (3.10).
  - We also update $\nabla\theta^{\text{r}}_{\text{avg}}[k]$ using Eq. (3.11).
  - We then calculate $\theta^{\text{r}}_{\text{ss}}[k]$ using Eq. (3.12).
  - We solve for $\phi^{\text{n}}_{\text{s-e}}[0,k]$ and $\phi^{\text{p}}_{\text{s-e}}[3,k]$ using Eqs. (3.15)–(3.16).
  - Finally, we solve for cell voltage using Eq. (3.17).

Validating the $\bar{\psi}$ estimate

- The PSS method was compared extensively to COMSOL full-order-model results in the original reference by Guest et al.
- Here, we quickly comment on results when using it to estimate $\bar{\psi}$.

- The first set of results sought to estimate $\bar{\psi}$ for the NMC30 cell when all other parameter values were considered to be known exactly.
- Table shows optimization relative errors in estimating $\bar{\psi}$ when using simulated constant-current discharges.

Estimating $\bar{\psi}$ in simulation using the PSS method. The true value was $8.15\times10^{-5}\,\mathrm{V\,K^{-1}}$.

Rate	Estimate	Rel. Error
C/10	6.55×10^{-5}	19.7 %
C/5	8.63×10^{-5}	−5.9 %
C/2	1.05×10^{-4}	−28.6 %
1C	1.10×10^{-4}	−34.7 %

- At both very low and high discharge rates, the voltage-prediction PSS-model approximation errors rival the contribution to voltage by $\bar{\psi}$ and so the results begin to degrade.
- However, at moderate rates in the neighborhood of C/5 for this simulation test case, estimates of $\bar{\psi}$ are very good.
- We also applied the methods to the Panasonic cell using C/2 data.
- The optimized value of $\bar{\psi}$ compares favorably with the value for the NMC30 cell.

3.16: MATLAB toolbox

- We return to the overview of the MATLAB toolbox from Ch. 2.

Lithium-ion toolbox functions for parameter estimation and model simulation

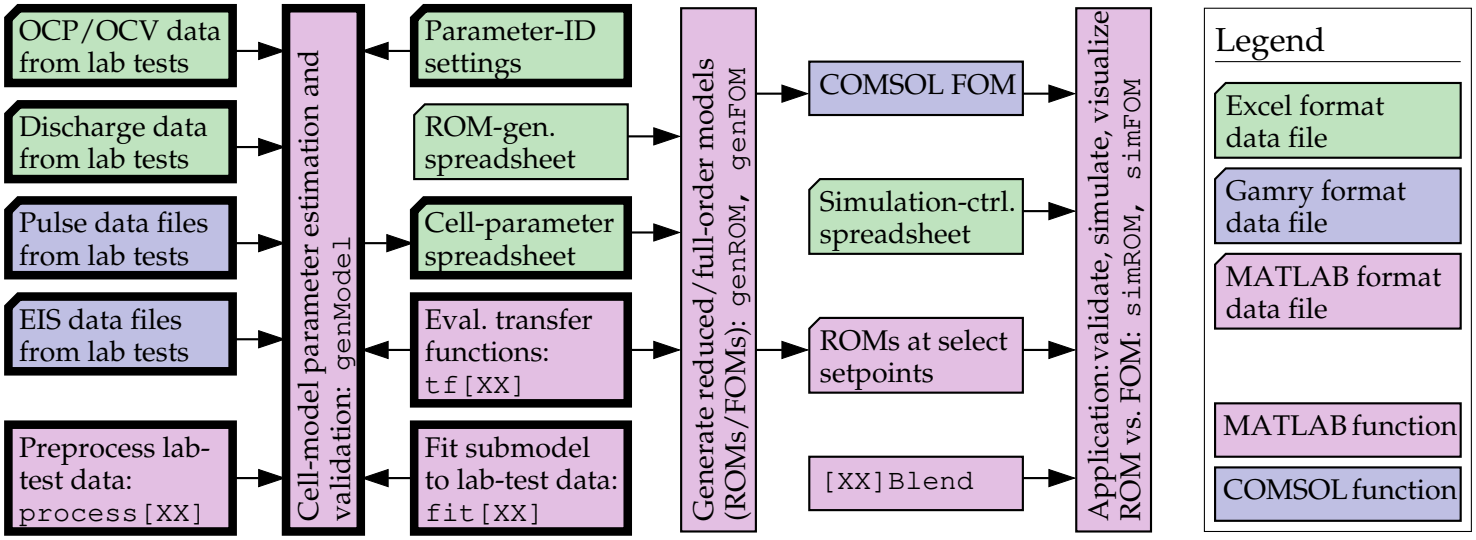

- Lab data from different tests are preprocessed by different routines denoted `process[XX]` for each test.
- Then, optimization routines `fit[XX]` are executed to fit subsets of model parameter values to the data from individual lab tests.
- The process can be automated via `genModel` or subfunctions can be executed manually.
- The figure on the next page presents in more detail the functionality of the toolbox related to parameter estimation.
- In general, lab-test data collected from different equipment will originate in multiple formats.
- For example, data collected from Arbin cell-cycling equipment is stored in Excel spreadsheet format; data collected from Gamry Instruments potentiostats is stored in text "`dat`" file format.

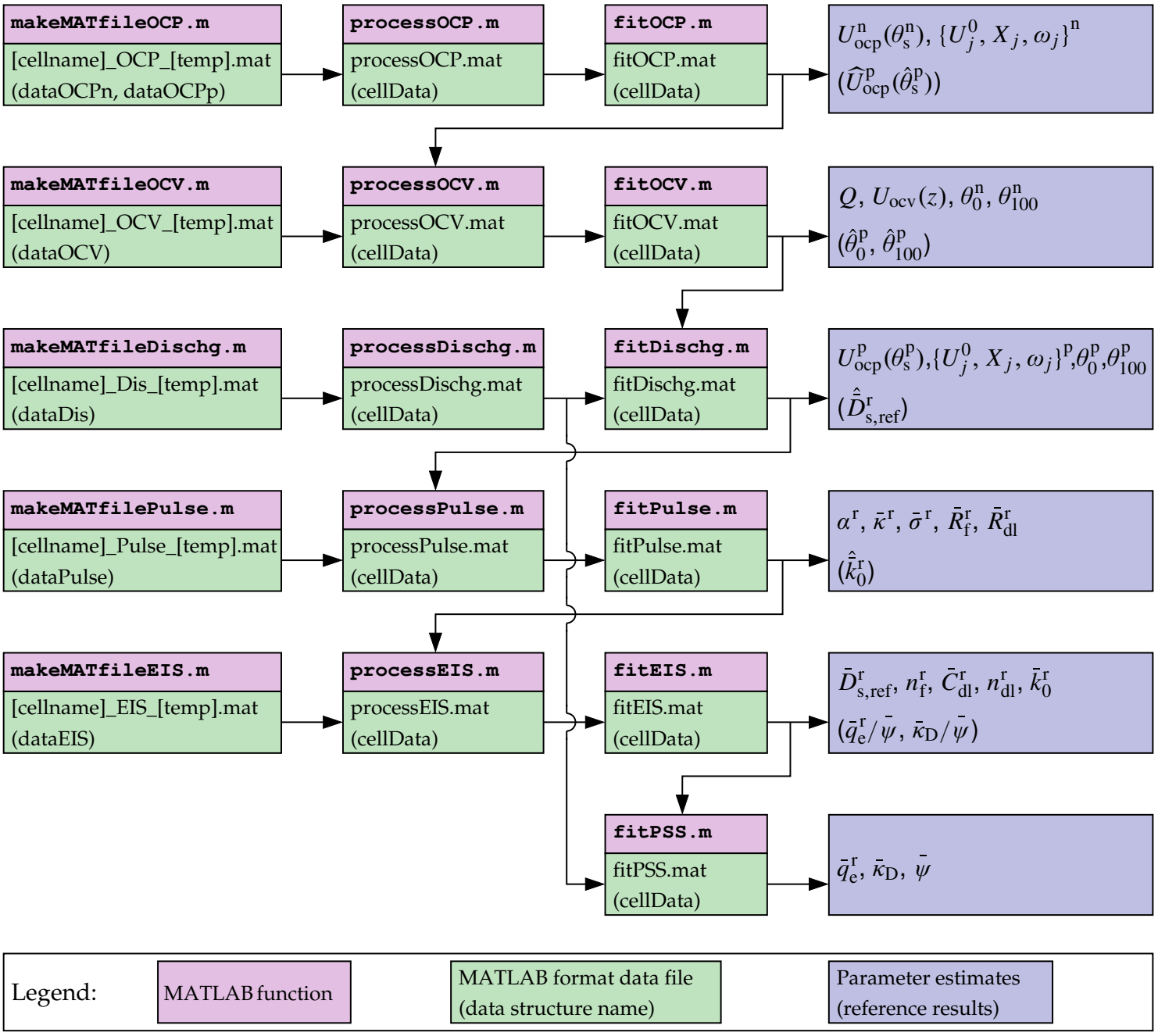

- These data must be converted to a standard format to be used by the processing routines.
- The toolbox provides functions `makeMATfile[XX]` that convert the demonstration data provided with the toolbox to the standard format.

- If you happen to use different equipment, you will need to create your own `makeMATfile` codes to convert between the format exported by that equipment and the required format for use by the toolbox.
- Examining the code in the existing `makeMATfile[XX]` functions should help to see what these required formats happen to be.
- Once the data are in the desired format, different `process[XX]` functions perform some preliminary preprocessing steps on the data.
- For example, `processOCP` uses the histogram method to compute calibrated discharge voltage versus capacity and charge voltage versus capacity curves, along with differential capacity estimates.
- As another example, `processPulse` estimates the $\widehat{R}_0$ values for every testing setpoint.
- The `process[XX]` functions do not directly run optimizations to determine estimates of LPM parameter values; they simply preprocess data to make them ready for the optimizations.
- The `fit[XX]` functions perform the parameter-estimation optimizations using the data collected at the present process step.
- The final parameter estimates produced at each step are indicated in the figure, as are reference results that are produced for use as initial guesses in later steps in the parameter-estimation process.
- The figure also shows the variables and files produced by each toolbox function.
- The most common variable is the `cellData` structure, which ultimately contains estimates of all model parameter values.

- These parameters can be written to a human-readable Excel spreadsheet format using the `saveCellParams` function (not shown in the figure).
- The spreadsheet can be loaded into MATLAB using `loadCellParams`, as discussed in Ch. 2.
- For further reference, the reader is encouraged to examine the MATLAB example functions in the Ch. 3 folder of the toolbox.
- These will help to illustrate how the toolbox functions.

Where to from here?

- Physics-based parameter estimation is not yet a mature topic.
- Still evolving and results improving over time.
- Have not discussed cell-teardown methods in much detail.
  - Until data-based methods are validated, will probably use some combination of cell teardown and optimization.
- Key point: Can't tear down physical cells during operation.
  - Some kind of data method will be needed to adapt model values as cells age.
  - This is why we continue to seek to understand and improve in this direction.
- But, what can we do once we have found the parameter values?
  - Should be able to simulate cells and packs and use models for BMS tasks like state estimation, computing performance limits, etc.
- In next chapter, we look at time-domain simulations.

Appendix 3.a: Half-cell testing to determine electrode OCP

- The half-cell OCP test protocol is presented here: it includes careful calibration steps to ensure highest-quality results.
- Before test begins, half cell is resting at $v_{\max}$ (via running Script #4).

OCP test Script #1 (at test temperature)

- The first OCP script determines low-rate constant-current discharge voltage as a function of ampere-hours discharged:

1. Soak the fully charged half cell at the test temperature for at least two hours to ensure a uniform temperature throughout.
2. Discharge half cell at a constant rate until its voltage equals $v_{\min}$.
   - The constant-current rate might be C/30 or C/100, for example.

- Note: terminal and resting voltages are not equal; if the half cell were allowed to rest following step #2, voltage would rebound above $v_{\min}$.
- Therefore the OCP of the half cell at the test temperature at the final moment of step #2 is known to be above $v_{\min}$.

OCP test Script #2 (at 25 °C*)*

- Electrode OCP is temperature-dependent. Therefore, for all of our OCP relationships at all temperatures to be consistent, we must calibrate the tests at a fixed temperature.
- We choose to do so at 25 °C since this is the default calibration temperature for cell-level OCV testing.
- The goal of test script #2 is to move the half-cell (resting) OCP to $v_{\min}$ at this calibration temperature. We perform these steps:

3. Soak the half cell at 25 °C for at least two hours to ensure a uniform temperature throughout the cell.
4. Dis/charge the half cell to $v_{\min}$ at same constant-current rate as step #2. Then, hold the half cell at that voltage for several hours.

- At the end of step #4, the OCP of the electrode under test in the half cell is as close to $v_{\min}$ as we are able to achieve at the calibration temperature in a lab setting.
- We will assume that the OCP is equal to $v_{\min}$ although we realize that there will be some testing error introduced by this assumption.

OCP test Script #3 (at test temperature)

- Next, we determine the charge voltage as a function of Ah charged:
  5. Soak the half cell at the test temperature for at least two hours to ensure a uniform temperature throughout.
  6. Charge the half cell at a constant-current rate until the half-cell terminal voltage equals $v_{\max}$.
- Note again: terminal and resting voltages are unequal; if cell were allowed to rest following step #6, voltage would relax below $v_{\max}$.
- Therefore the OCP of the half cell at the test temperature at the final moment of step #6 is known to be lower than $v_{\max}$.

OCP test Script #4 (at 25 °C)

- The final test script is implemented to calibrate the tests once again.
- The goal of test script #4 is to move the half-cell (resting) OCP to $v_{\max}$ at this calibration temperature. We now:

7. Soak the half cell at 25 °C for at least two hours to ensure a uniform temperature throughout.
8. Dis/charge the half cell to $v_{\max}$ at a constant-current rate. Then, hold the half cell at that voltage for several hours.

- At this point, we assume that the electrode OCP is equal to $v_{\max}$.
- During every step of the test, voltage, accumulated ampere-hours discharged, and accumulated ampere-hours charged are recorded periodically (*e.g.*, once per second).
- Script #4 is run first to "fully charge" the half cell; then others are run in sequence for a particular test temperature.
- Because a very low current rate is used, there is negligible heat generation in the cell, and we can consider all data points to be collected at the ambient test temperature for every script (but, temperature data can be measured as well to verify this assumption).

Initial data processing

- Measured data from OCP test scripts must undergo initial processing to create calibrated discharge voltage vs. relative stoichiometry $\tilde{\theta}_{\mathrm{s}}$ and calibrated charge voltage vs. relative stoichiometry $\tilde{\theta}_{\mathrm{s}}$.
- There are some subtle points if the test temperature is not 25 °C.
  - Prior to step 2, half cell is still resting at $\tilde{\theta}_{\mathrm{s}} = 0$, but its voltage is no longer $v_{\max}$ since $T \neq 25$ °C and OCP is temperature-dependent.
  - At end of step 2, half-cell $\tilde{\theta}_{\mathrm{s}} = 1$ *only* if the test temperature is 25 °C because, again, OCP is temperature-dependent, and the $v_{\min}$ specification defines $\tilde{\theta}_{\mathrm{s}} = 1$ only for 25 °C.

- At other temperatures, the actual value of $\tilde{\theta}_\mathrm{s}$ may be above or below 1.0 at the end of step 2.

- Similarly, at the end of step 6, the half cell will be at $\tilde{\theta}_\mathrm{s} = 0$ *only* if the test temperature is 25 °C.
  - At other temperatures, the actual value of $\tilde{\theta}_\mathrm{s}$ may be above or below zero at the end of step 6.
- This is why we must execute test scripts 2 and 4, to ensure that the half cell has reached a calibrated point before starting script 3 and then script 1 (for the next temperature to be tested).

- These considerations require some careful processing of the data.
- Let's consider processing data for test temperature 25 °C first.
  - This is the easiest case because all four scripts are then executed at 25 °C—no other temperatures are involved.
  - And, since voltages v_max and v_min are calibrated to 25 °C, the net ampere-hours discharged over all steps equals the capacity $\widetilde{Q}$ of the half cell over that voltage range.
- The net ampere-hours charged over all steps turns out to be slightly higher than $\widetilde{Q}$ since the coulombic efficiency of the half cell is not perfect. We compute the coulombic efficiency at 25 °C as

$$\eta(25\,^\circ\mathrm{C}) = \frac{\text{total ampere-hours discharged in all steps at } 25\,^\circ\mathrm{C}}{\text{total ampere-hours charged in all steps at } 25\,^\circ\mathrm{C}}.$$

- At a test temperature $T \neq 25\,^\circ\mathrm{C}$, we must follow a different approach.
- We don't know the value of $\tilde{\theta}_\mathrm{s}$ *a priori* at end of steps 2 and 6; but, we do know that $\tilde{\theta}_\mathrm{s} = 1$ at end of step 4 and that $\tilde{\theta}_\mathrm{s} = 0$ at end of step 8.

- Knowing this, we compute coulombic efficiency at temperature T:

$$\eta(T) = \frac{\text{total ampere-hours discharged}}{\text{total ampere-hours charged at temperature } T} - \eta(25\,^\circ\text{C})\frac{\text{total ampere-hours charged at } 25\,^\circ\text{C}}{\text{total ampere-hours charged at temperature } T}.$$

- We can now compute a value of $\tilde{\theta}_\text{s}$ corresponding to every data sample in the test.
- The depth-of-discharge (in Ah) at every point in time is calculated as

$$\begin{aligned}\text{DOD}(t) = {}& \text{total Ah discharged until } t \\ & - \eta(25\,^\circ\text{C}) \times \text{total Ah charged at } 25\,^\circ\text{C until } t \\ & - \eta(T) \times \text{total Ah charged at temperature } T \text{ until } t.\end{aligned}$$

- Using this metric, the half-cell capacity $\widetilde{Q}$ over the OCP range spanning v_min to v_max (measured at temperature T) is equal to the depth-of-discharge at the end of step 4.
- Likewise, the value of $\tilde{\theta}_\text{s}$ corresponding to every data sample is then

$$\tilde{\theta}_\text{s}(t) = \text{DOD}(t)/\widetilde{Q}.$$

- As a check, the value of $\tilde{\theta}_\text{s}$ at the end of step 4 must be 1, and the value of $\tilde{\theta}_\text{s}$ at the end of step 8 must be zero.
- In what follows, we use the calibrated lithiation (discharge) voltage versus $\tilde{\theta}_\text{s}$ from step #2 (always plotted as a blue line) and the calibrated delithiation (charge) voltage versus $\tilde{\theta}_\text{s}$ from step #6 (always plotted as a red line) in our calculations to determine electrode OCP.
- Here are some lab-test results that show the outcome of the process as described so far for a graphite material and an NMC material.

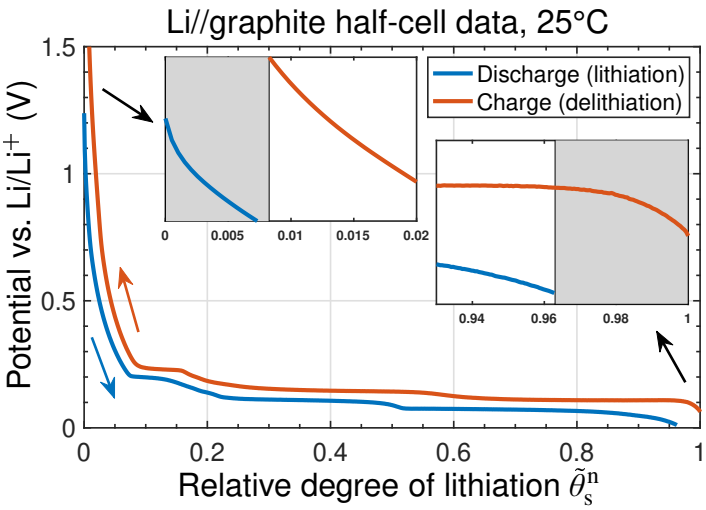

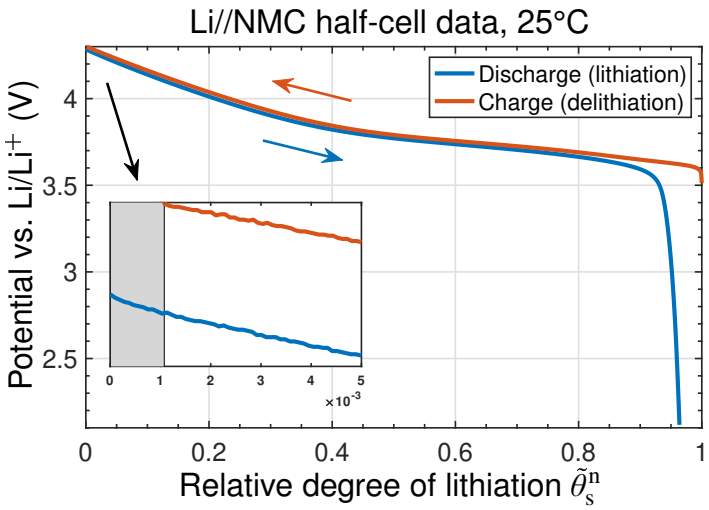

- Plot insets highlight regions of the calibrated dis/charge curves that illustrate the “missing-data problem”, described earlier.

Appendix 3.b: Practical computation of differential capacity

- In addition to the fundamental missing-data and inaccessible-lithium problems, we also encounter a practical data-quality problem.
- We wish to use differential-capacity estimates to identify equilibrium voltages and other electrochemical-reaction characteristics.
- Measured data always contain measurement noise and quantization errors.
- Quantization errors cause flat zero-change regions and result in divide-by-zero when evaluating $\mathrm{d}\tilde{\theta}_\mathrm{s}/\mathrm{d}\widetilde{U}_\mathrm{ocp}$ directly.

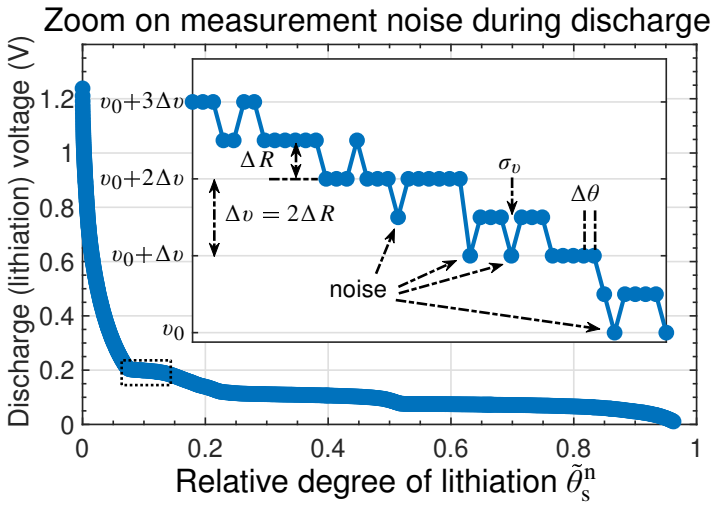

- Noise can cause OCP to appear to increase with $\tilde{\theta}_\mathrm{s}$ at some points.
- We know that the OCP function and differential capacity should be monotonically decreasing ($\mathrm{d}\widetilde{U}_\mathrm{ocp}/\mathrm{d}\tilde{\theta}_\mathrm{s} < 0$ and $\mathrm{d}\tilde{\theta}_\mathrm{s}/\mathrm{d}\widetilde{U}_\mathrm{ocp} < 0$), and so we can attempt to correct the data to enforce this feature.[14]
- Smoothing/filtering algorithms can be used to pre-process lab-test data before evaluating the differentiation.
  - However, many established smoothing methods can easily cause "under-fitting" or "over-fitting" problems, thereby distorting the information of the actual cell behaviors.
- In this section, we propose a simple "histogram counting" method, which can be programmed in MATLAB with only three lines of code.

[14] The differential figures in this chapter are drawn with positive magnitudes for clear visualizations among different data, even though actual functions are negative.

- The general idea is to partition the entire voltage range into constant-width intervals and count the number of data samples within each interval to determine the relative capacity per window.
  - A similar idea was proposed by Feng et al. and called the "Level Evaluation ANalysis" (LEAN) method.[15]
  - The "histogram counting" method is similar to the LEAN method but more straightforward to implement in MATLAB.
- There are three steps. First, we select a voltage interval, denoted as Δv, which is a critical term to impact the plateau resolution.
  - As suggested by Feng et al., Δv should k times the data sampling resolution ΔR, where k is an integer.
  - To minimize fluctuation, Δv should also be greater than magnitude of data-sampling error σ_v, yielding $(k-1)\,\Delta R \leq \sigma_v < k \cdot \Delta R = \Delta v$.
- After selecting the voltage window, the second step is to count the number of occurrences of data within each window, denoted as n_v.
  - This can be achieved simply in MATLAB via `histcounts.m`.
- The last step is to compute the stoichiometric interval spanned by each voltage window and from that the differential capacity.
  - The change in relative stoichiometry $\Delta\tilde{\theta}_s$ across an interval Δv (for constant current) is equal to the number of data samples in that interval multiplied by stoichiometric "width" of each data sample.

[15] X. Feng, Y. Merla, C. Weng, M. Ouyang, X. He, B. Y. Liaw, S. Santhanagopalan, X. Li, P. Liu, L. Lu, X. Han, D. Ren, Y. Wang, R. Li, C. Jin, P. Huang, M. Yi, L. Wang, Y. Zhao, Y. Patel, and G. Offer, "A reliable approach of differentiating discrete sampled-data for battery diagnosis," *eTransportation*, 3, 100051, (2020).

- The stoichiometric "width" of each data sample is $\max(\tilde{\theta}_s) - \min(\tilde{\theta}_s)$ for the dis/charge segment being analyzed divided by the number of samples N across that entire dis/charge segment.
- Therefore, we can write for some interval centered at voltage v_0,

$$\begin{bmatrix} \Delta\tilde{\theta}_s \text{ across} \\ \text{an interval} \end{bmatrix} = \begin{bmatrix} \text{count of samples} \\ \text{in the interval, } n_v \end{bmatrix} \times \frac{\max(\tilde{\theta}_s) - \min(\tilde{\theta}_s)}{N}.$$

- Then, (where $[\max(\tilde{\theta}_s) - \min(\tilde{\theta}_s)] < 1$ because of "missing-data")

$$\left.\frac{\mathrm{d}\tilde{\theta}_s}{\mathrm{d}\widetilde{U}_{ocp}}\right|_{v_0} \approx \begin{bmatrix} \text{count of samples } n_v(v_0) \\ \text{in the interval for } v_0 \end{bmatrix} \times \frac{[\max(\tilde{\theta}_s) - \min(\tilde{\theta}_s)]}{N\,\Delta v}.$$

- In summary, we compute smoothed differential capacity via 3 steps:

1. Specify a constant voltage interval Δv (e.g., $\Delta v = 2\,\text{mV}$).
2. Determine count of data samples, n_v, within each Δv (e.g., via `histcounts.m`). A smoothed $\widetilde{U}_{ocp}(\tilde{\theta}_s)$ relationship can be also be extracted from this step by integrating the histogram.
3. Compute the differential capacity via

$$\left.\frac{\mathrm{d}\tilde{\theta}_s}{\mathrm{d}\widetilde{U}_{ocp}}\right|_{v_0} \approx n_v(v_0)\frac{[\max(\tilde{\theta}_s) - \min(\tilde{\theta}_s)]}{N\,\Delta v}.$$

- Sample results are shown below:

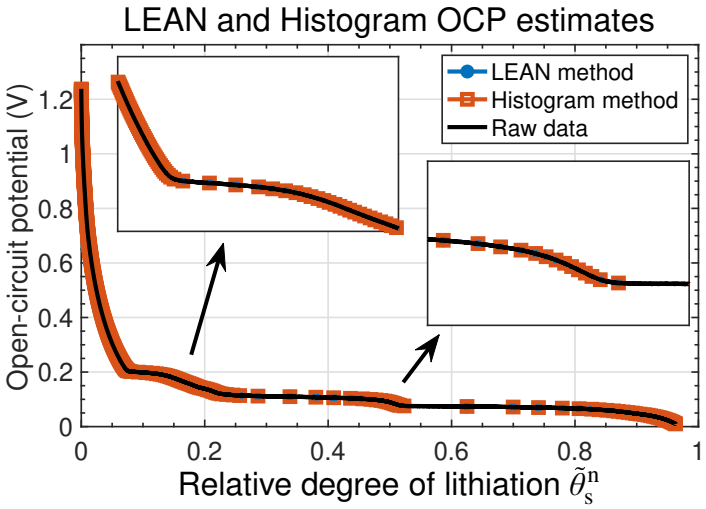

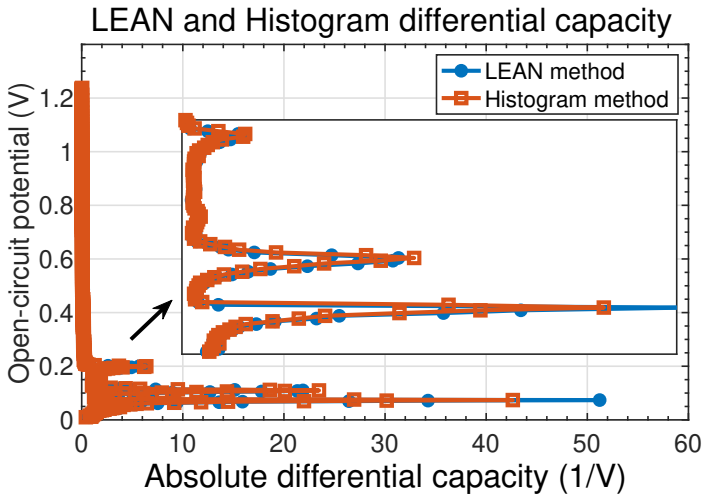

App. 3.c: Finding OCP without cell teardown: Observability problem

- We would like to find all PBM parameter values without cell teardown.
- So, we are compelled to ask, “can we determine both electrode OCP functions uniquely from the cell OCV function?”
- The answer turns out to be “no”: OCV information alone is insufficient to determine electrode OCP functions uniquely.
- We refer to this fact as the “observability problem,” which can be demonstrated fairly quickly.
- Consider an arbitrary function $f(z)$, where z is once again cell SOC.
- We can index $f(\cdot)$ using either $\theta_{\mathrm{s}}^{\mathrm{n}}$ or $\theta_{\mathrm{s}}^{\mathrm{p}}$ via:

$$z = \frac{\theta_{\mathrm{s}}^{\mathrm{n}} - \theta_{0}^{\mathrm{n}}}{\theta_{100}^{\mathrm{n}} - \theta_{0}^{\mathrm{n}}} = \frac{\theta_{\mathrm{s}}^{\mathrm{p}} - \theta_{0}^{\mathrm{p}}}{\theta_{100}^{\mathrm{p}} - \theta_{0}^{\mathrm{p}}}.$$

- Suppose we define biased estimates $\widehat{U}_{\mathrm{ocp}}^{\mathrm{r,bias}}$ of the true OCP by adding $f(z)$ to the true OCP function:

$$\widehat{U}_{\mathrm{ocp}}^{\mathrm{n,bias}}(\theta_{\mathrm{s}}^{\mathrm{n}}) = U_{\mathrm{ocp}}^{\mathrm{n}}(\theta_{\mathrm{s}}^{\mathrm{n}}) + f((\theta_{\mathrm{s}}^{\mathrm{n}} - \theta_{0}^{\mathrm{n}})/(\theta_{100}^{\mathrm{n}} - \theta_{0}^{\mathrm{n}}))$$

$$\widehat{U}_{\mathrm{ocp}}^{\mathrm{p,bias}}(\theta_{\mathrm{s}}^{\mathrm{p}}) = U_{\mathrm{ocp}}^{\mathrm{p}}(\theta_{\mathrm{s}}^{\mathrm{p}}) + f((\theta_{\mathrm{s}}^{\mathrm{p}} - \theta_{0}^{\mathrm{p}})/(\theta_{100}^{\mathrm{p}} - \theta_{0}^{\mathrm{p}})).$$

- Because $f(z)$ is arbitrary, $\widehat{U}_{\mathrm{ocp}}^{\mathrm{r,bias}} \neq U_{\mathrm{ocp}}$ in general. But, we cannot observe the bias in OCP estimates from an OCV measurement.
- If we attempted to do so, we would use the estimates of $\widehat{U}_{\mathrm{ocp}}^{\mathrm{r,bias}}$ to compute an estimate of OCV, $\widehat{U}_{\mathrm{ocv}}$:

$$\begin{aligned}\widehat{U}_{\mathrm{ocv}}(z) &= \widehat{U}_{\mathrm{ocp}}^{\mathrm{p,bias}}(\theta_{\mathrm{s}}^{\mathrm{p}}(z)) - \widehat{U}_{\mathrm{ocp}}^{\mathrm{n,bias}}(\theta_{\mathrm{s}}^{\mathrm{n}}(z)) \\ &= \left[U_{\mathrm{ocp}}^{\mathrm{p}}(\theta_{\mathrm{s}}^{\mathrm{p}}) + f((\theta_{\mathrm{s}}^{\mathrm{p}} - \theta_{0}^{\mathrm{p}})/(\theta_{100}^{\mathrm{p}} - \theta_{0}^{\mathrm{p}}))\right]\end{aligned}$$

$$- \left[U^{\mathrm{n}}_{\mathrm{ocp}}(\theta^{\mathrm{n}}_{\mathrm{s}}) + f((\theta^{\mathrm{n}}_{\mathrm{s}} - \theta^{\mathrm{n}}_{0})/(\theta^{\mathrm{n}}_{100} - \theta^{\mathrm{n}}_{0})) \right]$$

$$= U^{\mathrm{p}}_{\mathrm{ocp}}(\theta^{\mathrm{p}}_{\mathrm{s}}) - U^{\mathrm{n}}_{\mathrm{ocp}}(\theta^{\mathrm{n}}_{\mathrm{s}}) = U_{\mathrm{ocv}}(z).$$

- That is, the biased estimates of OCP combine in such a way that the biases cancel and the estimated OCV matches the true OCV exactly.
  - The error in electrode OCP estimates is not observable from a cell-level OCV measurement.
- We might also ask whether differential capacity might improve observability of the OCP functions from an OCV relationship.
  - Again, the answer is “no” (math omitted here).
- In retrospect, this result is not surprising.
  - We write OCV as the difference of two OCP functions.
  - We have two unknowns (the OCP functions) and a single equation.
  - We know that it is not possible to solve one equation uniquely for two unknowns.
- In sum, the “observability problem” is that cell-level OCV alone is insufficient to determine electrode-level OCP functions uniquely. Instead, we must proceed by making one of two assumptions:

  A1: We are able to fabricate half cells from electrode materials and measure OCP directly, as has been our assumption to this point.

  A2: Or, we will use a database approach, where we correlate cell-level OCV data with a database of OCP functions for known electrode materials.
- This section proposes two different strategies for how we might proceed if we cannot make Assumption A1:

1. We assume that the negative electrode has a known composition and identify positive-electrode characteristics from OCV tests; or
2. We assume that neither electrode is known but that we have a database of models of known materials against which we can compare cell measured OCV.

- These two approaches are presented below.

Assume that negative-electrode OCP is known

- We can combine a known negative-electrode OCP with a cell-level OPC estimate to develop a model of positive-electrode OCP.
- We restrict discussion to cells having graphite negative electrodes; however, we believe this approach can generalize to other materials.
- Graphite's OCP function has distinct features located at points "A", "B", and "C" that also appear quite visibly the cell's OCV function.

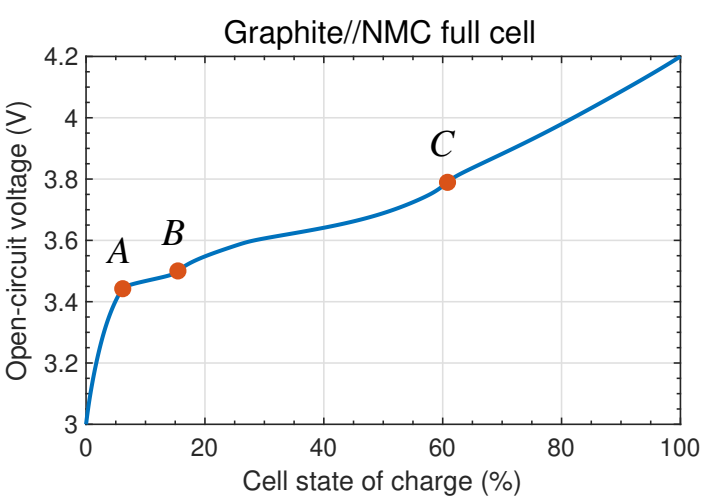

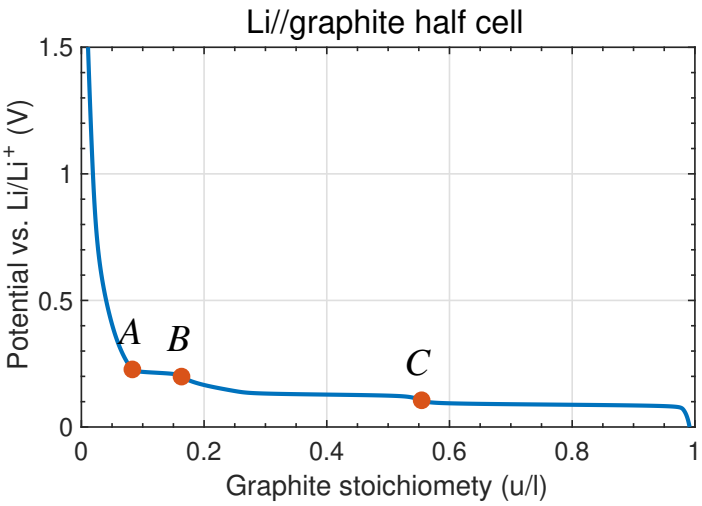

- These points can be found automatically:
  - A is determined from a peak in $\mathrm{d}^2U_{\mathrm{ocv}}/\mathrm{d}z^2$ and $\mathrm{d}^2U^{\mathrm{n}}_{\mathrm{ocp}}/\mathrm{d}\theta_{\mathrm{s}}^2$.
  - B and C are located at peaks in $\mathrm{d}U_{\mathrm{ocv}}/\mathrm{d}z$ and $\mathrm{d}U^{\mathrm{n}}_{\mathrm{ocp}}/\mathrm{d}\theta_{\mathrm{s}}$.

- Given the above information, the following four steps are then implemented to estimate cell- and electrode-level quantities:
  - Step 0: Use any of the four methods to produce an estimate of cell OCV vs. SOC, $\widehat{U}_{\rm ocv}\left(z\right)$, from cell dis/charge data.
  - Step 1: Correlate $\{A, B, C\}$ between cell OCV and graphite OCP.
    - Denote the cell-level SOCs of these points as z_A, z_B, and z_C, and the negative-electrode stoichiometries as $\theta^{\rm n}_{{\rm s},A}$, $\theta^{\rm n}_{{\rm s},B}$, and $\theta^{\rm n}_{{\rm s},C}$.
    - Use $\theta^{\rm n}_{\rm s}\left(z\right) = \theta^{\rm n}_0 + z\left(\theta^{\rm n}_{100} - \theta^{\rm n}_0\right)$ to solve for $\theta^{\rm n}_0$ and $\theta^{\rm n}_{100}$ via:

$$\begin{bmatrix} \theta^{\rm n}_{{\rm s},A} \\ \theta^{\rm n}_{{\rm s},B} \\ \theta^{\rm n}_{{\rm s},C} \end{bmatrix} = \begin{bmatrix} 1-z_A & z_A \\ 1-z_B & z_B \\ 1-z_C & z_C \end{bmatrix} \begin{bmatrix} \theta^{\rm n}_0 \\ \theta^{\rm n}_{100} \end{bmatrix}$$

$$\begin{bmatrix} \theta^{\rm n}_0 \\ \theta^{\rm n}_{100} \end{bmatrix} = \begin{bmatrix} 1-z_A & z_A \\ 1-z_B & z_B \\ 1-z_C & z_C \end{bmatrix}^{\dagger} \begin{bmatrix} \theta^{\rm n}_{{\rm s},A} \\ \theta^{\rm n}_{{\rm s},B} \\ \theta^{\rm n}_{{\rm s},C} \end{bmatrix},$$

      where the dagger (†) represents a matrix pseudo-inverse.
    - This is an over-determined set of equations: The pseudo-inverse solution gives the least-squares estimate of the unknown boundary values $\theta^{\rm n}_0$ and $\theta^{\rm n}_{100}$.
  - Step 2: Using computed negative-electrode operating boundaries, find MSMR model $\widehat{U}^{\rm p}_{\rm ocp}(\theta^{\rm p}_{\rm s})$ and optimize positive-electrode operating boundaries $\theta^{\rm p}_0$ and $\theta^{\rm p}_0$ by fitting to cell SOC vs. OCV.
    - To do so, we minimize the cost function:

$$J = \sum_k \left(z^{\rm cell}_k - z^{\rm ocp}_k\right)^2 + w\left(\frac{{\rm d}z_k}{{\rm d}U^{\rm cell}_{\rm ocv}} - \frac{{\rm d}z_k}{{\rm d}\widehat{U}^{\rm ocp}_{\rm ocv}}\right)^2$$

where $\mathrm{d}z_k/\mathrm{d}\widehat{U}_{\mathrm{ocv}}^{\mathrm{cell}}$ is cell differential capacity computed using OCV data and $\mathrm{d}z_k/\mathrm{d}\widehat{U}_{\mathrm{ocv}}^{\mathrm{ocp}}$ is cell differential capacity using electrode OCP data and ω is a weighting factor.

- The SOC estimates in the above cost function can be expressed using the MSMR model:

$$z_k^{\mathrm{ocp}} = \frac{\theta_{\mathrm{s}}^{\mathrm{p}}\left(z_k^{\mathrm{cell}}\right) - \theta_0^{\mathrm{p}}}{\theta_{100}^{\mathrm{p}} - \theta_0^{\mathrm{p}}}$$

$$\theta_{\mathrm{s}}^{\mathrm{p}}\left(z_k^{\mathrm{cell}}\right) = \sum_j \frac{X_j}{1 + \exp[f(\widehat{U}_{\mathrm{ocp}}^{\mathrm{p}}(\theta_{\mathrm{s}}^{\mathrm{p}}(z_k^{\mathrm{cell}})) - U_j)/\omega_j]}$$

$$\widehat{U}_{\mathrm{ocp}}^{\mathrm{p}}\left(\theta_{\mathrm{s}}^{\mathrm{p}}\left(z_k^{\mathrm{cell}}\right)\right) = \widehat{U}_{\mathrm{ocv}}\left(z_k^{\mathrm{cell}}\right) + U_{\mathrm{ocp}}^{\mathrm{n}}\left(\theta_{\mathrm{s}}^{\mathrm{n}}\left(z_k^{\mathrm{cell}}\right)\right).$$

- Step 3: Since the cost value J will not be exactly zero, we recompute the OCV estimates:

$$\widehat{U}_{\mathrm{ocv}}\left(z_k^{\mathrm{cell}}\right) = \widehat{U}_{\mathrm{ocp}}^{\mathrm{p}}\left(\theta_{\mathrm{s}}^{\mathrm{p}}\left(z_k^{\mathrm{cell}}\right)\right) - U_{\mathrm{ocp}}^{\mathrm{n}}\left(\theta_{\mathrm{s}}^{\mathrm{n}}\left(z_k^{\mathrm{cell}}\right)\right).$$

- When we implement this procedure, we encounter a variation of the observability problem discussed earlier.
- We find we can make a good model of positive-electrode OCP, but we cannot guarantee that the boundaries $\{\theta_0^{\mathrm{p}}, \theta_{100}^{\mathrm{p}}\}$ are physical.
- The estimate $\widehat{U}_{\mathrm{ocp}}^{\mathrm{p}}\left(\theta_{\mathrm{s}}^{\mathrm{p}}\left(z_k^{\mathrm{cell}}\right)\right)$ may be shifted and/or stretched with respect to the true function.
- To see this, consider that both boundaries might be offset by the same constant $\Delta\theta$:

$$z_k^{\mathrm{ocp}} = \frac{\theta_{\mathrm{s}}^{\mathrm{p}}\left(z_k^{\mathrm{cell}}\right) - \theta_0^{\mathrm{p}}}{\theta_{100}^{\mathrm{p}} - \theta_0^{\mathrm{p}}} = \frac{\left(\theta_{\mathrm{s}}^{\mathrm{p}}\left(z_k^{\mathrm{cell}}\right) + \Delta\theta\right) - \left(\theta_0^{\mathrm{p}} + \Delta\theta\right)}{\left(\theta_{100}^{\mathrm{p}} + \Delta\theta\right) - \left(\theta_0^{\mathrm{p}} + \Delta\theta\right)},$$

where

$$\theta_{\mathrm{s}}^{\mathrm{p}}\left(z_k^{\mathrm{cell}}\right)+\triangle\theta=\sum_j\left[\triangle\theta_j+\frac{X_j}{1+\exp\left[f\left(\widehat{U}_{\mathrm{ocp}}^{\mathrm{p}}\left(\theta_{\mathrm{s}}^{\mathrm{p}}\left(z_k^{\mathrm{cell}}\right)\right)-U_j\right)/\omega_j\right]}\right].$$

- There is no change in solution, regardless of the value of $\Delta\theta$.
- This infers that it is possible for the MSMR model to compute a result that has a constant offset (to the truth) by biasing both operating boundaries by the same amount.
  - $\triangle\theta$ is also eliminated by differentiation, so differential-capacity estimates do not overcome this observability problem.
- Based on these observations, in order to make a good MSMR model using this approach we must start our optimizations with initial values for $\left\{U_j, X_j, \omega_j\right\}_j^{\mathrm{p}}$ that are close to the true values and put narrow constraints on these values during optimization.
- This is not always feasible with physical cells; we rely on some insight regarding the material composition of the positive electrode and a literature MSMR model to use as an initialization for the optimizations.
- To summarize, in the process of estimating OCV and OCP, we have discovered two observability problems.
  1. Attempts to find both electrode OCP functions from cell-level OCV fail because the solution will be biased by a voltage offset
  2. Attempts to find positive-electrode OCP from cell-level OCV and negative-electrode OCP will be biased by a stoichiometric offset.
- These observability problems appear whenever the electrode data are missing, which underlines the recommendation that having data from both electrodes is always preferred when estimating the electrode-level quantities.

Assume that we have a database of known materials

- We quickly present a second alternative that might be used to determine electrode OCP functions and operating boundaries.
- We assume we are in possession of a database of MSMR models of $N^{\mathrm{n}} \geq 1$ negative-electrode and $N^{\mathrm{p}} \geq 1$ positive-electrode materials.
- We attempt to fit cell OCV using exhaustive combinations of these materials to see which fits cell OCV best.
- In principle, this requires $N^{\mathrm{n}} \times N^{\mathrm{p}}$ optimizations, but in practice some of these combinations will not make sense and can be skipped.
  - For example, cell chemistries having LFP positive electrodes have OCV relationships that are visually distinct from those having other electrodes; therefore, not every alternative from the database must to be checked if we can narrow the reasonable candidates down based on experience and simple observation.
- The procedure to follow is:
  1. Select one $U^{\mathrm{n}}_{\mathrm{ocp},j}$ and one $U^{\mathrm{p}}_{\mathrm{ocp},k}$ from the database of OCP functions, where $1 \leq j \leq N^{\mathrm{n}}$ and $1 \leq k \leq N^{\mathrm{p}}$.
  2. Optimize $\left\{\theta^{\mathrm{n}}_0, \theta^{\mathrm{n}}_{100}, \theta^{\mathrm{p}}_0, \theta^{\mathrm{p}}_{100}\right\}$ to fit OCV for this combination.
  3. Store the value of the optimization cost function as $J_{j,k} = J$ for this combination of j and k; similarly, store the optimized boundaries as $\Theta_{j,k} = \left\{\theta^{\mathrm{n}}_0, \theta^{\mathrm{n}}_{100}, \theta^{\mathrm{p}}_0, \theta^{\mathrm{p}}_{100}\right\}$.
  4. Repeat Steps (i)–(iii) for all distinct combinations (that make sense) of $1 \leq j \leq N^{\mathrm{n}}$ and $1 \leq k \leq N^{\mathrm{p}}$.
  5. Retain $U^{\mathrm{n}}_{\mathrm{ocp}} = U^{\mathrm{n}}_{\mathrm{ocp},j^*}$, $U^{\mathrm{p}}_{\mathrm{ocp}} = U^{\mathrm{p}}_{\mathrm{ocp},k^*}$, and $\left\{\theta^{\mathrm{n}}_0, \theta^{\mathrm{n}}_{100}, \theta^{\mathrm{p}}_0, \theta^{\mathrm{p}}_{100}\right\} = \Theta_{j^*,k^*}$ for the values of j^* and k^* that minimize $J_{j,k}$.

Appendix 3.d: Polynomial-type SPM

- Here, as reference, I present the development of a SPM that approximates the concentration of lithium in each particle using a polynomial function of the particle's radial dimension.
- The basic equation governing diffusion in the solid phase is given by Fick's Law as,

$$\frac{\partial \theta_{\mathrm{s}}}{\partial t} = \frac{1}{\tilde{r}^2}\frac{\partial}{\partial \tilde{r}}\left(\bar{D}_{\mathrm{s}}\tilde{r}^2\frac{\partial \theta_{\mathrm{s}}}{\partial \tilde{r}}\right), \tag{3.18}$$

with $\theta_{s,0} = \theta_0 + z_0\left(\theta_{100} - \theta_0\right)$ at $t = 0$ for $0 < \tilde{r} < 1$ and boundary conditions,

$$\bar{D}_{\mathrm{s}}\frac{\partial \theta_{\mathrm{s}}}{\partial \tilde{r}} = 0 \quad \text{at}\, \tilde{r} = 0,\ t \geq 0 \tag{3.19}$$

$$\bar{D}_{\mathrm{s}}\frac{\partial \theta_{\mathrm{s}}}{\partial \tilde{r}} = -\frac{|\theta_{100} - \theta_0|}{10800Q}i_{\mathrm{f}} \quad \text{at}\, \tilde{r} = 1,\ t \geq 0. \tag{3.20}$$

- We model θ_{s} using a fourth-order polynomial of the general form:

$$\theta_{\mathrm{s}}\left(\tilde{r}, t\right) = \alpha\left(t\right) + \beta\left(t\right)\tilde{r}^2 + \gamma\ \left(t\right)\tilde{r}^4. \tag{3.21}$$

- Due to the monotonic nature of the concentration profile under constant current, we need only consider even-ordered polynomials.
- Substituting expression (3.21) into (3.18) gives:

$$\begin{aligned}
\frac{\partial \theta_{\mathrm{s}}\left(\tilde{r}, t\right)}{\partial t} &= \frac{\partial \alpha\left(t\right)}{\partial t} + \frac{\partial \beta\left(t\right)}{\partial t}\tilde{r}^2 + \frac{\partial \gamma\ \left(t\right)}{\partial t}\tilde{r}^4 \\
&= \bar{D}_{\mathrm{s}}\left(\theta_{\mathrm{s}}\right)\frac{1}{\tilde{r}^2}\frac{\partial}{\partial \tilde{r}}\left(\tilde{r}^2 2\tilde{r}\beta\left(t\right) + \tilde{r}^2 4\tilde{r}^3\gamma\ \left(t\right)\right) \\
&= \bar{D}_{\mathrm{s}}\left(\theta_{\mathrm{s}}\right)\frac{1}{\tilde{r}^2}2\bar{r}^3\beta\left(t\right) + 4\tilde{r}^5\gamma\ \left(t\right) \\
&= \bar{D}_{\mathrm{s}}\left(\theta_{\mathrm{s}}\right)\frac{1}{\tilde{r}^2}6\tilde{r}^2\beta\left(t\right) + 20\tilde{r}^4\gamma\ \left(t\right) \\
&= \bar{D}_{\mathrm{s}}\left(\theta_{\mathrm{s}}\right)\left(6\beta\left(t\right) + 20\tilde{r}^2\gamma\ \left(t\right)\right).
\end{aligned}$$

- Examining the boundary conditions, we have

$$\left.\frac{\partial \theta_{\mathrm{s}}\left(\tilde{r}, t\right)}{\partial \tilde{r}}\right|_{\tilde{r}=0}=0$$

$$\left.\frac{\partial \theta_{\mathrm{s}}\left(\tilde{r}, t\right)}{\partial \tilde{r}}\right|_{\tilde{r}=1}=2 \beta\left(t\right)+4 \gamma\left(t\right)=-\frac{\left|\theta_{100}-\theta_{0}\right|}{\bar{D}_{\mathrm{s}} 10,800 Q} i_{\mathrm{f}}. \tag{3.22}$$

- We proceed to find expressions for time-dependent functions $\alpha\left(t\right)$, $\beta\left(t\right)$ and $\gamma\left(t\right)$ in terms of the solid surface concentration $\theta_{\mathrm{ss}}\left(t\right)$ and the average concentration θ_{avg}.
- The solid surface concentration is obtained by setting $\tilde{r}=1$ in (3.21) giving

$$\theta_{\mathrm{ss}}\left(t\right)=\alpha\left(t\right)+\beta\left(t\right)+\gamma\left(t\right). \tag{3.23}$$

- The volume-averaged concentration is again obtained by integrating the local concentration across the radial volume and dividing by the total volume, giving:

$$\begin{aligned}\theta_{\mathrm{avg}}\left(t\right) &= 3 \int_{\tilde{r}=0}^{\tilde{r}=1} \tilde{r}^{2} \theta\left(\tilde{r}, t\right) \mathrm{d}\tilde{r} \\ &= 3 \int_{\tilde{r}=0}^{\tilde{r}=1} \tilde{r}^{2}\left[\alpha\left(t\right)+\beta\left(t\right) \tilde{r}^{2}+\gamma\left(t\right) \tilde{r}^{4}\right] \mathrm{d}\tilde{r} \\ &= \left[\frac{3 \alpha\left(t\right) \tilde{r}^{3}}{3}+\frac{3 \beta\left(t\right) \tilde{r}^{5}}{5}+\frac{3 \gamma\left(t\right) \tilde{r}^{7}}{7}\right]_{0}^{1} \\ &= \alpha\left(t\right)+\frac{3}{5} \beta\left(t\right)+\frac{3}{7} \gamma\left(t\right).\end{aligned} \tag{3.24}$$

- We need a third equation as we have three time-dependent functions to identify.
- We introduce here the volume-averaged concentration flux, $\nabla \theta_{\mathrm{avg}}\left(t\right)$, for this purpose.

- The process for generating the volume-averaged concentration flux proceeds similar to that for the concentration; thus we write,

$$\begin{aligned}\nabla\theta_{\text{avg}}(t) &= 3\int_{\tilde{r}=0}^{\tilde{r}=1}\tilde{r}^2\frac{\partial\theta_{\text{s}}(\tilde{r},t)}{\partial\tilde{r}}\,\text{d}\tilde{r}\\ &= 3\int_{\tilde{r}=0}^{\tilde{r}=1}\tilde{r}^2\left[2\beta(t)\,\tilde{r}+4\gamma(t)\,\tilde{r}^3\right]\text{d}\tilde{r}\\ &= \int_{\tilde{r}=0}^{\tilde{r}=1}\left[6\beta(t)\,\tilde{r}^3+12\gamma(t)\,\tilde{r}^5\right]\text{d}\tilde{r}\\ &= \left[\frac{6\beta(t)\,\tilde{r}^4}{4}+\frac{12\gamma(t)\,\tilde{r}^6}{6}\right]_0^1\\ &= \frac{3}{2}\beta(t)+2\gamma(t)\,. \end{aligned} \tag{3.25}$$

- Equations (3.23) , (3.24) and (3.25) combine to form the linear system,

$$\begin{bmatrix}1 & 1 & 1\\ 1 & 3/5 & 3/7\\ 0 & 3/2 & 2\end{bmatrix}\begin{bmatrix}\alpha(t)\\ \beta(t)\\ \gamma(t)\end{bmatrix}=\begin{bmatrix}\theta_{\text{ss}}(t)\\ \theta_{\text{avg}}(t)\\ \nabla\theta_{\text{avg}}(t)\end{bmatrix}.$$

- Solving, we get

$$\begin{aligned}\alpha(t) &= \frac{39}{4}\theta_{\text{ss}}(t)-\frac{35}{4}\theta_{\text{avg}}(t)-3\nabla\theta_{\text{avg}}(t)\\ \beta(t) &= -35\theta_{\text{ss}}(t)+35\theta_{\text{avg}}(t)+10\nabla\theta_{\text{avg}}(t)\\ \gamma(t) &= \frac{105}{4}\theta_{\text{ss}}(t)-\frac{105}{4}\theta_{\text{avg}}(t)-7\nabla\theta_{\text{avg}}(t)\,. \end{aligned} \tag{3.26}$$

- We can now write a single expression for the concentration profile in terms of the solid surface and average concentrations and the concentration flux by substituting Eqs. (3.26) into Eq. (3.21) to write,

$$\theta_{\text{s}}(\tilde{r},t)=\left(\frac{39}{4}\theta_{\text{ss}}(t)-\frac{35}{4}\theta_{\text{avg}}(t)-3\nabla\theta_{\text{avg}}(t)\right)$$

$$
\begin{aligned}
&+ \left(-35\theta_{\text{ss}}\left(t\right) + 35\theta_{\text{avg}}\left(t\right) + 10\nabla\theta_{\text{avg}}\left(t\right)\right)\tilde{r}^2 \\
&+ \left(\frac{105}{4}\theta_{\text{ss}}\left(t\right) - \frac{105}{4}\theta_{\text{avg}}\left(t\right) - 7\nabla\theta_{\text{avg}}\left(t\right)\right)\tilde{r}^4 \\
&= \left(\frac{39}{4} - 35\tilde{r}^2 + \frac{105}{4}\tilde{r}^4\right)\theta_{\text{ss}}\left(t\right) - \left(\frac{1}{4} - \tilde{r}^2 + \frac{3}{4}\tilde{r}^4\right)\theta_{\text{avg}}\left(t\right) \\
&- \left(3 - 10\tilde{r}^2 + 7\tilde{r}^4\right)\nabla\theta_{\text{avg}}\left(t\right).
\end{aligned}
$$

- In order to obtain a complete solution for the fourth-order case, we will need three additional equations.
- These will come from: (i) the volume-averaged concentration, (ii) the volume-averaged concentration flux, and (iii) the boundary condition at the particle surface.
- The volume-averaged concentration flux is obtained via the following integration,

$$
\frac{\int_0^1 \frac{\partial}{\partial\tilde{r}}\left(\frac{\partial\theta_{\text{s}}}{\partial t}\right)4\pi\tilde{r}^2\,\text{d}\tilde{r}}{\int_0^1 \frac{4}{3}\pi\tilde{r}^3\,\text{d}\tilde{r}} = \frac{\bar{D}_{\text{s}}\int_0^1 \frac{\partial}{\partial\tilde{r}}\left[\frac{1}{\tilde{r}^2}\frac{\partial}{\partial\tilde{r}}\left(\tilde{r}^2\frac{\partial\theta_{\text{s}}}{\partial\tilde{r}}\right)4\pi\tilde{r}^2\right]\text{d}\tilde{r}}{\int_0^1 \frac{4}{3}\pi\tilde{r}^3\,\text{d}\tilde{r}}.
$$

- The left-hand side evaluates to equal the time derivative of the concentration flux, $\text{d}\nabla\theta_{\text{avg}}\left(t\right)/\text{d}t$. The right-hand side evaluates as follows:

$$
\frac{\bar{D}_{\text{s}}\int_0^1 \frac{\partial}{\partial\tilde{r}}\left[\frac{1}{\tilde{r}^2}\frac{\partial}{\partial\tilde{r}}\left(\tilde{r}^2\frac{\partial\theta_{\text{s}}}{\partial\tilde{r}}\right)4\pi\tilde{r}^2\right]\text{d}\tilde{r}}{\int_0^1 \frac{4}{3}\pi\tilde{r}^3\,\text{d}\tilde{r}} = 3\bar{D}_{\text{s}}\int_0^1 \frac{\partial}{\partial\tilde{r}}\left[\frac{1}{\tilde{r}^2}\frac{\partial}{\partial\tilde{r}}\left(\tilde{r}^2\frac{\partial\theta_{\text{s}}}{\partial\tilde{r}}\right)\right]\tilde{r}^2\,\text{d}\tilde{r}.
$$

- Taking first the inner derivative,

$$
\frac{\partial}{\partial\tilde{r}}\left(\tilde{r}^2\frac{\partial\theta_{\text{s}}}{\partial\tilde{r}}\right) = r^2\frac{\partial\theta_{\text{s}}^2}{\partial\tilde{r}^2} + 2\tilde{r}\frac{\partial\theta_{\text{s}}}{\partial\tilde{r}}.
$$

- Upon substituting,

$$\frac{\partial}{\partial\tilde{r}}\left[\frac{1}{\tilde{r}^2}\frac{\partial}{\partial\tilde{r}}\left(\tilde{r}^2\frac{\partial\theta_\mathrm{s}}{\partial\tilde{r}}\right)\right]=\frac{\partial}{\partial\tilde{r}}\left[\frac{1}{r^2}\left(r^2\frac{\partial\theta_\mathrm{s}^2}{\partial\tilde{r}^2}+2\tilde{r}\frac{\partial\theta_\mathrm{s}}{\partial\tilde{r}}\right)\right]=\frac{\partial}{\partial\tilde{r}}\left(\frac{\partial\theta_s^2}{\partial\tilde{r}^2}+2\tilde{r}^{-1}\frac{\partial\theta_\mathrm{s}}{\partial\tilde{r}}\right)$$
$$=\frac{\partial\theta_\mathrm{s}^3}{\partial\tilde{r}^3}+2\tilde{r}^{-1}\frac{\partial\theta_\mathrm{s}^2}{\partial\tilde{r}^2}-2\tilde{r}^{-2}\frac{\partial\theta_\mathrm{s}}{\partial\tilde{r}}.$$

- Again, substituting,

$$3\bar{D}_\mathrm{s}\int_0^1\frac{\partial}{\partial\tilde{r}}\left[\frac{1}{\tilde{r}^2}\frac{\partial}{\partial\tilde{r}}\left(\tilde{r}^2\frac{\partial\theta_\mathrm{s}}{\partial\tilde{r}}\right)\right]\tilde{r}^2\,\mathrm{d}\tilde{r}$$
$$=3\bar{D}_\mathrm{s}\int_0^1\left[\frac{\partial\theta_\mathrm{s}^3}{\partial\tilde{r}^3}+2\tilde{r}^{-1}\frac{\partial\theta_\mathrm{s}^2}{\partial\tilde{r}^2}-2\tilde{r}^{-2}\frac{\partial\theta_\mathrm{s}}{\partial\tilde{r}}\right]\tilde{r}^2\,\mathrm{d}\tilde{r} \tag{3.27}$$
$$=3\bar{D}_\mathrm{s}\int_0^1\left[\tilde{r}^2\frac{\partial\theta_\mathrm{s}^3}{\partial\tilde{r}^3}+2\tilde{r}\frac{\partial\theta_\mathrm{s}^2}{\partial\tilde{r}^2}-2\frac{\partial\theta_\mathrm{s}}{\partial\tilde{r}}\right]\mathrm{d}\tilde{r}. \tag{3.28}$$

- From the polynomial form, we compute the derivatives,

$$\frac{\mathrm{d}\theta_\mathrm{s}(t)}{\mathrm{d}\tilde{r}}=2\beta(t)\,\tilde{r}+4\gamma(t)\,\tilde{r}^3$$
$$\frac{\mathrm{d}^2\theta_\mathrm{s}(t)}{\mathrm{d}\tilde{r}^2}=2\beta(t)+12\gamma(t)\,\tilde{r}^2$$
$$\frac{\mathrm{d}^3\theta_\mathrm{s}(t)}{\mathrm{d}\tilde{r}^3}=24\gamma(t)\,\tilde{r},$$

- We insert these into Eq. (3.28) to write,

$$\frac{\mathrm{d}\nabla\theta_\mathrm{avg}(t)}{\mathrm{d}t}=3\bar{D}_\mathrm{s}\int_0^1\Big[\tilde{r}^2 24\gamma(t)\,\tilde{r}+2\tilde{r}\left(2\beta(t)+12\gamma(t)\,\tilde{r}^2\right)$$
$$-2\left(2\beta(t)\,\tilde{r}+4\gamma(t)\,\tilde{r}^3\right)\Big]\mathrm{d}\tilde{r} \tag{3.29}$$
$$=3\bar{D}_\mathrm{s}\int_0^1\Big[24\gamma(t)\,\tilde{r}^3+4\beta(t)\,\tilde{r}+24\gamma(t)\,\tilde{r}^3-4\beta(t)\,\tilde{r}$$
$$-8\gamma(t)\,\tilde{r}^3\Big]\mathrm{d}\tilde{r} \tag{3.30}$$

$$= 3\bar{D}_\mathrm{s} \int_0^1 40\gamma\ (t)\, \tilde{r}^3 d\tilde{r} = 30\bar{D}_\mathrm{s}\gamma\ (t)\,. \tag{3.31}$$

- At this point, we apply the boundary conditions at the particle surface. From Eq. (3.22), solving for $\beta\ (t)$ gives

$$\beta\ (t) = -2\gamma\ (t) - \frac{|\theta_{100} - \theta_0|}{2\bar{D}_\mathrm{s} 10800 Q} i_\mathrm{f}. \tag{3.32}$$

- Substituting into Eq. (3.25) gives,

$$\begin{aligned}\nabla\theta_\mathrm{avg}\ (t) &= -\frac{3}{2}\left[2\gamma\ (t) + \frac{|\theta_{100} - \theta_0|}{2\bar{D}_\mathrm{s} 10800 Q} i_\mathrm{f}\right] + 2\gamma\ (t) \\ &= -\gamma\ (t) - \frac{3}{4}\frac{|\theta_{100} - \theta_0|}{\bar{D}_\mathrm{s} 10800 Q} i_\mathrm{f}.\end{aligned}$$

- Solving for $\gamma\ (t)$ we obtain,

$$\gamma\ (t) = -\nabla\theta_\mathrm{avg}\ (t) - \frac{3}{4}\frac{|\theta_{100} - \theta_0|}{\bar{D}_\mathrm{s} 10800 Q} i_\mathrm{f}. \tag{3.33}$$

- Substituting Eq. (3.33) into Eq. (3.31) gives a first-order ordinary differential equation for the volume-averaged flux density,

$$\frac{\mathrm{d}\nabla\theta_\mathrm{avg}\ (t)}{\mathrm{d}t} + 30\bar{D}_\mathrm{s}\nabla\theta_\mathrm{avg}\ (t) + \frac{45}{2}\frac{|\theta_{100} - \theta_0|}{10800 Q} i_\mathrm{f} = 0. \tag{3.34}$$

Computational Algorithm: Fourth-order Form

- The fourth-order polynomial approximation features two dynamic states: (i) $\theta_\mathrm{avg}\ (t)$, and (ii) $\nabla\theta_\mathrm{avg}\ (t)$—both given by first-order ordinary differential equations—and a single output, $\theta_\mathrm{ss}\ (t)$, obtained from an algebraic equation.
- We find the differential equation for θ_avg as:

$$\frac{\mathrm{d}\theta_\mathrm{avg}}{\mathrm{d}t} = 3\bar{D}_\mathrm{s} \int_0^1 \frac{\partial}{\partial\tilde{r}}\left(\tilde{r}^2 \frac{\partial\theta_\mathrm{s}}{\partial\tilde{r}}\right) \mathrm{d}\tilde{r} = 3\bar{D}_\mathrm{s}\left[\tilde{r}^r \frac{\partial\theta_\mathrm{s}}{\partial\tilde{r}}\right]_0^1$$

$$= 3\bar{D}_{\rm s}\left(1\right)^2 \left.\frac{\partial\theta_{\rm s}}{\partial\tilde{r}}\right|_{\tilde{r}=1} = 3\bar{D}_{\rm s}\left(-\frac{|\theta_{100}-\theta_0|}{\bar{D}_s 10800Q}i_{\rm f}\right), \tag{3.35}$$

where the final term on the right-hand side is supplied from the boundary condition at $\tilde{r}=1$.

- This gives the final form of the equation as:

$$\frac{{\rm d}\theta_{\rm avg}}{{\rm d}t} = -\frac{3\left|\theta_{100}-\theta_0\right|}{10800Q}i_{\rm f}, \tag{3.36}$$

which is now an ordinary differential equation in $\theta_{\rm avg}\left(t\right)$.

- Employing a forward difference approximation we convert the differential equation (3.36) to discrete time as,

$$\frac{\theta_{\rm avg}\left[k+1\right]-\theta_{\rm avg}\left[k\right]}{\Delta T} = -\frac{3\left|\theta_{100}-\theta_0\right|}{10800Q}i_{\rm f}[k].$$

- The differential equation for the gradient is written in Eq. (3.34), which we rewrite here as

$$\frac{{\rm d}\nabla\theta_{\rm avg}\left(t\right)}{{\rm d}t} = -30\bar{D}_{\rm s}\nabla\theta_{\rm avg}\left(t\right) - \frac{45}{2}\frac{\left|\theta_{100}-\theta_0\right|}{10800Q}i_{\rm f}.$$

- We can discretize this as:

$$\frac{\nabla\theta_{\rm avg}[k+1]-\nabla\theta_{\rm avg}[k]}{\Delta T} = -30\bar{D}_{\rm s}\nabla\theta_{\rm avg}[k] - \frac{45}{2}\frac{\left|\theta_{100}-\theta_0\right|}{10800Q}i_{\rm f}[k].$$

- To find the output equation, we combine Eq. (3.23) and (3.24) to get:

$$\theta_{\rm ss}\left(t\right) = \theta_{\rm avg}\left(t\right) + \frac{2}{5}\beta\left(t\right) + \frac{4}{7}\gamma\left(t\right).$$

- We substitute $\beta(t)$ and $\gamma\left(t\right)$ from Eqs. (3.32) and (3.33):

$$\theta_{\rm ss}\left(t\right) = \theta_{\rm avg}\left(t\right) + \frac{8}{35}\nabla\theta_{\rm avg}(t) - \frac{\left|\theta_{100}-\theta_0\right|}{35\bar{D}_{\rm s}10800Q}i_{\rm f}(t).$$

- In discrete time, the form remains the same:

$$\theta_{\rm ss}\left[k\right] = \theta_{\rm avg}[k] + \frac{8}{35}\nabla\theta_{\rm avg}[k] - \frac{\left|\theta_{100}-\theta_0\right|}{35\bar{D}_{\rm s}10800Q}i_{\rm f}[k].$$

- To simplify notation, we define,

$$Q^{\mathrm{r}} = \frac{Q}{\left|\theta^{\mathrm{r}}_{100} - \theta^{\mathrm{r}}_{0}\right|}.$$

- We condense the model equations into a time-varying "state-space" form.
  - In continuous time, they are:

$$\begin{bmatrix} \dot{\theta}^{\mathrm{r}}_{\mathrm{avg}}(t) \\ \nabla\dot{\theta}^{\mathrm{r}}_{\mathrm{avg}}(t) \end{bmatrix} = \begin{bmatrix} 0 & 0 \\ 0 & -30\bar{D}^{\mathrm{r}}_{\mathrm{s}}(\theta^{\mathrm{r}}_{\mathrm{ss}}(t^{-})) \end{bmatrix} \begin{bmatrix} \theta^{\mathrm{r}}_{\mathrm{avg}}(t) \\ \nabla\theta^{\mathrm{r}}_{\mathrm{avg}}(t) \end{bmatrix} + \begin{bmatrix} -\dfrac{1}{3600Q^{\mathrm{r}}} \\ -\dfrac{1}{480Q^{\mathrm{r}}} \end{bmatrix} i^{\mathrm{r}}_{\mathrm{f}}(t)$$

$$\left[\theta^{\mathrm{r}}_{\mathrm{ss}}(t)\right] = \begin{bmatrix} 1 & \dfrac{8}{35} \end{bmatrix} \begin{bmatrix} \theta^{\mathrm{r}}_{\mathrm{avg}}(t) \\ \nabla\theta^{\mathrm{r}}_{\mathrm{avg}}(t) \end{bmatrix} + \left[-\frac{(1/378\,000)}{Q^{\mathrm{r}}\bar{D}^{\mathrm{r}}_{\mathrm{s}}(\theta^{\mathrm{r}}_{\mathrm{ss}}(t^{-}))}\right] i^{\mathrm{r}}_{\mathrm{f}}(t).$$

  - In discrete time, using Euler's rule, they are:

$$\begin{bmatrix} \theta^{\mathrm{r}}_{\mathrm{avg}}[k+1] \\ \nabla\theta^{\mathrm{r}}_{\mathrm{avg}}[k+1] \end{bmatrix} = \begin{bmatrix} 1 & 0 \\ 0 & 1 - 30\bar{D}^{\mathrm{r}}_{\mathrm{s}}(\theta^{\mathrm{r}}_{\mathrm{ss}}[k])\,\Delta T \end{bmatrix} \begin{bmatrix} \theta^{\mathrm{r}}_{\mathrm{avg}}[k] \\ \nabla\theta^{\mathrm{r}}_{\mathrm{avg}}[k] \end{bmatrix} + \begin{bmatrix} -\dfrac{\Delta T}{3600Q^{\mathrm{r}}} \\ -\dfrac{\Delta T}{480Q^{\mathrm{r}}} \end{bmatrix} i^{\mathrm{r}}_{\mathrm{f}}[k]$$

$$\left[\theta^{\mathrm{r}}_{\mathrm{ss}}[k]\right] = \begin{bmatrix} 1 & \dfrac{8}{35} \end{bmatrix} \begin{bmatrix} \theta^{\mathrm{r}}_{\mathrm{avg}}[k] \\ \nabla\theta^{\mathrm{r}}_{\mathrm{avg}}[k] \end{bmatrix} + \left[-\frac{(1/378\,000)}{Q^{\mathrm{r}}\bar{D}^{\mathrm{r}}_{\mathrm{s}}(\theta^{\mathrm{r}}_{\mathrm{ss}}[k-1])}\right] i^{\mathrm{r}}_{\mathrm{f}}[k]\,.$$

Appendix 3.e: Finding $\tilde{\phi}_{\mathrm{e}}^{\mathrm{p}}(3,0^+)$ from $\tilde{\phi}_{\mathrm{s\text{-}e}}^{\mathrm{r}}(\tilde{x},0^+)$

- The MATLAB `bvp5c` solver finds $\tilde{\phi}_{\mathrm{s\text{-}e}}^{\mathrm{r}}(\tilde{x},0^+)$ directly, but we also need $\tilde{\phi}_{\mathrm{e}}^{\mathrm{p}}(3,0^+)$ in order to compute the voltage change.
- Here, we see how to use the available information to do so.
- To begin, the ionic current flowing through the electrolyte is related to the following two equations:

$$\varepsilon_{\mathrm{e}}^{\mathrm{r}} A i_{\mathrm{e}}^{\mathrm{r}}(\tilde{x},t) = -\bar{\kappa}^{\mathrm{r}} \frac{\partial \phi_{\mathrm{e}}^{\mathrm{r}}(\tilde{x},t)}{\partial \tilde{x}} \tag{3.37}$$

$$\varepsilon_{\mathrm{e}}^{\mathrm{r}} A \frac{\partial i_{\mathrm{e}}^{\mathrm{r}}(\tilde{x},t)}{\partial \tilde{x}} = F \dot{n}^{\mathrm{r}}(\tilde{x},t)\,. \tag{3.38}$$

- Since the electrolyte supports ionic currents only, $i_{\mathrm{e}}(0,t) = i_{\mathrm{e}}(3,t) = 0$, and $\varepsilon_{\mathrm{e}} A i_{\mathrm{e}}(1,t) = \varepsilon_{\mathrm{e}} A i_{\mathrm{e}}(2,t) = i_{\mathrm{app}}$.
- In the following steps, we will omit the superscript (cell region) on ε_{e} and i_{e} because they will not appear in the final solutions.

Negative electrode

- Integrate both sides of Eq. (3.38) using dummy variable of integration χ to arrive at a solution for $i_{\mathrm{e}}(\tilde{x},t)$:

$$\int_0^{\tilde{x}} \varepsilon_{\mathrm{e}} A \frac{\partial i_{\mathrm{e}}(\chi,t)}{\partial \chi} \mathrm{d}\chi = \int_0^{\tilde{x}} F \dot{n}^{\mathrm{n}}(\chi,t)\,\mathrm{d}\chi$$

$$\varepsilon_{\mathrm{e}} A \left[i_{\mathrm{e}}(\tilde{x},t) - i_{\mathrm{e}}(0,t) \right] = F \int_0^{\tilde{x}} \dot{n}^{\mathrm{n}}(\chi,t)\,\mathrm{d}\chi$$

$$\varepsilon_{\mathrm{e}} A i_{\mathrm{e}}(\tilde{x},t) = F \int_0^{\tilde{x}} \dot{n}^{\mathrm{n}}(\chi,t)\,\mathrm{d}\chi\,.$$

- Then, combining the knowledge from Eq. (3.37) and performing integration again can help us find ϕ_e in the negative electrode:

$$-\int_0^{\tilde{x}} \bar{\kappa}^n \frac{\partial \phi_e^n(\chi,t)}{\partial \chi} d\chi = \int_0^{\tilde{x}} \varepsilon_e^r A i_e^r(\chi_1,t)\, d\chi_1$$

$$= F \int_0^{\tilde{x}} \int_0^{\chi_1} \dot{n}^n(\chi_2,t)\, d\chi_2 d\chi_1$$

$$-\bar{\kappa}^n \left[\phi_e^n(\tilde{x},t) - \phi_e^n(0,t)\right] = F \int_0^{\tilde{x}} \int_0^{\chi_1} \dot{n}^n(\chi_2,t)\, d\chi_2 d\chi_1$$

$$\tilde{\phi}_e^n(\tilde{x},t) = -\frac{F}{\bar{\kappa}^n} \int_0^{\tilde{x}} \int_0^{\chi_1} \dot{n}^n(\chi_2,t)\, d\chi_2 d\chi_1. \quad (3.39)$$

Separator

- In the separator region,

$$\varepsilon_e A i_e(\tilde{x},t) = i_{app}$$

$$\varepsilon_e A i_e(\tilde{x},t) = -\bar{\kappa}^s \frac{\partial \phi_e^s(\tilde{x},t)}{\partial \tilde{x}}.$$

- We now integrate again over the separator region only:

$$-\int_1^{\tilde{x}} \bar{\kappa}^s \frac{\partial \phi_e^s(\chi,t)}{\partial \chi} d\chi = \int_1^{\tilde{x}} \varepsilon_e A i_e(\chi,t)\, d\chi = \int_1^{\tilde{x}} i_{app} d\chi$$

$$-\bar{\kappa}^s \left[\phi_e^s(\tilde{x},t) - \phi_e(1,t)\right] = i_{app}(\tilde{x}-1)$$

$$\tilde{\phi}_e^s(\tilde{x},t) - \tilde{\phi}_e^n(1,t) = -\frac{i_{app}}{\bar{\kappa}^s}(\tilde{x}-1)$$

$$\tilde{\phi}_e^s(\tilde{x},t) = \tilde{\phi}_e^n(1,t) - \frac{i_{app}}{\bar{\kappa}^s}(\tilde{x}-1). \quad (3.40)$$

Positive electrode

- Similarly,

$$\varepsilon_{\mathrm{e}} A i_{\mathrm{e}}\left(\tilde{x}, t\right) = -\bar{\kappa}^{\mathrm{p}} \frac{\partial \phi_{\mathrm{e}}^{\mathrm{p}}\left(\tilde{x}, t\right)}{\partial \tilde{x}}$$

$$\varepsilon_{\mathrm{e}} A \frac{\partial i_{\mathrm{e}}\left(\tilde{x}, t\right)}{\partial \tilde{x}} = F \dot{n}^{\mathrm{p}}\left(\tilde{x}, t\right).$$

- We now integrate over the positive-electrode region only:

$$\int_2^{\tilde{x}} \varepsilon_{\mathrm{e}} A \frac{\partial i_{\mathrm{e}}\left(\chi, t\right)}{\partial \chi} \mathrm{d}\chi = \int_2^{\tilde{x}} F \dot{n}^{\mathrm{p}}\left(\chi, t\right) \mathrm{d}\chi$$

$$\varepsilon_{\mathrm{e}} A \left[i_{\mathrm{e}}\left(\tilde{x}, t\right) - i_{\mathrm{e}}(2, t)\right] = F \int_2^{\tilde{x}} \dot{n}^{\mathrm{p}}\left(\chi, t\right) \mathrm{d}\chi$$

$$\varepsilon_{\mathrm{e}} A i_{\mathrm{e}}\left(\tilde{x}, t\right) = i_{\mathrm{app}} + F \int_2^{\tilde{x}} \dot{n}^{\mathrm{p}}\left(\chi, t\right) \mathrm{d}\chi.$$

- Again,

$$-\bar{\kappa}^{\mathrm{p}} \int_2^{\tilde{x}} \frac{\partial \phi_{\mathrm{e}}^{\mathrm{p}}\left(\chi, t\right)}{\partial \chi} \mathrm{d}\chi = \int_2^{\tilde{x}} i_{\mathrm{app}} \mathrm{d}\chi + F \int_2^{\tilde{x}} \int_2^{\chi_1} \dot{n}^{\mathrm{p}}\left(\chi_2, t\right) \mathrm{d}\chi_2 \mathrm{d}\chi_1$$

$$-\bar{\kappa}^{\mathrm{p}} \left[\phi_{\mathrm{e}}^{\mathrm{p}}\left(\tilde{x}, t\right) - \phi_{\mathrm{e}}^{\mathrm{s}}\left(2, t\right)\right] = i_{\mathrm{app}}\left(\tilde{x} - 2\right) + F \int_2^{\tilde{x}} \int_2^{\chi_1} \dot{n}^{\mathrm{p}}\left(\chi_2, t\right) \mathrm{d}\chi_2 \mathrm{d}\chi_1$$

$$\tilde{\phi}_{\mathrm{e}}^{\mathrm{p}}\left(\tilde{x}, t\right) = \tilde{\phi}_{\mathrm{e}}^{\mathrm{s}}\left(2, t\right) - \frac{i_{\mathrm{app}}\left(\tilde{x} - 2\right)}{\bar{\kappa}^{\mathrm{p}}} - \frac{F}{\bar{\kappa}^{\mathrm{p}}} \int_2^{\tilde{x}} \int_2^{\chi_1} \dot{n}^{\mathrm{p}}\left(\chi_2, t\right) \mathrm{d}\chi_2 \mathrm{d}\chi_1.$$

- Substitute Eqs. (3.39) and (3.40) into the electrolyte-potential expression in the positive electrode:

$$\tilde{\phi}_{\mathrm{e}}^{\mathrm{p}}\left(\tilde{x}, t\right) = -\frac{F}{\bar{\kappa}^{\mathrm{n}}} \int_0^1 \int_0^{\chi_1} \dot{n}^{\mathrm{n}}\left(\chi_2, t\right) \mathrm{d}\chi_2 \mathrm{d}\chi_1 - \frac{i_{\mathrm{app}}}{\bar{\kappa}^{\mathrm{s}}} - \frac{i_{\mathrm{app}}\left(\tilde{x} - 2\right)}{\bar{\kappa}^{\mathrm{p}}} - \frac{F}{\bar{\kappa}^{\mathrm{p}}} \int_2^{\tilde{x}} \int_2^{\chi_1} \dot{n}^{\mathrm{p}}\left(\chi_2, t\right) \mathrm{d}\chi_2 \mathrm{d}\chi_1. \tag{3.41}$$

- Cell voltage computation requires only that we know $\tilde{\phi}_{\mathrm{e}}^{\mathrm{p}}(3,t)$. Evaluating the previous equation at $\tilde{x}=3$ gives:

$$\tilde{\phi}_{\mathrm{e}}^{\mathrm{p}}(3,t) = -\frac{F}{\bar{\kappa}^{\mathrm{n}}}\int_0^1\int_0^{\chi_1}\dot{n}^{\mathrm{n}}(\chi_2,t)\,\mathrm{d}\chi_2\mathrm{d}\chi_1 - \frac{i_{\mathrm{app}}}{\bar{\kappa}^{\mathrm{s}}} - \frac{i_{\mathrm{app}}}{\bar{\kappa}^{\mathrm{p}}} - \frac{F}{\bar{\kappa}^{\mathrm{p}}}\int_2^3\int_2^{\chi_1}\dot{n}^{\mathrm{p}}(\chi_2,t)\,\mathrm{d}\chi_2\mathrm{d}\chi_1. \tag{3.42}$$

The double integral of $\dot{n}^{\mathrm{r}}(\tilde{x},t)$

- The double-integration of $\dot{n}$ in the negative and positive electrodes can be evaluated directly from ODE-solver solutions.
- In the negative electrode, we have found

$$\tilde{\phi}_{\mathrm{e}}^{\mathrm{n}}(1,t) = -\frac{F}{\bar{\kappa}^{\mathrm{n}}}\int_0^1\int_0^{\chi_1}\dot{n}^{\mathrm{n}}(\chi_2,t)\,\mathrm{d}\chi_2\mathrm{d}\chi_1.$$

- We will find a simpler solution by double-integrating

$$\frac{\partial^2\tilde{\phi}_{\mathrm{s\text{-}e}}^{\mathrm{n}}(\tilde{x},t)}{\partial\tilde{x}^2} = F\left(\frac{1}{\bar{\sigma}^{\mathrm{n}}}+\frac{1}{\bar{\kappa}^{\mathrm{n}}}\right)\dot{n}^{\mathrm{n}}(\tilde{x},t).$$

- We begin with

$$\int_0^{\chi_1}\frac{\partial^2\tilde{\phi}_{\mathrm{s\text{-}e}}^{\mathrm{n}}(\chi_2,t)}{\partial\chi_2^2}\,\mathrm{d}\chi_2 = F\left(\frac{1}{\bar{\sigma}^{\mathrm{n}}}+\frac{1}{\bar{\kappa}^{\mathrm{n}}}\right)\int_0^{\chi_1}\dot{n}^{\mathrm{n}}(\chi_2,t)\,\mathrm{d}\chi_2$$

$$\left.\frac{\partial\tilde{\phi}_{\mathrm{s\text{-}e}}^{\mathrm{n}}(\chi_2,t)}{\partial\chi_2}\right|_{\chi_1} - \underbrace{\frac{\partial\tilde{\phi}_{\mathrm{s\text{-}e}}^{\mathrm{n}}(0,t)}{\partial\chi_2}}_{-i_{\mathrm{app}}(t)/\bar{\sigma}^{\mathrm{n}}} = F\left(\frac{\bar{\sigma}^{\mathrm{n}}+\bar{\kappa}^{\mathrm{n}}}{\bar{\sigma}^{\mathrm{n}}\bar{\kappa}^{\mathrm{n}}}\right)\int_0^{\chi_1}\dot{n}^{\mathrm{n}}(\chi_2,t)\,\mathrm{d}\chi_2$$

$$\frac{\partial\tilde{\phi}_{\mathrm{s\text{-}e}}^{\mathrm{n}}(\chi_1,t)}{\partial\chi_1} = F\left(\frac{\bar{\sigma}^{\mathrm{n}}+\bar{\kappa}^{\mathrm{n}}}{\bar{\sigma}^{\mathrm{n}}\bar{\kappa}^{\mathrm{n}}}\right)\int_0^{\chi_1}\dot{n}^{\mathrm{n}}(\chi_2,t)\,\mathrm{d}\chi_2 - \frac{i_{\mathrm{app}}(t)}{\bar{\sigma}^{\mathrm{n}}}.$$

- We integrate once again:

$$\int_0^{\tilde{x}} \frac{\partial \tilde{\phi}_{\text{s-e}}^{\text{n}}(\chi_1, t)}{\partial \chi_1} \, \mathrm{d}\chi_1 = F \left(\frac{\bar{\sigma}^{\text{n}} + \bar{\kappa}^{\text{n}}}{\bar{\sigma}^{\text{n}} \bar{\kappa}^{\text{n}}} \right) \int_0^{\tilde{x}} \int_0^{\chi_1} \dot{n}^{\text{n}}(\chi_2, t) \, \mathrm{d}\chi_2 \mathrm{d}\chi_1 - \int_0^{\tilde{x}} \frac{i_{\text{app}}(t)}{\bar{\sigma}^{\text{n}}} \, \mathrm{d}\chi_1$$

$$\tilde{\phi}_{\text{s-e}}^{\text{n}}(\tilde{x}, t) - \tilde{\phi}_{\text{s-e}}^{\text{n}}(0, t) = F \left(\frac{\bar{\sigma}^{\text{n}} + \bar{\kappa}^{\text{n}}}{\bar{\sigma}^{\text{n}} \bar{\kappa}^{\text{n}}} \right) \int_0^{\tilde{x}} \int_0^{\chi_1} \dot{n}^{\text{n}}(\chi_2, t) \, \mathrm{d}\chi_2 \mathrm{d}\chi_1 - \frac{\tilde{x} i_{\text{app}}(t)}{\bar{\sigma}^{\text{n}}}.$$

- Solving for the term of interest:

$$\frac{\bar{\sigma}^{\text{n}} \bar{\kappa}^{\text{n}}}{\bar{\sigma}^{\text{n}} + \bar{\kappa}^{\text{n}}} \left(\tilde{\phi}_{\text{s-e}}^{\text{n}}(\tilde{x}, t) - \tilde{\phi}_{\text{s-e}}^{\text{n}}(0, t) + \frac{\tilde{x} i_{\text{app}}(t)}{\bar{\sigma}^{\text{n}}} \right) = F \int_0^{\tilde{x}} \int_0^{\chi_1} \dot{n}^{\text{n}}(\chi_2, t) \, \mathrm{d}\chi_2 \mathrm{d}\chi_1$$

$$\tilde{\phi}_{\text{e}}^{\text{n}}(1, t) = -\frac{\bar{\sigma}^{\text{n}}}{\bar{\sigma}^{\text{n}} + \bar{\kappa}^{\text{n}}} \left(\tilde{\phi}_{\text{s-e}}^{\text{n}}(1, t) - \tilde{\phi}_{\text{s-e}}^{\text{n}}(0, t) \right) - \frac{i_{\text{app}}(t)}{\bar{\sigma}^{\text{n}} + \bar{\kappa}^{\text{n}}}.$$

- In the positive electrode, we follow the same strategy to find

$$-\frac{F}{\bar{\kappa}^{\text{p}}} \int_2^3 \int_2^{\chi_1} \dot{n}^{\text{p}}(\chi_2, t) \, \mathrm{d}\chi_2 \mathrm{d}\chi_1.$$

- We simplify by double-integrating

$$\frac{\partial^2 \tilde{\phi}_{\text{s-e}}^{\text{p}}(\tilde{x}, t)}{\partial \tilde{x}^2} = F \left(\frac{1}{\bar{\sigma}^{\text{p}}} + \frac{1}{\bar{\kappa}^{\text{p}}} \right) \dot{n}^{\text{p}}(\tilde{x}, t).$$

- We begin with

$$\int_2^{\chi_1} \frac{\partial^2 \tilde{\phi}_{\text{s-e}}^{\text{p}}(\chi_2, t)}{\partial \chi_2^2} \, \mathrm{d}\chi_2 = F \left(\frac{1}{\bar{\sigma}^{\text{p}}} + \frac{1}{\bar{\kappa}^{\text{p}}} \right) \int_2^{\chi_1} \dot{n}^{\text{p}}(\chi_2, t) \, \mathrm{d}\chi_2$$

$$\left. \frac{\partial \tilde{\phi}_{\text{s-e}}^{\text{p}}(\chi_2, t)}{\partial \chi_2} \right|_{\chi_1} - \underbrace{\frac{\partial \tilde{\phi}_{\text{s-e}}^{\text{p}}(2, t)}{\partial \chi_2}}_{i_{\text{app}}(t)/\bar{\kappa}^{\text{p}}} = F \left(\frac{\bar{\sigma}^{\text{p}} + \bar{\kappa}^{\text{p}}}{\bar{\sigma}^{\text{p}} \bar{\kappa}^{\text{p}}} \right) \int_2^{\chi_1} \dot{n}^{\text{p}}(\chi_2, t) \, \mathrm{d}\chi_2$$

$$\frac{\partial \tilde{\phi}_{\text{s-e}}^{\text{p}}(\chi_1, t)}{\partial \chi_1} = F \left(\frac{\bar{\sigma}^{\text{p}} + \bar{\kappa}^{\text{p}}}{\bar{\sigma}^{\text{p}} \bar{\kappa}^{\text{p}}} \right) \int_2^{\chi_1} \dot{n}^{\text{p}}(\chi_2, t) \, \mathrm{d}\chi_2 + \frac{i_{\text{app}}(t)}{\bar{\kappa}^{\text{p}}}.$$

- We integrate once again:

$$\int_2^{\tilde{x}} \frac{\partial \tilde{\phi}_{\text{s-e}}^{\text{p}}(\chi_1, t)}{\partial \chi_1} \, \mathrm{d}\chi_1 = F \left(\frac{\bar{\sigma}^{\text{p}} + \bar{\kappa}^{\text{p}}}{\bar{\sigma}^{\text{p}} \bar{\kappa}^{\text{p}}} \right) \int_2^{\tilde{x}} \int_2^{\chi_1} \dot{n}^{\text{p}}(\chi_2, t) \, \mathrm{d}\chi_2 \mathrm{d}\chi_1 + \int_0^{\tilde{x}} \frac{i_{\text{app}}(t)}{\bar{\kappa}^{\text{p}}} \, \mathrm{d}\chi_1$$

$$\tilde{\phi}_{\text{s-e}}^{\text{p}}(\tilde{x}, t) - \tilde{\phi}_{\text{s-e}}^{\text{p}}(2, t) = F \left(\frac{\bar{\sigma}^{\text{p}} + \bar{\kappa}^{\text{p}}}{\bar{\sigma}^{\text{p}} \bar{\kappa}^{\text{p}}} \right) \int_2^{\tilde{x}} \int_2^{\chi_1} \dot{n}^{\text{p}}(\chi_2, t) \, \mathrm{d}\chi_2 \mathrm{d}\chi_1 + \frac{(\tilde{x} - 2) i_{\text{app}}(t)}{\bar{\kappa}^{\text{p}}}.$$

- Solving for the term of interest:

$$\frac{\bar{\sigma}^{\text{p}} \bar{\kappa}^{\text{p}}}{\bar{\sigma}^{\text{p}} + \bar{\kappa}^{\text{p}}} \left(\tilde{\phi}_{\text{s-e}}^{\text{p}}(\tilde{x}, t) - \tilde{\phi}_{\text{s-e}}^{\text{p}}(2, t) - \frac{(\tilde{x} - 2) i_{\text{app}}(t)}{\bar{\kappa}^{\text{p}}} \right) = F \int_2^{\tilde{x}} \int_2^{\chi_1} \dot{n}^{\text{p}}(\chi_2, t) \, \mathrm{d}\chi_2 \mathrm{d}\chi_1.$$

- Overall, we are seeking to find a solution to Eq. (3.42):

$$\begin{aligned}
\tilde{\phi}_{\text{e}}^{\text{p}}(3, t) &= -\frac{F}{\bar{\kappa}^{\text{n}}} \int_0^1 \int_0^{\chi_1} \dot{n}^{\text{n}}(\chi_2, t) \, \mathrm{d}\chi_2 \mathrm{d}\chi_1 - \frac{i_{\text{app}}}{\bar{\kappa}^{\text{s}}} \\
&\quad - \frac{i_{\text{app}}}{\bar{\kappa}^{\text{p}}} - \frac{F}{\bar{\kappa}^{\text{p}}} \int_2^3 \int_2^{\chi_1} \dot{n}^{\text{p}}(\chi_2, t) \, \mathrm{d}\chi_2 \mathrm{d}\chi_1 \\
&= -\frac{\bar{\sigma}^{\text{n}}}{\bar{\sigma}^{\text{n}} + \bar{\kappa}^{\text{n}}} \left(\tilde{\phi}_{\text{s-e}}^{\text{n}}(1, t) - \tilde{\phi}_{\text{s-e}}^{\text{n}}(0, t) \right) - \frac{i_{\text{app}}(t)}{\bar{\sigma}^{\text{n}} + \bar{\kappa}^{\text{n}}} - \frac{i_{\text{app}}(t)}{\bar{\kappa}^{\text{s}}} \\
&\quad - \frac{i_{\text{app}}}{\bar{\kappa}^{\text{p}}} - \frac{\bar{\sigma}^{\text{p}}}{\bar{\sigma}^{\text{p}} + \bar{\kappa}^{\text{p}}} \left(\tilde{\phi}_{\text{s-e}}^{\text{p}}(3, t) - \tilde{\phi}_{\text{s-e}}^{\text{p}}(2, t) - \frac{i_{\text{app}}(t)}{\bar{\kappa}^{\text{p}}} \right) \\
&= -\frac{i_{\text{app}}(t)}{\bar{\sigma}^{\text{n}} + \bar{\kappa}^{\text{n}}} - \frac{i_{\text{app}}(t)}{\bar{\kappa}^{\text{s}}} - \frac{i_{\text{app}}}{\bar{\sigma}^{\text{p}} + \bar{\kappa}^{\text{p}}} - \frac{\bar{\sigma}^{\text{n}}}{\bar{\sigma}^{\text{n}} + \bar{\kappa}^{\text{n}}} \left(\tilde{\phi}_{\text{s-e}}^{\text{n}}(1, t) - \tilde{\phi}_{\text{s-e}}^{\text{n}}(0, t) \right) \\
&\quad - \frac{\bar{\sigma}^{\text{p}}}{\bar{\sigma}^{\text{p}} + \bar{\kappa}^{\text{p}}} \left(\tilde{\phi}_{\text{s-e}}^{\text{p}}(3, t) - \tilde{\phi}_{\text{s-e}}^{\text{p}}(2, t) \right).
\end{aligned}$$

Appendix 3.f: Code for vonNeuman's elephant

- Can we find parameter values well for such a high-dimensional model? Hard to say. This code is provided for fun. Try it!

```
% vonNeuman:
%    "With four parameters I can fit an elephant,
%       and with five I can make him wiggle his trunk."
% From Mayer, Khairy, Howard, "Drawing an elephant with four complex
%      parameters", Am. J. Phys. 78(6), 2010, 648-649
% Translated and modified from Python code: Original Version
%     Author: Piotr A. Zolnierczuk (zolnierczukp@ornl.gov)
%     www.johndcook.com/blog/2011/06/21/how-to-fit-an-elephant/
% Modified to wiggle trunk:
%     2 October 2011 by David Bailey (www.physics.utoronto.ca/~dbailey)
close all
p = [50-30i; 18+8i; 12-10i; -14-60i; 40+20i]; % FIVE parameters
B1x=50; B1y=-30;
B2x=18; B2y=8;
A3x=12; B3y=-10;
A5x=-14; A1y=-60;
Wiggle = 50;

p1 = 0.3; p2 = 1.25; p3 = 3;
bodyt=linspace(p1+p2*pi,p3*pi,1000);
trunkt=linspace(p3*pi,p1+(2.01+p2)*pi,1000);

for i = 0:200
  t = bodyt;
  x = A3x*cos(3*t) + A5x*cos(5*t) + B1x*sin(1*t) + B2x*sin(2*t);
  y = A1y*cos(1*t) + B1y*sin(1*t) + B2y*sin(2*t) + B3y*sin(3*t);
  hold off; plot(y,-x,'k','linewidth',2); hold on
  plot(20,20,'k.','markersize',10); plot(20,20,'ko','markersize',10);

  % wiggle // partially a guess at how to do it
  t = trunkt;
  x = A3x*cos(3*t) + A5x*cos(5*t) + B1x*sin(1*t) + B2x*sin(2*t);
  y = A1y*cos(1*t) + B1y*sin(1*t) + B2y*sin(2*t) + B3y*sin(3*t);
  yWiggle = sin((x-x(1))*pi/(length(y)))*sin(i)*Wiggle;
  plot(y - yWiggle,-x,'k','linewidth',2); drawnow
  pause(0.01)
end
```

